Daniela Eira Araújo

Application of antisense oligonucleotides to prevent *Candida albicans* infections

Application of antisense oligonucleotides to prevent *Candida albicans* infections

Daniela Araújo

UMinho | 2021

october 2021

Universidade do Minho
Escola de Engenharia

Daniela Eira Araújo

Application of antisense oligonucleotides to prevent *Candida albicans* infections

Doctoral Thesis
Chemical and Biological Engineering

Work supervised by
Dr. Sónia Silva
Dr. Mariana Henriques
Dr. Jesper Wengel

october 2021

COPYRIGHT AND CONDITIONS FOR THE USE OF WORK BY THIRD PARTIES

This is an academic work that can be used by third parties in accordance with internationally accepted rules and good practice in respect of copyright and related rights.

Thus, the present work can be used under the terms of the license indicated below. In case the user needs permission to be able to make use of the work under conditions not foreseen in the indicated license, he should contact the author through the RepositóriUM of the University of Minho.

Acknowledgments

STATEMENT OF INTEGRITY

I hereby declare having conducted this academic work with integrity. I confirm that I have not used plagiarism or any form of undue use of information or falsification of results along the process leading to its elaboration.

I further declare that I have fully acknowledged the Code of Ethical Conduct of the University of Minho.

Application of antisense oligonucleotides to prevent *Candida albicans* infections

Abstract

Candida albicans is the main cause of candidiasis and its pathogenicity is supported by a series of virulence factors, including the switch from yeast to filamentous forms. The transcription factor *EFG1* plays a central role in *C. albicans* regulation morphology. In addition, there is rise of *C. albicans* multidrug resistance accompanied by the scarcity of new classes of fungal drugs. Antisense oligonucleotides (ASOs) can hold great promise as a therapeutic agent, however yet they are poorly explored for controlling *Candida* infections. Therefore, the main goal of this work was to develop a therapeutic approach based on antisense therapy (AST) to track *C. albicans* filamentation. To this end, two major objectives were addressed: I) Exploitation and application of ASOs to control *C. albicans* filamentation; II) Creation of strategies for ASOs cargo and delivery.

The first goal of this research was the exploitation of the second and third generations of ASOs to control *EFG1* gene and *C. albicans* filamentation. To this end, the anti-*EFG1* 2'OMethylRNA was firstly projected based on second generation of ASOs and was proved to have an impact on the reduction of *EFG1* gene expression (by 60 %) and on Efg1p protein translation (by 60 %). Interestingly, the ASO was able to inhibit filamentation and to attenuate the virulence of *C. albicans* on *in vivo Galleria mellonella* (increasing its survival on 30 % at 72h with a double-dose administration). Based on the third generation of ASOs, a set of anti-*EFG1* LNA (Locked nucleic acids) ASOs were developed, and their performance was tested *in vitro* and *in vivo*. All LNA-ASOs were able to reduce *EFG1* gene expression (by 40-80 %) and consequently filamentation (by 45-55 %) *in vitro*. The *in vivo* results revealed that the LNA-ASO modified with PS-linkages and palmitoyl-2'-amino-LNA as the most favorable for an *in vivo* application (increasing *G. mellonella* survival by 40 % only with a single-dose administration).

The second goal of this research was the development of strategies for anti-*EFG1* ASO cargo and delivery. Two distinct approaches were tested: (i) development of polyplexes based on polyamide 4 and 6, that revealed to be feasible carriers, once the ASO maintains its activity against *C. albicans* cells; (ii) application of lipid-based formulations, where the DOTAP/DOPC 80/20 ρ=3 revealed to be the most promising when tested in a *G. mellonella* model (25 % of increase on larvae survival in comparison to ASO-free at 72 h).

In summary, this research underlines the therapeutic potential of ASOs for controlling *C. albicans* virulence determinants, as is the case of *EFG1* gene, as well as the importance of developing carriers' systems for ASOs cargo. Considering the future research into the management of *C. albicans* infections, this research provides valuable information to the development of a credible and alternative method to control *C. albicans* infections, based on AST.

Keywords: antisense oligonucleotides, *Candida albicans, EFG1* gene, filamentation, non-viral vectors

Aplicação de oligómeros de antisense para prevenir infeções por _Candida albicans_

Sumário

Candida albicans é uma das principais causas de candidíase e a sua patogenicidade é suportada por um conjunto de fatores de virulência, incluindo a capacidade de filamentar. _EFG1_ é um fator de transcrição com papel fundamental na filamentação. O aumento da multirresistência de _C. albicans_ é acompanhado pela escassez de novos antifúngicos. Os oligonucleotídeos de antisense (OAS) têm revelado potencial como agentes terapêuticos, contudo ainda pouco explorados no controlo da candidíase. Assim, o principal objetivo deste trabalho foi desenvolver uma abordagem terapêutica baseada na Terapia Antisense (TA) para controlar a filamentação de _C. albicans_. Para tal, dois grandes objectivos complementares foram definidos: I) Exploração e aplicação de OAS para controlar a filamentação e II) Criação de estratégias para o transporte e entrega dos OASs.

Como primeiro objetivo explorou-se a segunda e terceira gerações de OASs para controlar o gene _EFG1_. O anti-_EFG1_ 2'_O_MethylRNA foi projetado com base na segunda geração, e provou ter um impacto na redução da expressão do gene _EFG1_ (em 60 %) e na tradução da proteína Efg1p (em 60 %). O OAS foi capaz de inibir a filamentação e atenuar _in vivo_ a virulência de _C. albicans_ em _Galleria mellonella_ (30 % de aumento de sobrevivência às 72 h após dupla administração). Por outro lado, um conjunto de OAS modificados com LNA (terceira geração) foram desenvolvidos e testados _in vitro_ e _in vivo_. _In vitro_, os OAS-LNA inibiram a expressão do gene de _EFG1_ (em 40-80 %) e a filamentação (em 45-55 %). _In vivo_, o OAS-LNA com as modificações de PS e palmitoyl-2'amino-LNA revelou ser o mais favorável (40 % de aumento de sobrevivência da _G. mellonella_ com uma administração).

Como segundo objetivo exploraram-se poliplexos e lipoplexos como estratégias para o transporte e entrega do anti-_EFG1_ 2'OMe. Como primeira abordagem, desenvolveram-se poliplexos à base de poliamida 4 e 6, que revelaram ser veículos viáveis, uma vez que o OAS manteve a sua atividade contra as células de _C. albicans_. Em seguida, foram exploradas formulações lipídicas, sendo que o DOTAP/DOPC 80/20 ρ=3 revelou ser a mais promissora quando testada _in vivo_ (25 % de aumento de sobrevivência da _G. mellonella_ em comparação com o OAS livre às 72 h).

Em suma, esta investigação destaca o potencial terapêutico de OAS para o controlo de determinantes de virulência de _C. albicans_, como o caso do gene _EFG1_, bem como a importância do desenvolvimento de sistemas de veículos para o seu transporte. Considerando futuros trabalhos sobre o controlo de infeções por _C. albicans_, esta investigação fornece informação valiosa para o desenvolvimento de um método credível e alternativo para o controlo destas infeções, com base na TA.

Palavras-chave: _Candida albicans,_ filamentação, gene _EFG1_, oligonucleotídeos antisense, vetores não-víricos

Index

Chapter II.3 Antisense locked nucleic acid gapmers to control *Candida albicans* filamentation

List of Figures

Chapter II. Exploitation of the antisense oligonucleotides to control *Candida albicans* filamentation

Chapter II.1 Application of 2'-*O*MethylRNA antisense oligonucleotide to control *Candida albicans EFG1* virulence determinant

Chapter II.2 Anti-*EFG1* 2'-*O*MethylRNA antisense oligonucleotide inhibits *Candida albicans* filamentation and attenuates the candidiasis in *Galleria mellonella*

Chapter II.3 Antisense locked nucleic acid gapmers to control *Candida albicans* filamentation

Chapter III. Creation of strategies for *C. albicans* antisense oligonucleotides cargo and delivery

Chapter III.1 Polyamide microsized particulate polyplex carriers for 2'-*O*MethylRNA *EFG1* ASO

List of Tables

Chapter III. Creation of strategies for *C. albicans* antisense oligonucleotides cargo and delivery

Chapter III.1 Polyamide microsized particulate polyplex carriers for 2'-*O*MethylRNA *EFG1* ASO

Chapter III.2 Cationic lipid-based formulations for encapsulation and delivery of anti-*EFG1* 2'OMethylRNA ASO

Annex IV

Symbols

σ_M charge density

ρ_{chg} charge ratio

P Significance value

% Percent

°C Degrees

Nomenclature

2'OMe 2'-*O*-Methyl

2'-MOE 2'-*O*-methoxyethyl

2'-F 2'-fluoro

AAROP Activated anionic ring opening polymerization

ALS Agglutinin-like sequence

ANOVA Analysis of variance

AP Amplification product

ARP Arginine-rich peptide

AS Artificial saliva

ASO Antisense oligonucleotides

AST Antisense Therapy

ATCC American type culture collection

AU Artificial urine

bHLH Basic helix-loop-helix-type

BLAST Basic local alignment search tool

bp Base pairs

cAMP Cyclic adenosine monophosphate

CAN acetonitrile

cDNA Complementary DNA

CFU Colony forming units

CGD Candida genome database

CHROMagar™ Chromogenic media agar

DCI Dicyanoimidazole

DDS Drug delivery system

DL Dilactamate

DMEM Dulbecco's modified eagle medium

DMSO Dimethyl-sulfoxide

DMT Dimethoxytrityl cation

DNA Deoxyribonucleic acid

DOPC 1,2-dioleoylsn-glycero-3-phosphatidylcholine

DOPE Di-Oleoyl-Phosphatidyl-Ethanoalamine

DOTAP 1,2-DiOleoyl-3-TrimethylAmmonium Propane

DOX Doxycycline

ds double-stranded

DSC Differential scanning calorimetry

DSPC 1,2-DiStearoyl-sn-glycero-3- PhosphoCholine

DTT Dithiothreitol

ECL ε-caprolactam

EDT1 Efg1-dependent transcript 1

EDTA Ethylenediamine tetraacetic acid

EED1 Epithelial Escape and Dissemination 1

EMA European Medicines Agency

FA Formic acid

FASP Filter-aided sample preparation

FBS Fetal Bovine Serum

FDA Food and Drug Administration

FISH Fluorescence *in situ* hybridization

FTIR-ATR Fourier-transform infra-red spectroscopy with attenuated total reflection

GBL γ-*butyrolactam*

GC Guanine-cytosine

GPI Glycosylphosphatidylinositol

GUVs Giant Unilamellar Vesicles

HE Haematoxylin-eosin

HPLC High-pressure liquid chromatography

Hwp Hyphal wall protein

ICU Intensive Care Unit

IDT Integrated DNA Technologies

ITS Internal transcribed spacer

IE-HPLC Ion-exchange High-pressure liquid chromatography

LC-MS/MS Liquid chromatography-tandem mass spectrometry

LNA Locked nucleic acids

LNPs lipid based nanoparticles

LUVs Large Unilamellar Vesicles

MALDI-TOF Matrix-assisted laser desorption ionization time-to-flight mass spectrometry

MAP Mitogen-activated protein

MLVs Multilamellar Vesicles

MOPS 3-(N-Morpholino) propanesulfonicacid

MP microparticles

mRNA Messenger RNA

MTS 3-(4,5-dimethylthiazol-2-yl)-5-(3-carboxymethoxyphenyl)-2-(4-sulfophenyl)-2H-tetrazolium

MVVs Multi Vesicular Vesicles

NAM Nucleic acid mimics

NCAC non-Candida albicans Candida

NRT Non-reverse transcriptase

NTC No-template control

OD Optical density

PA4 poly(γ-butyrolactam)

PA6 poly(ε-caprolactam)

PAS Periodic acid Schiff

PBS Phosphate Buffered Saline

PCR Polymerase chain reaction

pDMAEMA poly[(2-dimethylamino) ethyl methacrylate]

PEI Polyethylenimine

PKA Protein kinase A

PLA poly-L-arginine

PLL poly(l-lysine)

PMO Phosphoroamidate morpholino oligomer

PMSF Phenylmethylsulfonyl fluoride

PNA Peptide nucleic acid

PS Phosphorothioate

qRT-PCR Quantitative real-time PCR

RAM Regulation of Ace2p transcription factor and morphogenesis

RIM101 Regulator of IME2 protein 1

RNA Ribonucleic acid

RPMI Roswell Park Memorial Institute

Sap Secreted aspartyl proteinase

SAXS Small-angle X-ray scattering

SDA Sabouraud dextrose agar

SDB Sabouraud dextrose broth

SDS Sodium dodecyl sulfate

SEM Scanning electron microscopy

ss single-stranded

SUVs Small Unilamellar Vesicles

Tc-DNA Tricyclo-DNA

TFA Trifluoroacetic acid

TGA Thermogravimetric analysis

THF Tetrahydrofuran

Tm Melting temperature

WAXS Synchrotron wide X-ray scattering

XTT 2,3-(2-methoxy-4-nitro-5-sulfophenyl)-5-[(phenylamino)carbonyl]-2Htetrazoliumhydroxide

YPD Yeast peptone dextrose

Scientific outputs

Papers in peer reviewed journals:

1. Araújo D, Azevedo N, Barbosa A, Almeida C, Rodrigues E,Henriques M, Silva S. (2019) Application of 2'OMethylRNA antisense oligomer to control *Candida albicans EFG1* virulence determinant. *Molecular Therapy – Nucleic Acids*, Published. DOI: 10.1016/j.omtn.2019.09.016.

2. Barbosa, A.; **Araújo, D.**; Ribeiro, E.; Henriques, M.; Silva, S. (2020). *Candida albicans* adaptation on simulated human body fluids under different pH. *Microorganisms*, 8, 511

3. Araújo D, Braz J, Dencheva N, Henriques M, Denchev Z, Malfois M, Silva S. (2021) Polyamide microsized particulate polyplex carriers for 2'-*O*MethylRNA *EFG1* antisense oligonucleotide. *ACS Applied Bio Materials*. doi.org/10.1021/acsabm.1c00334

Submitted

1. Araújo D, Mil-Homens D, Henriques M, Silva, S. (2021) Anti-*EFG1* 2'-*O*MethylRNA oligomer inhibits *Candida albicans* filamentation and attenuates the candidiasis in *Galleria mellonella*. *Molecular Therapy – Nucleic Acids*, MTNA-D-21-00236

2. Araújo D, Mil-Homens D, Rodrigues ME, Henriques M, Jørgensen PT, Wengel J, Silva S. (2021) Antisense locked nucleic acid gapmers to control *Candida albicans* filamentation. *Nanomedicine – Nanotechnology, Biology and Medicine*, JN202197

3. Barbosa A, **Araújo D**, Henriques M, Silva S. (2021) The combined application of the anti-*RAS1* and anti-*RIM101* 2'-*O*MethylRNA oligomers enhances *Candida albicans* filamentation control. *Medical Mycology*, MM-2021-0038

Patent:

1. Silva, S.; **Araújo, D.**; Azevedo, N.; Azeredo, J.; Henriques, M. (2020). Antisense oligomers for controlling *Candida albicans* infections. WO 2020/174366 A1

Posters in conference:

1. **Araújo, D.**; Azevedo, N.; Henriques, M.; Silva, S., Antisense oligomers based approaches for controlling *Candida albicans* filamentation, *14*th *ASM Conference on Candida and Candidiasis*, Providence, Rhode Island, USA, 15-19 April, 2018.

2. Barbosa A, **Araújo D**, Henriques M, Silva S. Anti-*EFG1* oligomer able to control *Candida albicans* filamentation in human body fluids. *4*th *Meeting of Medicinal Biotechnology*, Porto, Portugal, 17 May, 2019.

3. **Araújo, D.**; Azevedo, N., Barbosa, A., Almeida, C., Rodrigues, M.E., Henriques, M.; Silva, S., 2'OMethylRNA *EFG1* antisense oligomer to control *Candida albicans* filamentation, *15*th *Annual Meeting of the Oligonucleotide Therapeutics Society*, Munich, Germany, 13-16 October, 2019.

4. **Araújo D**, Jørgensen PT, Wengel J, Mil-Homens D, Fialho AM, Henriques M, Silva S. Exploration of anti-*EFG1* derivatives of locked nucleic acid gapmers to control *Candida albicans* filamentation. *Candida and Candidiasis 2021*, Digital event, 21-27 March, 2021

Oral communications:

1. **Araújo D,** Azevedo N, Barbosa A, Almeida C, Rodrigues E, Henriques M, Silva S. Anti-*EFG1* 2'*O*me oligomer is able to control *Candida albicans* filamentation. 17 September, 2020. *CBEDS – Chemical and Biological Engineering Doctoral Symposium*, Centre of Biological Engineering, Braga, Portugal

2. **Araújo D**. Aplicação de Oligómeros de Antisense para prevenir infeções por *Candida albicans*. 14 January, 2021. *Café com Engenharia*, Braga, Portugal

Objectives and structure of the thesis

Nosocomial infections are currently a major health problem, which include life-threatening mycoses. These infections are mainly caused by the genus *Candida*, particularly *Candida albicans* that remains the most prevalent of all *Candida* species. Candidiasis is supported by a series of virulence factors, and one of the most important is the ability of *C. albicans* cells to switch from yeast to filamentous forms. The filamentation phenomenon is essential for *C. albicans* pathogenicity and it is regulated by a complex network of genes in which *EFG1* is one of the most important virulence determinants.

In addition to the rise of multidrug resistance, the scarcity of new classes of fungal drugs, has led to the stagnation in antifungal discovery. This evidence highlights the need for new strategies to manage candidiasis which allow a fast-accurate and effective control of *C. albicans* virulence. A prospective candidate for rapidly designing antifungal agents is antisense oligonucleotides (ASOs), which are nucleic mimics (NAMs) that base pair with target mRNA to obstruct translation. Antisense technology (AST) holds great promise as a therapeutic agent for the treatment of human chronic non-infectious diseases and more recently to target bacteria resistance, however it is poorly explored for the control of *Candida* infections.

Therefore, the main goal of this PhD thesis was to promote the development of a novel therapeutic approach based on AST to track *C. albicans* filamentation employing established and emerging generations of ASOs. To reach such aim, two complementary objectives were addressed: I) Exploitation and application of ASOs to control the *EFG1* gene and consequently *C. albicans* filamentation; II) Creation of strategies for *C. albicans* ASOs cargo and delivery.

This thesis is organized into four main chapters, which address the hypothesis of the use of ASOs to control *C. albicans* filamentation. So, **Chapter I** – "Literature review" is a brief review of the current knowledge about the epidemiology of *C. albicans* infections, biology, and virulence factors. The principals of concepts about AST, including ASOs chemical modifications, mechanism of action, cargo and delivery strategies, pharmacokinetic properties, and toxicology were also addressed. The other chapters present the different parts of the experimental work performed.

The **Chapter II** – "Exploitation of the antisense oligonucleotides to control *Candida albicans* filamentation" is focused on exploration of the 2'-*O*Methyl (second generation of ASOs) and Locked nucleic acid (third generation of ASOs) chemical modification to control *EFG1* gene and *C. albicans* filamentation. The Chapter II is sub-divided into three complementary sub-chapters. In **Chapter II.1** – "Application of 2-OMethylRNA antisense oligonucleotide to control *Candida albicans EFG1* virulence determinant" is

described the effect of anti-*EFG1* 2'OMe ASO on *EFG1* gene expression, on Efg1p protein translation and on *C. albicans* cell filamentation in simulated human body fluids. To complement the *in vitro* results presented in Chapter II.1, into **Chapter II.2** – "Anti-*EFG1* 2'-*O*MethylRNA antisense oligonucleotide inhibits *Candida albicans* filamentation and attenuates candidiasis in *Galleria mellonella*", the anti-*EFG1* 2'OMe ASO performance was validated *in vivo* using the *Galleria mellonella* model. The **Chapter II.3** – "Antisense locked nucleic acid gapmers to control *Candida albicans* filamentation" describes the application of a set of Locked nucleic acid gapmers to control *in vitro EFG1* gene expression, and *C. albicans* filamentation and the *in vivo* performance on the *G. mellonella* survival.

Afterwards, **Chapter III** – "Creation of strategies for *C. albicans* antisense oligonucleotides cargo and delivery" is focused on the development of different vectors for anti-*EFG1* 2'OMe ASO cargo and delivery. The Chapter III is sub-divided into two complementary sub-chapters. **Chapter III.1** – "Polyamide microsized particulate polyplex carriers for 2'-*O*MethylRNA *EFG1* ASO" describes the application of anionic and cationic polyplexes based on poly(γ-butyrolactam) (PA4) or poly(ε-caprolactam) (PA6) respectively as a valid strategy to anti-*EFG1* 2'OMethyl ASO cargo. In **Chapter III.2** – "Cationic lipid-based formulations for encapsulation and delivery of anti-*EFG1* 2'-*O*Methyl antisense oligonucleotide" is described the application of cationic lipid-based formulations for encapsulation and delivery of anti-*EFG1* 2'OMethyl ASO.

Finally, **Chapter IV** - "General conclusions and work perspectives" comprehends the major conclusions, obtained in this work, concerning the application of ASOs to control *EFG1* gene expression and *C. albicans* filamentation and proposes suggestions for future research that can contribute for enhanced knowledge about applicability of AST to control *Candida* infections.

Chapter I

Literature review

I.1 *Candida* and Candidiasis

The members of the genus *Candida* are the most frequently recovered from fungal infections and there is an extremely heterogeneous group of over 200 species. However, it is well established that only 20 have been associated with human infectious disease [1,2]. These *Candida* infections are collectively referred to as candidiasis and may either be superficial, affecting the skin or mucosal membranes, or systemic, which involves the major body organs. The increase of candidiasis has been associated to many factors, in which the increase of immunocompromised patients and the use of broad-spectrum antibiotics are the most reported. In this sense, fungal infections have emerged as an important public health challenge with high economic and medical relevance due to the increased costs of care, time of hospitalization and high levels of mortality, with rates of about 30-50 % in the last years [3,4]. *Candida* species normally exist as commensals; therefore, this status depends on the host microbiome as a whole and the immune condition of the host. Obviously, if some perturbation of mucosal microbiota or weakening of host immunity happens, *Candida* species switch from commensal to pathogen microorganism, increasing its ability to cause superficial and systemic infections [5]. Most of candidiasis cases are attributed to *Candida albicans*, however, in the recent decades, the improved diagnostic methods and the multi-drug resistance to certain antifungals have led to the emergence of non-*Candida albicans Candida* (NCAC) species, particularly *Candida glabrata*, *Candida parapsilosis*, *Candida tropicalis*, *Candida Krusei* and more recently *Candida auris* [6–8].

I.1.1 Epidemiology and risk factors of candidiasis

Fungal infections have become increasingly important as a public health problem since invasive candidiasis is a severe infection associated with high morbidity and mortality rates [3,4,9–11]. Normally, the most common presentation of invasive candidiasis is the development of a candidemia [11]. In fact, *Candida* species are in the first three pathogens causing health-care associated bloodstream infections, and approximately 50 % of candidemia episodes occurs in the Intensive Care Unit (ICU) [4]. There are many risk factors associated with candidiasis, however the most common include exposure to broad-spectrum antibacterial agents, long-term ICU stay, a recent major surgery and the presence of an indwelling central venous catheter [7,9,12]. In fact, catheters could be a problem in ICU that required an important attention since candidemia associated with intravenous lines can act as substrates for biofilm production [3,10,13].

Candida species can also colonize several human body sites as skin, oropharynx, lower respiratory tract, and gastrointestinal and genitourinary tract [1,13]. It is important to refer that Candida species are commensal yeasts and there are part of the normal human skin and gut microbiota, so normally they are found in up to 60 % of healthy individuals [13,14].

Candida albicans remains the predominant species recovered from infections counting with 70-90 % cases among all candidiasis-causing fungi [13]. In a report of Montagna et al. [15] in 2014, C. albicans represented 50-70 % of all Candida infections in European countries. In the last decades, it has been confirmed that in 95 % of the Candida infection's cases, the most common species involved are C. albicans, C. glabrata, C. tropicalis, C. parapsilosis and Candida krusei [1,13]. However, the distribution of C. albicans varies from region to region and depend upon the study and the time of surveillance. In addition, other reasons can explain the differences from region to region, such as, differences in medical practices, a reduced number of health care workers and difficulties in the implementation of infection control programs in hospitals and the excessive use of antifungal agents. Indeed, Koehler et al. [4] reported recently that the incidence rate (IR) for candidemia has been higher in Southern Europe than in Northern or Western Europe (Table I.1). In that work the differences in the regions are explained by factors as climatic differences, the methods used for antibiotic prescription and demographic development [4]. However, the local health care systems have significant impact in candidemia incidence. In terms of a pooled crude mortality rate (MR) was about of 40 % in population-based studies [16,17], and in the case of ICU-only studies, the report of crude MR was approximately 49 %. In the population-based studies reported in Koehler et al. [4], C. albicans remained the most prevalent species involved in candidemia, even though cases with non-Candida species were increasing.

Table I.1 Incidence and mortality rate of population-based studies and hospital based-studies in European countries for candidemia based on the report by Koehler et al. [4]

European Countries	Population-based studies (per 100.000 inhabitants)	Hospital-based studies (per 100.000 inhabitants)	Mortality rate (%)
Southern	5.29	1.13	37
Northern	3.77	0.31	35
Western	2.5	0.47	37

I.1.2 *Candida albicans*

a. Biology of *Candida albicans*

Candida albicans is a diploid polymorphic yeast that is part of the human microflora and is found in the human gastrointestinal (GI), respiratory and genitourinary tracts [7,18]. Normally, *C. albicans* is present as blastoconidia, which is a harmless commensal fungus, however, in immunocompromised patients, this fungal species can become into an opportunistic pathogen causing superficial, as well as systemic infections [7,19–21].

Candida albicans cells present a range of size between 4-6 μm in the blastoconidia form, reaching higher sizes when grow to a filamentous form [22]. Polymorphism ability of *C. albicans* corresponds to a reversible morphologic transition between yeast and filamentous forms, which can be a pseudohyphae or true hyphae (Figure I.1 A) [2,7,23,24]. In addition to microscopic differences, it is possible to distinguish from other *Candida* species by colony colour on through CHROMagar™ *Candida*, based on a set of reactions of species-specific enzymes with a proprietary chromogenic substrate [25]. In the case of *C. albicans*, the colonies produce a light green colour (Figure I.1 B) [25].
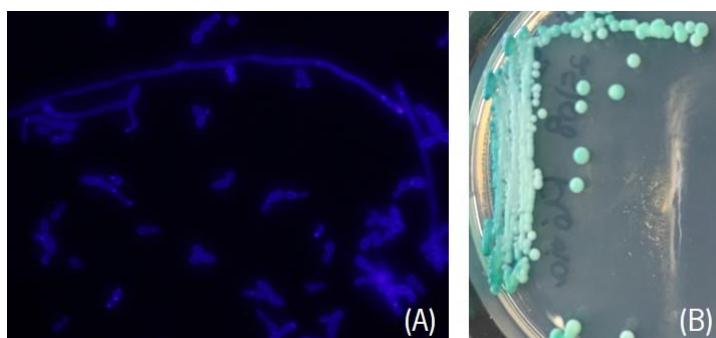
Figure I.1 (A) *Candida albicans* cells stained with calcofluor obtained by microscopic epifluorescence and **(B)** macroscopic colonies on CHROMagar™ of *Candida albicans*.

b. *Candida albicans* virulence factors

As mentioned before, *C. albicans* can become pathogenic invading host tissues and leading to superficial and systemic infections. The pathogenicity of *C. albicans* is supported by several virulence factors, including hydrolytic enzyme secretion, the ability to adhere to medical devices and/or on host cells and to form biofilms, and the morphological transition from yeast to hyphal forms.

Hydrolytic enzymes production

Candida albicans cells have the ability to produce and secrete some enzymes that facilitate penetration into the host cells. These enzymes are involved in adhesion, cell damage and tissue invasion and there are three different classes of secreted hydrolases expressed by *C. albicans*: proteinases, phospholipases and lipases.

The secreted aspartic proteinases (*SAP* genes) are involved in the invasion and colonization of host tissues, promoting the disruption of host mucosal membranes and degradation of defence proteins [6,26,27]. The family of *SAP* genes consists a group of 10 members (*SAP1* to *SAP10*), which eight of them (*SAP1* to *SAP8*) are secreted into the extracellular space and *SAP9* and *SAP10* are part of membrane-anchored GPI proteins [6,28]. According to the some studies, the regulation of *SAP* genes is depending on the transition from yeast to hyphal form, changes in growth environment, and expression of alternative switch phenotypes [28–30]. In the case of *SAP1* and *SAP3*, they are involved in the regulation of phenotypic switching, being expressed in the 'opaque', but it is not expressed during 'white' form [28,31]. The genes *SAP4-SAP6* are mostly expressed during the development of hyphal forms at neutral pH [28,32,33]. In contrast, it has been described that *SAP9* and *SAP10* are expressed in all growth conditions, so these genes are not regulated by environmental conditions [28,34,35]. Phospholipases (PL) are responsible for the hydrolyse one or more ester linkages in glycerophospholipids, leading to the host cell membrane damage and adhesion of yeasts to host tissues [36]. The ability of *C. albicans* to produce these extracellular phospholipases is significantly higher [36] and these enzymes have been differentiated according to its mode of action and the target within the phospholipid molecule. There are four subclasses of PL genes identified in *C. albicans*, which are classified as A, B, C and D [28]. In *C. albicans*, seven phospholipases were reported to be involved in the pathogenesis, namely, *PLA*, *PLB1-2*, *PLC1-3* and *PLD1* [37]. The secreted hydrolytic lipases are involved in the hydrolysis of ester bonds of monodi- and triacylglycerols. So far, 10 genes have been identified in *C. albicans* called as *LIP1-10* and the first extracellular lipase identified was *LIP1*. In contrast to other enzymes, these enzymes are less studied. It was known that deletion of *LIP8* in *C. albicans* produced significant effects on its virulence [38].

Adhesion

Adherence of *C. albicans* to mucosal surfaces and/or synthetic materials is the early step leading to proliferation and consequently biofilm formation and infection (Figure I.2) [27]. The adhesion

mechanism is based on interaction between the *C. albicans* cell wall and the host cells' surface and is ruled by environmental conditions [39]. The adhesion process can be modulated by microbial adhesins or host cell receptors, or by physical and chemical manipulations [40]. Figure I.2 presents the gene cascades that are involved in *Candida* adhesion and biofilm formation. One of those genes is *BCR1*, a C_2H_2 zinc finger protein essential for biofilm formation in *C. albicans* and which is essential for the expression of several cell wall proteins in *C. albicans* [41], namely Als1, Als3 and Hwp1 [42,43]. Nobile et *al.* [41] described that the expression of *ALS3* and *HWP1* is reduced in a Δ*bcr1/bcr1* strain [41,44]. The CFEM (common in fungal extracellular membranes) family of proteins are targets of *BCR1* and can act as cell surface receptors or as adhesins [45]. However, the CFEM family, namely *RBT5*, *PGA10* and *CSA1* has just been described in *C. albicans* as having a role in biofilm development [46,47]. The presence of specific cell-wall proteins, designated normally as adhesins, is a trigger in the modulation of the adhesion process [6]. In *C. albicans*, the adhesion is mediated by the family of agglutinin-like sequence (Als) proteins, which comprises eight members, Als1-7 and 9, with a similar structure containing an N- terminal secretory signal sequence [48,49]. In the literature, it is reported that *ALS1* and *ALS3* are involved in biofilm surface attachment, however their expression is depending on *C. albicans* cell morphology (Figure I.2) [50]. *ALS1* expression is detectable in both growth forms, yeast, and hyphal cell [51], in contrast to *ALS3* which is only expressed in the hyphal lifestyle [52]. The hyphal forms of *C. albicans* that are deficient to *ALS3* exhibit defective adhesion to endothelial cells [49,53].
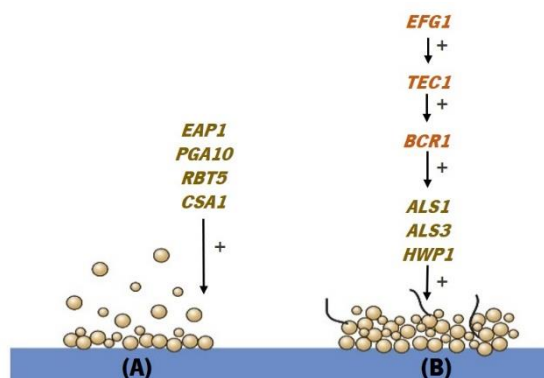
Figure I.2 Regulatory genes involved in **(A)** initial adhesion process and **(B)** in the basal layers of biofilm formation.

Eap1 is a glycosylphosphatidylinositol-dependent (GPI-linked) cell wall protein, which is also involved in the cell-cell adhesion in *C. albicans* and it is expressed in both yeast and hyphal cells (Figure I.2) [54]. This protein mediates surface binding, affecting cell adhesion and biofilm formation *in vitro* and *in vivo* and its expression is regulated by the transcription factor *EFG1* [51]. The *EAP1* mutants showed

reduced adhesion to plastic surfaces and epithelial cells and it was demonstrated that are involved in the control of adhesion to yeast cells [51,54]. Hyphal wall protein I (*HWP1*) is a fungal cell wall mannoprotein that promotes attachment of *Candida* cells to the host surface (Figure I.2) [43]. In the literature, this gene is described as involved in the formation of germ-tubes and the hyphal forms of *C. albicans*, promoting physical contact between epithelial cells and the fungi, concluding that *HWP1* is an important effector of *C. albicans* pathogenicity [24,55,56].

Biofilm formation

Biofilms are communities of microorganisms properly organized and embedded in an extracellular matrix [57]. *Candida albicans* isolates are good biofilms formers, and their presence during infection has been related to higher morbidity and mortality rates compared to isolates incapable of forming biofilms [58]. It is important to address that biofilms have variability in their structure and matrix composition differing between species and strains [59]. The biofilm structure of *C. albicans* normally consists of two layers, a basal deposit of blastospores covered by a thick matrix film with hyphal forms (Figure I.3). The matrix of *C. albicans* biofilm is composed mainly by carbohydrates, proteins, phosphorus and hexosamines [23,60,61].
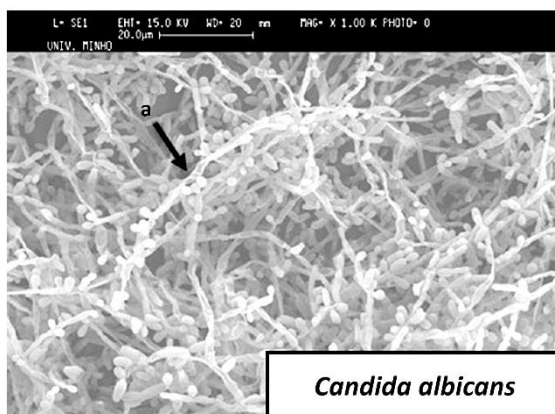
Figure I.3 *Candida albicans* biofilm structure. **(a)** Filamentous forms (hyphae and/or pseudohyphae). Images obtained with scanning electron microscopy after 24 h of biofilm growth.

Biofilm formation is a sequential phenomenon, which involves attachment, maturation and detachment [62]. Attachment and colonisation of yeast cells to an abiotic or/and biotic surface is the first step of biofilm development, as described in the previous section (Figure I.2 A). Initial attachment of *C. albicans* cells is followed by cells division, leading to the formation of a basal layer of anchoring microcolonies [62,63] (Figure I.2 B), and then subsequent biofilm maturation (Figure I.4 A). The biofilm

maturation is, generally, characterized by the presence of filamentous forms, pseudohyphae and/or hyphae, and by the production of extracellular matrix [63,64]. The matrix role is to protect *Candida* cells from phagocytic cells and to act as a barrier to drugs and toxic substances [65,66]. Moreover, this matrix allows the maintenance of nutrients within reach of biofilm cells [65,66]. Finally, mature biofilms have the ability to initiate detachment and dispersion (Figure I.4 B) on their own and this cells release from the original biofilm community is a step forward in generating novel communities at new locations [67].
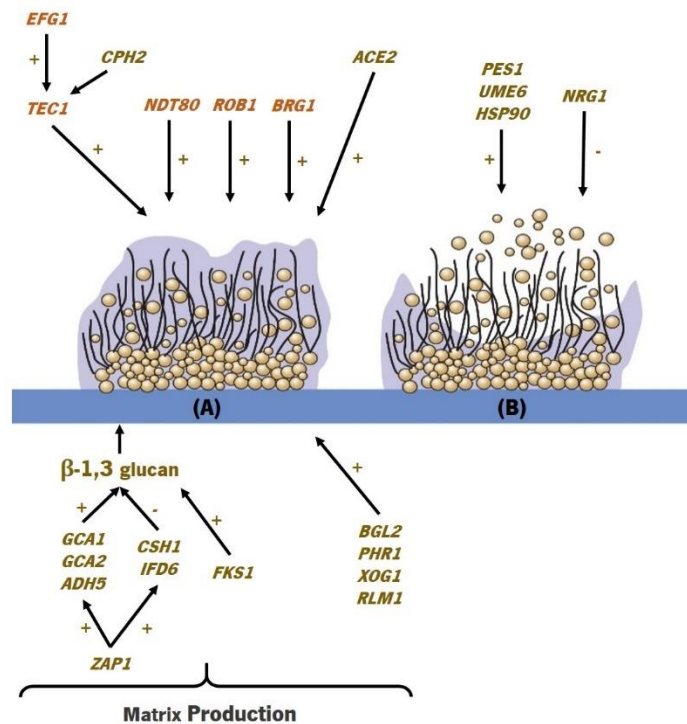
Figure I.4 Final stages of *Candida albicans* biofilm formation and its corresponding networks genes. **(A)** Mature biofilm constituted by cells with diverse morphologies and extracellular matrix; **(B)** Biofilm detachment and dispersion.

The biofilm formation in *C. albicans* is regulated by several transcription factors that play a fundamental role in various pathways and they have an important potential in the regulation of other genes involved in biofilm formation [24,41]. Nobile et *al.* [62] investigated the transcriptional network and identified a set of six transcription factors in *C. albicans* that play an important role in the regulation of biofilm formation, namely *BCR1*, *EFG1, TEC1, NDT80, ROB1* and *BRG1* (Figure I.2 and I.4) [62]. Furthermore, *C. albicans* biofilms are defective when any of these regulators are deleted [62]. *EFG1* is one transcription factor required for biofilm formation that regulates the cell surface and hyphal formation [68]. Holland et *al.* [69] demonstrated a reduction in *C. albicans* biofilm when *EFG1* is eliminated. Moreover, Δ*efg1/efg1* strains were unable to form hyphae in *C. albicans*, even grown under hypha-

inducing conditions [70]. *TEC1* is a gene required for hyphal formation and virulence in *C. albicans* [42] and is a member of TEA/ATTS transcription factor family [71].

The production of extracellular matrix is another important feature in biofilm maturation [63]. One of the carbohydrates present in *C. albicans* matrix is β-1,3 glucan [72]. However, recent study by Zarnowski et *al.* [73] demonstrated that β-1,6 glucan is also an important matrix component, that it is highly dependent on the environmental conditions used. The gene responsible for glucan synthase is *FKS1* (Figure I.4), more commonly designated by *GSC1*, and it has been implicated in *C. albicans* biofilm resistance to fluconazole [72]. The susceptibility to fluconazole is the result of *FKS1* disruption which reduces the deposition of β-1,3 glucan in the biofilm matrix [74]. Furthermore, the increase in *FKS1* transcript is due to the reduction of the delivery of glucan to matrix [75]. In *C. albicans*, *RLM1* and *ZAP1* are consider two other biofilm regulators involved in matrix production in biofilms (Figure I.4). The transcription factor *ZAP1* is predominantly a negative regulator of biofilm matrix production, Δ*zap1/zap1* produces a biofilm with high levels of β-1,3 glucan both *in vitro* as *in vivo* [76]. Some targets genes of *ZAP1* are *CSH1, IFD6, GCA1, GCA2* and *ADH5*, which modulate levels of β-1,3 glucan in the biofilm matrix (Figure I.4) [76]. In the case of *CSH1* and *IFD6*, when *ZAP1* activates the expression of these genes, the production of β-1,3 glucan decreases and therefore these genes are considered as negative regulators of matrix production [76]. However, *GCA1, GCA2* and *ADH5* are positive regulators, since there is an increase of β-1,3 glucan when these genes are activated by the *ZAP1* gene [76]. Another regulator of matrix production is *RLM1*, a positive regulator, which deletion promoted a reduction in its matrix levels [77]. Taff et *al.* [75] described a role for *BGL2, PHR1* and *XOG1* (Figure I.4) as glucan modifying genes involved in glucan delivery and matrix incorporation. The *BGL2* and *PHR1* genes encode glucanosyltransferases and *XOG1* is a β-1,3 exoglucanase [78–80].

The last step of biofilm formation is characterized by the dispersion of yeast cells and/or pieces of the biofilm from its mature form which allows the organism to colonize new sites for further adherence and colonization [62], completing the biofilm life-cycle (Figure I.4). Biofilm dispersion occurs in response to environmental changes, such as a decrease or lack of nutrients or other modifications in the growth media composition [81]. Furthermore, the dispersion of biofilm cells can lead to a development of infections in deep organs due to the ability to invade the blood stream [81]. In the past decade, early events associated with *Candida* biofilm formation have received considerable attention. Recent studies in *C. albicans* biofilms have reported that the majority of dispersed cells are yeast cells and *PES1, UME6* and *NRG1* are three main regulators genes in this step (Figure I.4) [63]. Uppuluri et *al.* [81] demonstrated that the major yeast cells dispersed from biofilm were released from the upper hyphal layers.

Furthermore, overexpression of *PES1* results in an increase of yeast growth when cells were grown on medium without doxycycline (DOX) [82]. On other hand, when *NRG1* was overexpressed, in the absence of DOX, the biofilm contained only a monolayer of yeast and pseudohyphae cells [83], since the *NRG1* is a negative regulator of filamentation [84,85].

Dimorphic ability

One of the major causes of *C. albicans* pathogenicity is the ability to switch from yeast to a filamentous form (Figure I.5), increasing its capability to invade epithelial cells, causing tissue damage, as well as allowing to escape the host's immune system [19,86]. There are three major points in that filamentation is required for the success of *C. albicans* as pathogen and to cause candidiasis. First, filament is stimulated in circumstances that mimic the host environment, such as at 37 °C [87], contact with serum and neutral or even alkaline pH [88]. Secondly, filament form is more invasive to human tissues than yeast cells [89]. Third, filament formation provides a mechanism for evasion of host's defence mechanism once yeast cells taken up by macrophages produce filaments which can lyse them [90]. *Ex vivo* studies demonstrated the high capability of *C. albicans* to colonize and invade vaginal and oral epithelia with an enhanced invasiveness along time [6,91]. An *in vitro* research has shown that *C. albicans* in the yeast form presented lower ability to invade epithelium, confirming the fact that hyphae plays an important role in tissue invasion [89,92]. The possible reason for this phenomenon is related with the fact that the cell wall of filamentous form has more chitin than the yeast form, which increases its resistance to phagocytosis and enhances epithelium colonisation and invasion into tissues [93].
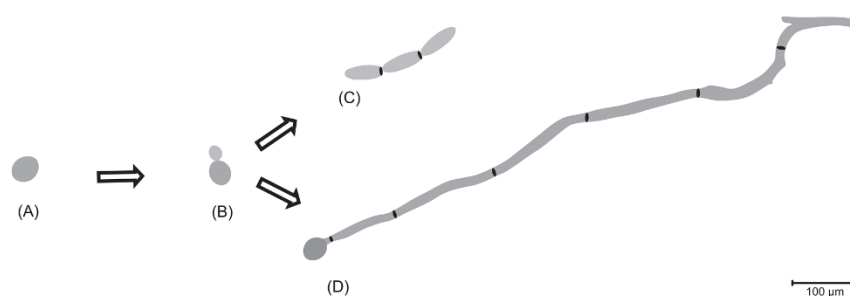
Figure I.5 Photomicrograph of the different morphological growth forms of *Candida albicans*: **(A)** yeast form (blastoconidia); **(B)** reproduction by budding; **(C)** pseudohyphae and **(D)** hyphae formation.

Important scientific advances have been facilitated to generate a set of data on genomic, transcriptomic, and proteomic, that is essential to discover the molecular biology undergo switching between yeast and filamentous growth, identifying important networks of genes and the pathways involved in *C. albicans* dimorphism. There are many genes identified and characterized as involved positively in

C. albicans filamentation, which are included into distinct pathways. The cyclic adenosine monophosphate (cAMP)/protein kinase A (PKA) pathway and mitogen-activated protein (MAP) kinase cascade have in common the fact to be up-regulated by *RAS1* gene, a member of a highly conserved family of GTPase binding proteins [94]. Regulation of Ace2p transcription factor and polarized morphogenesis (RAM) network is a signalling pathway that regulates polarized morphogenesis in yeasts. Specifically, RAM pathway directly regulates two distinct cellular processes, the maintenance of cell polarity during the filamentation and daughter cell–specific nuclear localization of Ace2p [95]. Additionally, genes induced by pH through the regulator of IME2 protein 1 (*RIM101*) transcription factor governs *C. albicans* cellular morphology taking account the environment pH [96,97]. It is well known that acidic pH inhibit the transition between yeast and hyphae, while neutral and alkaline pH promote the growth as filamentous form [87,97]. The responses to pH are thought to be dependent on changes in *RIM101* expression, which plays a major role in pH-dependent genes regulation in *C. albicans* [98,99].

Additionally, *EFG1* which is a transcription factor involved in biofilm formation, is also a major transcriptional regulator of filamentous growth (Figure I.6). This gene is a member of the APSES proteins containing a novel conserved DNA-binding domain related to a basic helix-loop-helix-type (bHLH) domain [68]. Although, depending on environmental cues, the *EFG1* have a double role in filamentation acting as a repressor or as an activator. Under normoxia conditions, *EFG1* reveals to be a strong inducer of hyphal growth [90,100], while under hypoxic conditions, *EFG1* acts as a repressor of the hyphal growth on agar at temperature below 35 °C [101,102]. Under hypha-inducing conditions, the deletion of *EFG1* provokes a defect in filamentation, while, under microaerophilic or embedded conditions, the hyphal growth occurs normally.
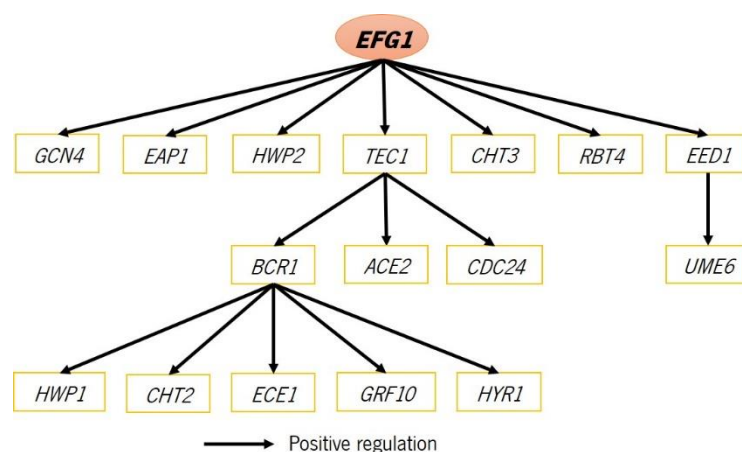
Figure 1.6 Illustrative scheme of the genes involved in *EFG1* network and cross-link among them.

The expression of *TEC1, HWP2, EAP1, CHT3, EED1* and *RBT4* are up-regulated by *EFG1* and there are all involved in the morphogenesis process (Figure I.6). It is well known that *TEC1*, which is a transcription factor involved in the biofilm formation, is able to regulate directly the expression levels of *BCR1, ACE2* and *CDC24* genes (Figure I.6) [41,60,103]. Moreover, it is known that the expression of *TEC1* is directly regulated by *CPH2*, which is another gene involved in the induction of hypha-specific genes [104]. According to the literature, *BCR1* is involved in the regulation of *HYR1, HWP1, CHT2, GRF10* and *ECE1* genes, and it is known that in *bcr1* and *tec1* mutants, the expression of these genes were considerably committed when compared to the wild-type reference strain [42]. *HWP1* and *HYR1* are two genes that are associated directly with hyphal development. In the case of *HWP1*, encodes a mammalian transglutaminase substrate protein that is only found on germ tubes and on the cell surface of *C. albicans* true hyphae [105,106] and in the case of *HYR1*, it is induced specifically during hyphal development. The other three genes, *CHT2, GRF10* and *ECE1*, directly regulated by *BCR1* and indirectly regulated by *EFG1* have different roles in the hyphal formation. *CHT2* gene is responsible for the remodulation of chitin in the *C. albicans* cell wall and some works demonstrated that levels of expression are higher in the *C. albicans* hyphal form than in the yeast form [107,108]. The deletion of homeobox transcription factor-encoding, identified as *GRF10* gene, resulted in defects in filamentous growth *in C.* albicans in opposite to its overexpression that triggers the formation of hyphae forms on solid and liquid media [109,110]. The extent of cell elongation 1, *ECE1*, is also considered as a hyphae-specific gene, which means that when the expression levels of *ECE1* are increased, the elongation of the cells is increased too [111]. However, it is not essential for hyphal formation, since the null mutant presents a normal morphology [111].

HWP2, another hyphal cell wall protein likely *HWP1,* it was also detected in *C. albicans* filaments but only when the transcriptional activator *EFG1* is present (Figure I.6) [112]. In fact, Sohn *et al.* [105] demonstrated that in the *efg1* mutant, the *HWP1* and *HWP2* were downregulated under the hyphae-inducing conditions (YPD with serum at 37 °C).

The *C. albicans EED1*, unique to this species, is a specific gene essential for hyphal extension on solid surfaces and during interactions with host cells (Figure I.6) [113–115]. It is called Epithelial Escape and Dissemination 1 once the deletion of this gene failed to maintain hyphal growth [114,115]. This gene was originally named *EDT1*, more exactly, Efg1-dependent transcript 1, since *EED1* expression depends on Efg1 [116]. In the same study, it was demonstrated that the second step of the hyphal extension cycle is dependent of *EED1* and *UME6* expression levels [114]. The *eed1* and *ume6* mutants have similar phenotypes, presenting defects in hyphal extension, so it can be concluded that both genes perform a

major role in filamentation [114,117,118]. In the *eed1* mutant cells, it was observed that the overexpression of *UME6* re-established filamentation and the expression of hyphal-associated genes like *ECE1, HWP1* and *HYR1* [114]. Thus, *EED1* and *UME6* act together in order to keep the hyphal growth of *C. albicans* cells and avoid transition of hypha-to-yeast [114]. The *EAP1,* a GPI-anchored cell wall adhesin, is described as important for adhesion of *C. albicans* cells and as having a role in filamentation growth [51,54]. The expression of this gene is directly affected by the *EFG1* transcription factor and therefore activate by the cAMP-PKA pathway [51,54].

c. *Candida albicans* antifungal resistance

There are major classes of antifungal drugs commonly used to treat *C. albicans* infections, namely azoles, polyenes and echinocandins [119–123]. However, the intensification of antifungal resistance has been increased due to the strong virulence factors involved in *C. albicans* infections and commonly causing therapeutic clinical failure. The biofilm structure of *C. albicans* has been identified as the main responsible for the increased of the resistance to antifungal agents [123,124]. The antifungal resistance is a complex multifactorial phenomenon, and traditionally the impact of known mechanisms such as to prevent a drug from entering the cell, promote drug extrusion, inactivate the drug or prevent it from inhibiting its target, plays the main role in drug resistance [125]. There are some mechanisms of resistance related with *C. albicans* biofilm, including the high density of cells presented in biofilm structure, the limitation in terms of nutrients, the formation of biofilm matrix, the presence of persister cells, and the increase of sterols on the cells presented in the biofilm (Figure I.7) [123].
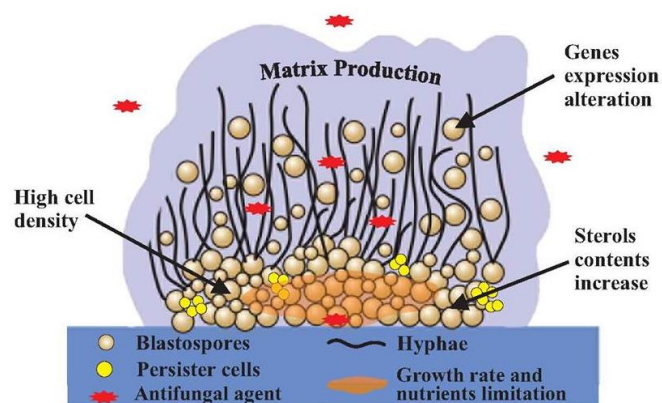
Figure I.7 Mechanisms related with *C. albicans* biofilm resistance. Adapted from [123].

Taking in account, the *C. albicans* pathogenicity and the increasing emergence of antifungal resistance, new alternative therapeutic therapies with novel mechanisms of action, enhanced therapeutic potential, improved pharmacokinetics, and less toxicity are urgently needed to reach into marketplace to control *C. albicans* infections.

I.2 Antisense Therapy

Over the last 25 years there was a great development on the therapies based on proteins and small molecules, by the pharmaceutical and biotechnology industries. It is well known that protein is derived from specific mRNAs, which can be used as therapeutic targets by modulating mRNA or pre-mRNA. Until now, there are different therapeutic strategies to modulate mRNA function in cells, including, gene therapy, small molecules targeting RNA, genome editing, delivery of exogenously expressed mRNAs and synthetic antisense oligonucleotides (ASOs).

The antisense therapy (AST) is relatively straightforward: the use of an ASO, which is a complementary sequence to a specific mRNA that can inhibit expression of the latter and induce a 'blockage' in the transfer of genetic information from DNA to protein [126]. This hybridization results in reduced levels of translation of the target transcript and depends on the chemical of the ASO and the location of hybridization [127].

The ASO is a short strand of nucleic acids with a mean length of 12 to 25 nucleotides, which is complementary to the target mRNA, and bind to the target by means of standard Watson-Crick base pairing [126,128]. ASOs are easy to produce, can be extensively modulated and they have a good cell penetration, enabling them as an excellent strategy to be used in gene therapy [129].

I.2.1 ASOs chemical modifications

The unmodified oligonucleotides are found in nature [130], however its clinical use was limited since they were easily degraded by intracellular endonucleases and exonucleases due to weak binding affinities [126,131]. The unmodified ASOs are often destroyed before binding their target receptor and have been reported to have half-life on the order of minutes, in which there are rapidly filtered and excreted because of the small size that it is enough to be filtered by the glomerulus and poorly protein-bound in plasma. Lastly, the affinity is compromised, because the antisense drug must be able to compete with the structure of mRNA within a cell. It is important to emphasize that the massive dose requirements and limited clinical efficiency commits the use of these unmodified oligonucleotides [132]. To overcome these problems, ASOs have been chemically modified and there are available with a range of different

modifications, which are classified into three generations (Figure I.8), in order to increase nuclease resistance, reduce toxicity, increase affinity and potency and extend tissue half-life [126,131,133].
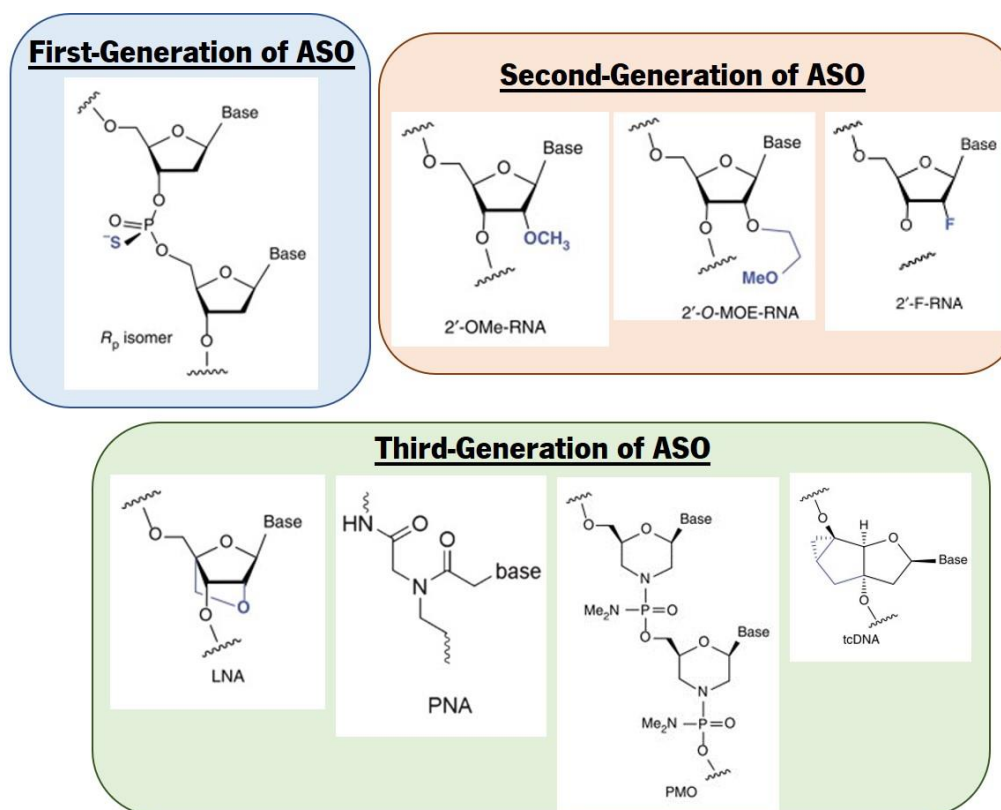
Figure I.8 Chemical structure of the chemical modification generations of antisense oligonucleotides.

a. First-generation of ASOs

In first-generation ASOs, the nonbridging phosphate oxygen is replaced by sulfur group, which generates phosphorothioate (PS) modification (Figure I.8) [130,134]. The first PS DNA oligonucleotides synthesized was in 1960, by Eckstein et *al.* [135]. The ASO modified with PS modifications prolongs the half-life from minutes to days compared to unmodified ASO, since the resistance against nuclease degradation is improved, and consequently the stability in plasma, tissue and cells is enhanced, preventing the metabolism prior to reaching the target RNA [136,137]. An important factor is the ability to recruit the enzyme RNaseH which is an enzyme that promotes the degradation of RNA strand in a DNA-RNA duplex [130]. However, this first generation does not protect completely ASOs from nucleases [132] and the melting temperature of heteroduplex decreases which compromise the affinity of the ASO for its mRNA, affecting ASO potency [127]. Furthermore, it was demonstrated that the *in vivo* efficacy of ASOs is dependent on the administration of high doses [132].

b. Second-generation of ASOs

The alkyl modifications are characterized by modifying the 2' position of the ribose sugar, which belongs to the second-generation of ASOs. These chemical modifications were developed to enhance nuclease resistance and increase binding affinity for target mRNA [126] and also reduces immune stimulation [138]. The second generation is formed by 2'-*O*-Methyl (2'-OMe) and 2'-*O*-Methoxyethyl (2'-MOE), characterized by the introduction of an oxygenated group (Figure I.8) [139]. This generation is less toxic than PS, described in first generation, and increases the nuclease resistance. Moreover, there is a jump in hybridization affinity [140–142]. For ASO with 2'-OMe-PS, the toxicity presented was very mild, which in fact has been shown to not interfere, after delivery in rodent brain, with their desired effects [143,144]. The ASO sequence can be modified also with 2'-fluoro (2'-F) modification, which increase the ASO affinity. In terms of mechanism of action, the second generation does not allow the recruitment of RNase H [139]. To overcome this limitation, the RNase H activity can be restored through the insertion of a central unmodified or PS-DNA sequence, called as gapmer, which consist of regions of 2'-modified residues that flank a central DNA region of the oligonucleotide. These "wings" increase affinity and nuclease resistance, and additionally allows RNase H to join in the central gap and activate the degradation of target mRNA [126,130].

c. Third-generation of ASOs

In addition to promoting target affinity and nuclease resistance, third-generation is created to further enhance biostability and pharmacokinetics and it is the most heterogeneous generation [145]. The most common modification include locked nucleic acid (LNA), peptide nucleic acid (PNA) and phosphorodiamidate morpholino oligomer (PMO) (Figure I.8) [145].

LNA modification is a sugar modification, in which nucleotides are chemically modified with a ribose containing a methylene bridge between the 2'-oxygen and the 4'-carbon of the ribose [146]. LNA substitution improve the binding affinity with mRNA target through the increase of thermal stability between DNA and RNA heteroduplexes [147]. Moreover, the LNA-modified sequence show low toxicity in biological systems [148], which explains the fact of LNAs being used as an ASO molecule, both *in vitro* and *in vivo* [149,150]. Tricyclo-DNA (tc-DNA) is a sugar modification that belongs to the conformational constraint of the LNA modification. It is characterized by the addition of an ethylene bridge merged with a cyclopropane unit that lead to a decrease of flexibility around the C3'-C4' and C4'-C5' bounds [143].

This modification is not compatible with RNase H and the binding affinity of tc-DNA is lower than in the case of LNA [151]. However, the studies in cells has shown more potent splice-switching applications compared to 2'-OMe-PS oligonucleotides [132,152].

PNA modification is an uncharged synthetic DNA and was firstly described by Nielsen et *al.* [153]. This modification is characterized by the substitution of sugar phosphate backbone by *N*-(3-aminoethyl) glycine units [154]. PNA is not degraded by nucleases or peptidases, showing high biostability in biological fluids [126].

PMO modification is a non-charged agent that binds and sterically blocks translation machinery or alters splicing of pre-mRNA, since PMO does not support RNase H activity [155]. This modification is characterized by the replacement of ribose sugar by morpholino ring and phosphodiester bond by phosphoroamidate linkage [155]. It has been known that PMO ASOs have a great resistance to nucleases and proteases in biological fluid [126]. Recent studies have conjugated PMO modification with arginine-rich peptide (ARP) in order to increase the thermal stability of heteroduplex cellular uptake, leading to an increase of cellular uptake and ASO potency [156].

I.2.2 ASO mechanism of action

In absence of ASO, the normal gene expression leads to a protein expression (Figure I.9 A). According to Stanley Crooke [157], the activity of ASOs can be divided into three phases, namely prehybridization, hybridization and posthybridization. After the ASO enters and distributes in the cell, it must recognize the nucleic acid sequence space to hybridize to its cognate site, which is a complex process involving interactions within proteins [157]. The events before hybridization between ASO and target sequence need to be better understood. It is important to determine the effective concentrations in the region and identify the major intracellular proteins that bind ASOs which allow the hybridization between ASO and the "receptor" [157,158]. However, proteins or lipids involved in the hybridization step have not been yet identified and for the researchers this step is considered a "black box". Crooke *et al.* [159] demonstrated that the RNA structure is a major factor on potency and specificity of the potential hybridization. On the other hand, they shown that the number of copies of target RNA and the RNA half-life is irrelevant for this step. After hybridization, the target RNA can be degraded, disabled, or modified by several mechanisms which is dependent on the ASO chemistry and design, the position of the RNA where ASO will bind and the function of the target RNA.
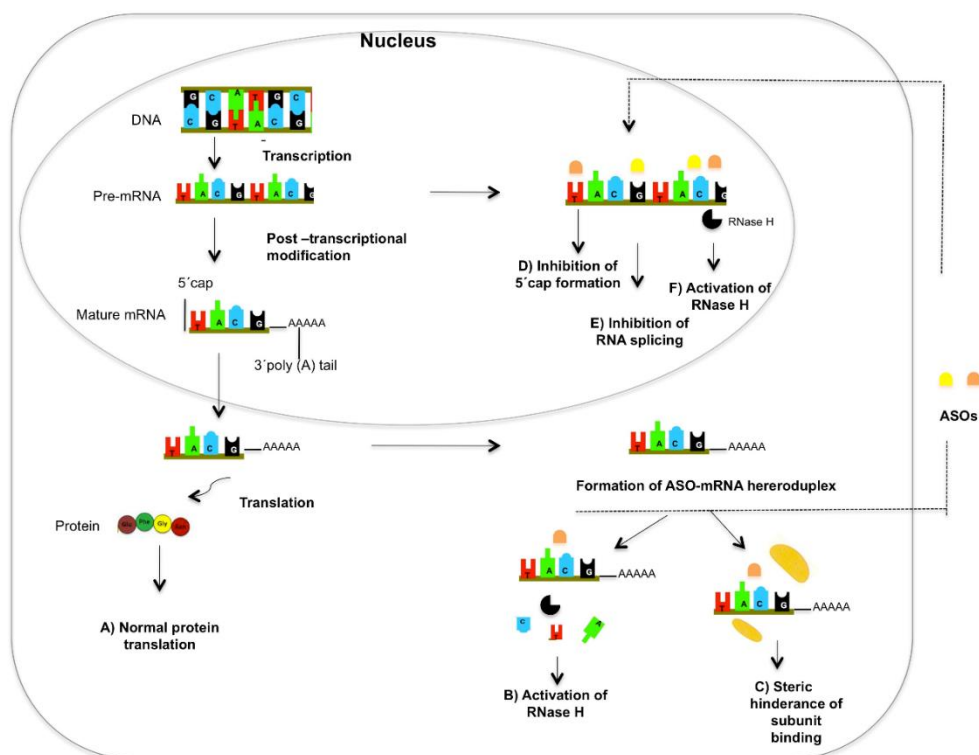
Figure I.9 Antisense oligonucleotides modes of action. A) normal gene protein expression in absence of ASO. **B)** formation of an ASO-mRNA heteroduplex capable to induce RNase H activation, leading to selective degradation of bound mRNA or **C)** steric interference of ribosomal assembly into cell cytoplasm. Alternatively, the ASO can enter the nucleus and regulate mRNA maturation **D)** inhibition of 5´cap formation, **E)** inhibition of mRNA splicing and **F)** activation of RNase H.

Basically, the mechanism of action are divided into two broad categories: the ASO which activate RNase H (Figure I.9 B, F), and those that do not (Figure I.9 C, D, E) [145]. The first ASOs activate the RNase H, which is a ubiquitous enzyme that hydrolyses the RNA strand of an RNA/DNA duplex, which means that recognizes RNA-DNA heteroduplexes, and induce the degradation of mRNA, releasing the intact DNA [160]. The kinetics associated to molecular pharmacology of RNase H1 activating ASOs is extremely slow [161] and it was demonstrated that the onset of action occurs about two hours after ASO enters the cell [157]. It was necessary 60 min for intracellular distribution, 20 min for ASO search the RNA sequence and hybridize to the site and 40 min for RNase H1 recruitment and cleavage [157]. It has been shown that RNase H1, specifically, mediates the RNA cleavage and the intact ASO released from RNase H1 can be used in cleavage of many RNA molecules, which increase ASO potency [130,160]. The ideal ASO should be designed with perfect match to the target sequence and more than 3 base pair mismatches to all other genes [162]. Thus, the inactivation of RNase H is very dependent of sequence specificity because RNase H loses the degrading activity when 3 or more mismatches exist [130,162].

The ASOs that do not activate RNase H, prevent or inhibit the progression of translation by sterically blocking the ribosomal subunits or modulating alternative splicing. In the first case, ASOs can be involved in the prevention of the movement of ribosomes down the transcript and/or inhibit the construction of ribosomal subunits (40S and 60S) [130]. On the other hand, several studies demonstrated that ASOs can also bind to pre-mRNA structure and modulate splicing, both *in vitro* as *in vivo*, leading to exons inclusion or exclusion [163,164].

MicroRNAs are sequences of RNAs with approximately 21 to 23 nucleotides that inhibit translation of several mRNAs targets, leading to the control of the regulation of around 200-300 genes [130,165,166]. Thus, ASOs can be designed to bind microRNAs, blocking the possible linkage with RNA sequences and one miRNA could be an effective strategy once microRNAs block translation of multiple targets [167,168]. The first miRNA which inhibits miR-122 in hepatitis C infection show therapeutic promise *in vivo* [169], since decreased the hepatitis C in monkeys as well as human patients in phase II human trial [170,171].

I.2.3 ASO cargo and delivery strategies

The major problem for ASO-based therapeutics is the cargo and the delivery of the molecule to its site of action, since this delivery shall be in the tissue of therapeutic interest and in the right intracellular compartment [172]. It is very difficult to administer systematically the ASO in its naked form, due to its negative charge that cause a repulsion with the cell membrane, leading to a low uptake by target cells. Moreover, naked ASOs present more toxicity and are easily eliminated and degraded by serum nucleases [126]. The precise mechanisms involved in ASO penetration into the targeted cells is not clear, so it is important to understand how these ASOs enter the cell. The uptake of the ASO depends on temperature, the structure and the concentration of the ASO and the cell line [173–175]. The mechanisms of internalization are dependent on ASO concentration and the two major mechanisms are adsorptive endocytosis and fluid phase pinocytosis. For a low concentration, the membrane-bound receptors are enough, so the internalization occurs mainly by endocytosis [173,174]. However, for the high concentration, the pinocytosis process occurs since these receptors are saturated.

It is known that ASOs tend to localize in endosomes/lysosomes and become unavailable for antisense technology. In order to improve the cellular uptake and ASO activity, in addition to the variety of chemical modifications developed, it has also been introduced Drug Delivery System (DDS): techniques and transporters, such as vectors [128]. So, it is important to develop vectors for efficient and stable delivery of ASO to the target cells and these vectors could be a viral or non-viral system. The most common

vector to deliver the ASO is the incorporation into a non-viral system, which determines the tissue distribution and cellular interactions of the oligonucleotide [172]. These non-viral vectors present many advantages to viral vectors, in terms of the relative safety, lack of immunogenicity, ease large-scale production and their surface is easy to modify for tissue-specific targeting [176–180].

As mentioned above, a single piece of ASO (Figure I.10 A) present a rapid renal clearance and can easily activate the immune response. The strategy to deliver the ASO can be divided into two broad strategies, molecular and nanoscale [172]. It is possible to conjugate the ASO with a ligand (Figure I.10 B) or a polymer (Figure I.10 C). The association of the ASO to a ligand allows to improve the half-life of the ASO in blood, providing time to transit to the targeted organ or cell [181]. The conjugation of ASO with a ligand allows a selective delivery to cells or tissue through receptor mediated mechanisms, which can be an advantage in relation to naked ASO [181]. Alternatively, the ASO can be conjugated with a polymer, as described in Figure I.10 C and in this case, the retention in blood circulation is improved [182]. Through the biodegradable bonds that can be readily dissociated, the ASO can be released intact into the cytoplasm [181,182].

A) Single piece of oligonucleotide   B) Ligand-oligonucleotide conjugate   C) Polymer-oligonucleotide conjugate   D) Lipid or polymer nanoparticle
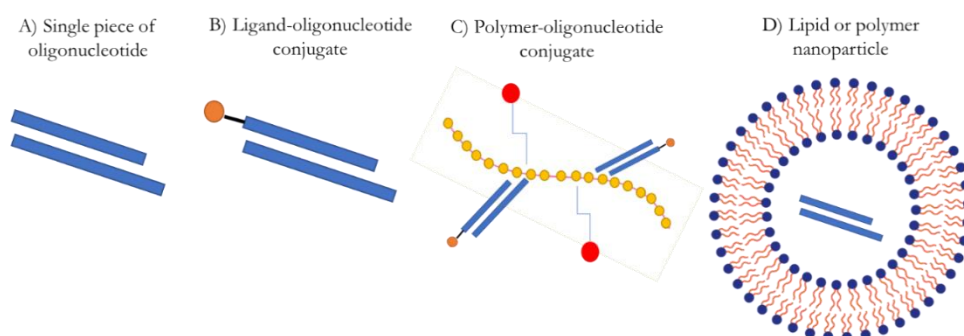
Figure I.10 Delivery systems of oligonucleotides. A) single piece of oligonucleotide, **B)** ligand-oligonucleotide conjugate, **C)** polymer-oligonucleotide conjugate and **D)** lipid or polymer nanoparticle.

Because of the negative charge of ASO, the non-viral vectors more commonly used are the cationic liposomes and polymers (Figure I.10 D), forming a complex more easily [177,183].

a. Polymeric complexes: Polyplexes

An example of ASO delivery strategy is the use of polymeric particles, which have a shell of polymer with the ASO inside (Figure I.10 D). Cationic polymers have been an alternative class of non-viral vectors and poly(L-lysine) (PLL) and polyethylenimine (PEI), being the earlier polymeric vectors used [178]. Very recently, polyamide porous microparticles (MP) were developed by activated anionic ring

opening polymerization (AAROP) of lactams [184,185] and proven useful for protein recognition [186] or enzyme carriers [187].

The interaction between the vectors and ASO is via electrostatic interactions [128] and normally, the ASO is internalized via an endocytosis mechanism. The first application of PLL polymer was in the late 1980s for non-viral liver-targeted gene delivery, where PLL was conjugated with a glycoprotein [188,189]. However, to reduce the *in vitro* cytotoxicity of unmodified PLL, some variants have been reported. One example is the use of the hydrophilic polymer PEG to cover the PLL, since PEG helps to minimize nonspecific interactions with serum components, increasing the circulation time of nanoparticles [190,191]. Another polymeric material most studied for gene delivery was PEI and its variants, and the first demonstration of its application for transfection *in vitro* and *in vivo* was in 1995 [192]. In this case, the transfection efficiency and cytotoxicity depend on its structural properties [178]. To overcome the issues associated with the toxicity, other polymeric non-viral vectors have been developed, with poly[(2-dimethylamino) ethyl methacrylate] (pDMAEMA) as an example.

b. Liposomes complexes: Lipoplexes

Another strategy is to use the lipid based nanoparticles (LNPs), which are the most widely used and clinically advanced non-viral vectors and the first generation of vectors developed (Figure I.10 D) [178,179]. Liposomes are spherical particles composed of phospholipids that present different structures, dimensions, lipid composition and surface charge [193]. In relation to the structure, liposomes can be composed by several concentric bilayers separated by aqueous compartments or only one phospholipid bilayer surrounding an aqueous compartment [194]. In the first case, liposomes are called Multilamellar Vesicles (MLVs), with a size range between 500 nm and 5 µm [194,195]. In the second case, liposomes are called as Small Unilamellar Vesicles (SUVs), Large Unilamellar Vesicles (LUVs) and Giant Unilamellar Vesicles (GUVs), with a size range of 20 to 200 nm, 200 to 1 µm and larger than 1 µm, respectively [194]. Moreover, they can be formed by vesicles surrounded by other vesicles, which form a multi-compartmental structures, called Multi Vesicular Vesicles (MVVs) [194]. The LNP consist of vesicles composed of bilayers of phospholipids and the nature of the phospholipids determines the liposome charge, which can be neutral or cationic [128]. The positive charge of these vectors promote a high affinity with cell membrane, because of their negative charge under physiological conditions [179,195,196]. It can be used as a lipid with positive charge, i.e., the 1,2-DiOleoyl-3-TrimethylAmmonium Propane (DOTAP) [177–180,195,197] and include a "helper" lipid to promote a more efficiently intracellular uptake of ASO and their endosomal escape [179,180,195]. These "helper" lipids are

normally neutral lipids and the most common used are 1,2-dioleoylsn-glycero-3-phosphatidylcholine (DOPC) [177,180,197,198], Di-Oleoyl-Phosphatidyl-Ethanoalamine (DOPE) [178,180,197,198] and 1,2-DiStearoyl-sn-glycero-3- PhosphoCholine (DSPC) [178,180].

I.2.4 ASO pharmacokinetic properties

The pharmacokinetic properties of ASOs depend on its structure, if it is a single or double stranded, the charge, if it is negatively charged or neutral, and how it is the formulation (into a nanoparticle or not) [159,199]. As mentioned before, an unmodified ASO is generally rapidly filtered out of blood by the kidney and excreted in urine because there are normally small molecules. There are several routes of administration, namely intravenous administration, subcutaneous route, local administration, or inhalation. The most favourable route of administration depends on the site to reach its target. For systemic applications, the intraperitoneal, subcutaneous, or intravenous (IV) delivery of ASOs are the primary route of administration.

An ASO modified by PS chemical modification, is enough to prolong the time of circulation and to distribute to tissue, due to the increased binding to serum proteins. The administration of PS-modified ASO by subcutaneous or intravenous route allows a high biodistribution mainly in the peripheral tissues, taking liver and kidney the highest concentrations [199,200]. The dominant phase of distribution happens immediately after the administration when ASO are moved to tissues in minutes to hours, declining rapidly in the plasma after this initial distribution phase [201]. This initial clearance is dependent on protein binding, which it is saturable and the distribution kinetics is dose-dependent [159]. The cell uptake is predominantly facilitated by endocytosis, which ASOs transit into cells by moving down concentration gradients from extracellular to intracellular compartments [159,201]. The slower terminal elimination from tissues is the last phase, whose can be extended up to several weeks, leading to a balance between the post-distribution phase plasma concentrations and tissue concentrations. The ultimate clearance and elimination is facilitated by endo- and exonuclease metabolism, since the resultant small-molecular-weight fragments lose the ability to bind plasma proteins and they are easily eliminated in urine [201].

The second generation of ASOs is composed by chemical modifications that allows to improve pharmacokinetic and pharmacodynamic properties when compared to first generation (PS-ASOs). The pharmacokinetic properties of the second generation of ASOs after parenteral administration are very similar for both 2'-OMe and 2'-MOE modifications. The drugs are initially adsorptive from the plasma to the tissues, quickly and extensively, presenting a rapid distribution half-lives of plasma profiles, of about hours. The peak plasma concentrations when second generation of ASOs are injected intravenously, is

reached at the end of infusion, in contrast to subcutaneous injection where the ASOs are rapidly absorbed into the systemic circulation and the maximum concentration is reached on 3 to 5 h after injection [202,203]. After reaching the peak of concentration, the ASOs concentration decrease in a multiphasic decline, which is defined by a fast-initial distribution phase (intravenous distribution with a half-life of about 0.5 to 3 h and subcutaneous distribution of about 3 to 5 h). Consequently, the ASOs elimination is a slower phase and is characterized by very low plasma concentrations with elimination half-lives of about 2 to 4 weeks. The ASOs modified by the second generation are, in general, more stable against endo- and exonucleases than PS-ASOs, mainly due to the 'wings' at the 3' and 5' ends, which protect them from being metabolized, justifying the metabolization over 2 to 4 weeks. These oligonucleotides are highly bound to plasma proteins [201,204], which rates are above 90 % and have a higher bioavailability following subcutaneous injection [203]. Furthermore, these compounds are extremely excreted by urinary tract mainly in metabolites produced slowly within tissues [202,204].

When LNA ASOs are transfected without any delivery agent, called as 'Gymnosis', any cellular response is directly related with the administration of the ASO. It was shown that 'naked' LNAs present a higher uptake and potency in contact with cell cultures [205,206]. Normally, the cellular uptake of LNA ASOs is predominantly carried out by endocytosis, as happens with other chemical modification [206]. Recently, it was reported that after subcutaneous administration, LNA ASOs are highly bound to plasma proteins, however, the extension is dependent on species. After 24 h of the first dose, the plasma concentration decays for at least half of the concentration, since the oligonucleotides are rapid distributed to different tissues, firstly in the liver and kidney [206]. Following intravenous administration of the ASO, the concentration in the plasma declined rapidly in a multi-exponential phase. As in the case of second-generation of ASO, the initial phase is characterized by initial rapid distribution, wherein the ASO is distributed from circulation in the tissues, of about hours [207,208].

I.2.5 ASO toxicology

The pharmacological effect of any class of drug can result on one potential mechanism of toxicity and like any drug, the ASOs exhibit dose-dependent toxicities. These ASOs toxicities can be classified as hybridization dependent or hybridization independent [199]. The hybridization with nearly homologous sequences on nontarget mRNA, alterations of endogenous metabolic pathways and nonspecific interactions with proteins can induce toxicity. Exaggerated pharmacological effects and the hybridization to non-target RNAs are the most common processes associated to the hybridization-dependent toxicities [209]. These toxicities can be avoided through a proper and careful selection of the sequence with perfect

matches or a few mismatches by bioinformatic analysis. The shorter oligonucleotides can be a problem because of the interaction with non-targeted transcripts which are degraded if RNase is active [210]. Moreover, it is important to perform preclinical models in order to characterize the pharmacology and toxicology of the ASOs [199].

The interaction between oligonucleotides and proteins could be a second mechanism of ASO toxicity which can be sequence dependent or independent. Typically, there are two main factors associated to the sequence independent toxicity, which are the chemistry of the oligonucleotides and the chemical class of the proteins that ASO interact [199]. The most serious toxicities related to the systemic administration of ASOs are the coagulation activation and the complement and hypotension [211–213]. In the case of the first generation of ASOs, it is described in the literature that the toxicity is due to the combination of some factors, such as, the dose, extent of PS modification, sequence, and route and duration of administration [199,213,214]. The sequence that are fully modified by PS, ASO exhibit nonspecific effects, in contrast to partially modified sequence [214]. The first side effects associated with PS chemistry was reported in human trials of Bcl-2 PS ASOs which were increased blood glucose levels, dose-dependent thrombocytopenia, and mild hyperglycaemia [213,215].

The second generation of ASOs has been demonstrated to be better accepted than the PS-modified ASOs.[209,216]. For example, thrombocytopenia is a side effect with ASO treatment, and it was reported that in mice the administration of a first-generation ASO resulted frequently in a reduction in platelet counts [217–219]. In contrast, this incidence decreases with the administration of a 2'-MOE ASO. Moreover, in cancer studies which investigated the first-generation of ASO, the thrombocytopenia has been frequently reported [220,221], in contrast with the second-generation [217,219,222].

The LNA modified ASOs have the potential to increase the potency of the ASOs [223], however, comparing to the second generation of the ASO, LNA-modified ASOs provoke a risk of hepatotoxicity that was chemistry-, sequence- and design-dependent [147]. For example, it has also been shown that LNA ASOs with a size between 14 and 20 nucleotides significantly reduced the hepatotoxicity. Moreover, sequences with different positions of LNA modifications can present different hepatotoxic profiles [206,224].

I.2.6 Antisense Drugs approved by FDA and EMA

Numerous studies have documented the use of AST as biochemical tools for studying human target diseases. Up to now, there are ten antisense drugs that have been approved by Food and Drug Administration (FDA), as well as, by European Medicines Agency (EMA) [225–227]. These antisense drugs are presented in Table I.2. However, there are around 187 antisense drugs that are under different stages of clinical trials, and only 17 in the third phase [227,228]. The first antisense drug that received market authorization was formivirsen, that was a drug developed in a collaboration between Isis Pharmaceuticals with Novartis Ophthalmics approved by FDA in 1998 and by EMA in 1999 [229,230]. However, Novartis interrupted the drug marketing in 2002 in Europe and in 2006 in the United States [226]. In the last two years, three antisense drugs were approved, namely, Volanesorsen, Givosiran and Golodirsen [226,227]. The potential antisense therapeutics have been studied for the treatment of some human diseases, such as, cancer (e.g., leukemia, lung cancer, prostate cancer) [131,231–234] and, Huntington's disease [131,143,235]. In recent years, the AST has been applied to bind specific targets to treat infections, for example as targeting specific antibiotic resistance determinants. The first application of AST to bacteria was demonstrated through a PNA-modified ASO, which demonstrated an antisense inhibition of the *Escherichia coli* beta-lactamase gene [236]. More recently, a PMO-modified ASO was synthesized and conjugated with cell-penetrating peptides to enhance cellular delivery. An CPP-PMO was designed to target *E. coli gyrA* that is a conserved gene in several bacteria species, and it was demonstrated that the ASO has reduced the expression of *gyrA* mRNA and reduced the viability of *Enterococcus faecalis* and *Staphylococcus aureus* [237,238]. Another application was described by Liang *et al.* [239] that have designed a peptide-conjugated PNA (PPNA) to target the *ftsZ* gene, essential for cell division in *S. aureus* and it was demonstrated that PPNA ASO inhibited growth and expression of *ftsZ* mRNA [239–241]. However, application of AST as anti-*Candida* agents are still scarce and usually are limited to the first and the second generation of ASOs. Do authors knowledge there is only one study using the AST to interrupt and efficiently inhibit *C. albicans in vivo* splicing using a PS-modified ASO [242]. The most exciting long-term possibility is to develop antisense molecules for clinical application; however, this naturally requires much more research to develop a credible and alternative approach to control *Candida* infections.

Table I.2 Antisense drugs that received market authorization by FDA and/or EMA. Adapted from [227]

Chemical modification	Antisense Drug	Disease	Market approval
Unmodified	Defibrotide (Defitelio™)	Veno-occlusive disease	FDA in 2016 EMA in 2013
PS	Fomivirsen (Vitravene™)	Cytomegalovirus retinitis	FDA in 1998 EMA in 1999
2'OMe	Patisiran (Onpattro™)	Polyneuropathy in patients with hereditary transthyretin amyloidosis	FDA in 2018 EMA in 2018
PS/2'MOE	Mipomersen (Kynamro™)	Homozygous familial hypercholesterolemia	FDA in 2013
	Nusinersen (Spinraza™)	Spinal muscular atrophy	FDA in 2016 EMA in 2017
	Inotersen (Tegsedi™)	Polyneuropathy in patients with hereditary transthyretin amyloidosis	FDA in 2018 EMA in 2018
	Volanesorsen (Waylivra™)	Familial chylomicronaemia syndrome	EMA in 2019
PS/2'O-fluorine/2'MOE	Givosiran (Givlaari™)	Acute hepatic porphyria	FDA in 2019 EMA in 2020
PMO	Eteplirsen (Exondys 51™)	Duchenne muscular dystrophy	FDA in 2016
	Golodirsen (Vyondys 53™)	Duchenne muscular dystrophy	FDA in 2019

References

1   Pfaller M A and Diekema D J (2007) Epidemiology of invasive candidiasis: A persistent public health problem. *Clin. Microbiol. Rev.* 20, 133–163

2   Williams D W, Jordan R, Wei X, et al. (2013) Interactions of *Candida albicans* with host epithelial surfaces. *J. Oral Microbiol.* 5, 22434

3   Quindós, G. (2018) Epidemiology of invasive mycoses: A landscape in continuous change. *Rev. Iberoam.*

Micol. 35, 171–178

4   Koehler P, Stecher M, Cornely O A, et al. (2019) Morbidity and mortality of candidaemia in Europe: an epidemiologic meta-analysis. *Clin. Microbiol. Infect.* 25(10), 1200-1212

5   Berman J, and Sudbery P E (2002) *Candida albicans*: a molecular revolution built on lessons from budding yeast. *Nat. Rev. Genet.* 3, 918–930

6   Silva S, Negri M, Henriques M, et al. (2011) Adherence and biofilm formation of non-*Candida albicans Candida* species. *Trends Microbiol.* 19, 241–247

7   Dadar M, Twari R, Karthik K, et al (2018) *Candida albicans* - Biology, molecular characterization, pathogenicity, and advances in diagnosis and control – An update. *Microb. Pathog.* 117, 128–138

8   Lone S A and Ahmad A (2019) *Candida auris*–the growing menace to global health. *Mycoses* 62, 620–637

9   Yapar N and Nur Y (2014) Epidemiology and risk factors for invasive candidiasis. *Ther. Clin. Risk Manag.* 10, 95–105

10   Guinea J (2014) Global trends in the distribution of *Candida* species causing candidemia. *Clin. Microbiol. Infect.* 20, 5–10

11   Quindós G (2014) Epidemiology of candidaemia and invasive candidiasis . A changing face. *Rev. Iberoam. Micol.* 31, 42–48

12   Gonçalves B, Ferreira C, Alves C T, et al. (2016) Vulvovaginal candidiasis: Epidemiology, microbiology and risk factors. *Crit. Rev. Microbiol.* 42, 905–927

13   Pappas P G, Lionakis M S, Arendrup M C, et al. (2018) Invasive candidiasis. *Nat. Publ. Gr.* 4, 1–20

14   Pappas P G, Rex J H, Lee J, et al. (2003) A prospective observational study of candidemia: epidemiology, therapy, and influences on mortality in hospitalized adult and pediatric patients. *Clin. Infect. Dis.* 37, 634–643

15   Montagna M T, Lovero G, Borghi E, et al. (2014) Candidemia in intensive care unit : a nationwide prospective observational survey (GISIA-3 study) and review of the European literature from 2000 through 2013. 18, 661-674

16   Pemán J, Cantón E and Gobernado M (2005) Epidemiology and antifungal susceptibility of *Candida* species isolated from blood: Results of a 2-year multicentre study in Spain. *Eur. J. Clin. Microbiol. Infect. Dis.* 24, 23–30

17   Bitar D, Lortholary O, Strat Y, et al. (2014) Population-based analysis of invasive fungal infections, France, 2001–2010. *Emerg. Infect. Dis.* 20, 1149–1155

18   Nobile C and Johnson A (2015) *Candida albicans* biofilms and human disease. *Annu. Rev. Microbiol.* 69, 71–92

19   Kim J and Sudbery P (2011) *Candida albicans*, a major human fungal pathogen. *J. Microbiol.* 49, 171–177

20   Lim C, Rosli R, Seow H, et al. (2012) *Candida* and invasive candidiasis: Back to basics. *European Journal of Clinical Microbiology and Infectious Diseases,* 31, 21–31

21   Romanowski K, Zaborin A, Valuckaite V, et al. (2012) *Candida albicans* isolates from the gut of critically Ill patients respond to phosphate limitation by expressing filaments and a lethal phenotype. *PLoS One* 7, 7(1), e30119

22   Walsh T, Hayden R, Larone D (2018) Medically Important Fungi: A Guide to Identification, 6th edition, ASM Press, Washington

23   Gulati M and Nobile C J (2016) *Candida albicans* biofilms: development, regulation, and molecular mechanisms. *Microbes Infect.* 18, 1–12

24   Araújo D, Henriques M and Silva S (2017) Portrait of *Candida* species biofilm regulatory network genes. *Trends Microbiol.* 1, 62–75

25   Odds F C and Bernaerts R (1994) CHROMagar *Candida*, a new differential isolation medium for presumptive identification of clinically important *Candida* species. *J. Clin. Microbiol.* 32, 1923–1929

26   Monod M, Capoccia S, Léchenne, et al (2002) Secreted proteases from pathogenic fungi. *Int. J. Med. Microbiol.* 292, 405–19

27   Silva S, Negri M, Henriques M, et al (2012) *Candida glabrata*, *Candida parapsilosis* and *Candida tropicalis*: Biology, epidemiology, pathogenicity and antifungal resistance. *FEMS Microbiol. Rev.* 36, 288–305

28   Schaller M, Borelli C, Korting H, et al (2005) Hydrolytic enzymes as virulence factors of *Candida albicans*. *Mycoses* 48, 365–77

29   Hube B, Hess D, Baker C, et al (2001) The role and relevance of phospholipase D1 during growth and dimorphism of *Candida albicans*. *Microbiology* 147, 879–889

30   Naglik J, Challacombe S and Hube B (2003) *Candida albicans* secreted aspartyl proteinases in virulence and pathogenesis. *Microbiol. Mol. Biol. Rev.* 67, 400–28

31   White T, Miyasaki S, Agabian N (1993) Three distinct secreted aspartyl proteinases in *Candida albicans*. Journal of Bacteriology, 175(19), 6126-6133

32   Hube B, Monod M, Schofield D, et al (1994) Expression of seven members of the gene family encoding secretory aspartyl proteinases in *Candida albicans*. *Mol. Microbiol.* 14, 87–99

33   White T C and Agabian N (1995) *Candida albicans* secreted aspartyl proteinases: isoenzyme pattern is determined by cell type, and levels are determined by environmental factors. Journal of Bacteriology. 177(18), 5215-5221

34   Felk A, Kretschmar M, Albrecht A (2002) *Candida albicans* hyphal formation and the expression of the Efg1-regulated proteinases Sap4 to Sap6 are required for the invasion of parenchymal organs. *Infect. Immun.* 70, 3689–3700

35   Schaller M, Bein M, Korting H, et al (2003) The secreted aspartyl proteinases Sap1 and Sap2 cause tissue damage in an *in vitro* model of vaginal candidiasis based on reconstituted human vaginal epithelium. *Infect. Immun.* 71, 3227–3234

36   Ghannoum M A (2000) Potential role of phospholipases in virulence and fungal pathogenesis. *Clin. Microbiol. Rev.* 13, 122–143

37   Samaranayake Y H, Dassanayake R, Cheung B, et al (2006) Differential phospholipase gene expression by *Candida albicans* in artificial media and cultured human oral epithelium. *APMIS* 114, 857–866

38   Gácser A, Schäfer W, Nosanchuk J, et al (2007) Virulence of *Candida parapsilosis*, *Candida orthopsilosis*, and *Candida metapsilosis* in reconstituted human tissue models. *Fungal Genet. Biol.* 44, 1336–41

39   Wang Y C, Huang S, Lan C, et al (2012) Prediction of phenotype-associated genes via a cellular network approach: A *Candida albicans* infection case study. *PLoS One* 7, 1–7

40   Lima-Neto R G, Beltrão E, Oliveira P, et al (2011) Adherence of *Candida albicans* and *Candida parapsilosis* to epithelial cells correlates with fungal cell surface carbohydrates. *Mycoses* 54, 23–29

41   Nobile C and Mitchell A P. (2005) Regulation of cell-surface genes and biofilm formation by the *C. albicans* transcription factor Bcr1p. *Curr. Biol.* 15, 1150–1155

42   Nobile C J, Andes D R, Nett J E, et al (2006) Critical role of Bcr1-dependent adhesins in *C. albicans* biofilm formation *in vitro* and *in vivo*. *PLoS Pathog.* 2, 0636–0649

43   Henriques M, Azeredo J and Oliveira R (2006) *Candida* species adhesion to oral epithelium: factors involved and experimental methodology used. *Crit. Rev. Microbiol.* 32, 217–226

44   Filler S G (2006) *Candida*-host cell receptor-ligand interactions. *Curr. Opin. Microbiol.* 9, 333–339

45   Kulkarni R, Kelkar H and Dean R (2003) An eight-cysteine-containing CFEM domain unique to a group of fungal membrane proteins. *Trends Biochem. Sci.* 28, 118–121

46   Ding C, Vidanes G, Maguire S, et al (2011) Conserved and divergent roles of Bcr1 and CFEM proteins in *Candida parapsilosis* and *Candida albicans*. *PLoS One* 6, 1–11

47   Pérez A, Pedrós B, Murgui A, et al (2006) Biofilm formation by *Candida albicans* mutants for genes coding fungal proteins exhibiting the eight-cysteine-containing CFEM domain. *FEMS Yeast Res.* 6, 1074–1084

48   Mayer F, Wilson D and Hube B (2013) *Candida albicans* pathogenicity mechanisms. *Virulence* 4, 119–28

49   Grubb S, Murdoch C, Sudbery P, et al (2008) *Candida albicans* -endothelial cell interactions: a key step in the pathogenesis of systemic candidiasis . *Infect. Immun.* 76, 4370–4377

50   Nobile C J, Schneider H A, Nett J E, et al (2008) Complementary adhesin function in C. albicans biofilm formation. *Curr Biol.* 18(14), 1017-1024

51   Li F and Palecek S P (2003) *EAP1*, a *Candida albicans* gene involved in binding human epithelial cells. *Eukaryot Cell* 2, 1266–73

52   Green C B, Zhao X, Yeater K M, et al (2005) Construction and real-time RT-PCR validation of *Candida albicans* PALS-GFP reporter strains and their use in flow cytometry analysis of ALS gene expression in budding and filamenting cells. *Microbiology* 151, 1051–1060

53   Zhao X, Oh S, Cheng G, et al (2004) ALS3 and ALS8 represent a single locus that encodes a *Candida*

albicans adhesin; functional comparisons between Als3p and Als1p. *Microbiology* 150, 2415-2428

54   Li F, Svarovsky M, Karlsson A, et al (2007) Eap1p, an adhesin that mediates *Candida albicans* biofilm formation *in vitro* and *in vivo*. *Eukaryot. Cell* 6, 931–939

55   Staab J F, Bradway S D, Fidel P L, et al (1999) Adhesive and mammalian transglutaminase substrate properties of *Candida albicans* Hwp1. *Science* 283, 1535–8

56   Orsi C F, Borghi E, Colombari B, et al (2014) Impact of *Candida albicans* hyphal wall protein 1 (*HWP1*) genotype on biofilm production and fungal susceptibility to microglial cells. *Microb. Pathog.* 69-70C, 20–27

57   Silva S, Henriques M, Martins A, *et al.* (2009) Biofilms of non-*Candida albicans Candida* species: quantification, structure and matrix composition. *Med. Mycol.* 47, 681–689

58   Desai J, Mitchell A P and Andes D R (2014) Fungal biofilms, drug resistance, and recurrent infection. *Cold Spring Harb. Perspect. Med.* 4(10), a019729

59   Jain N, Kohli R, Cook E, et al (2007) Biofilm formation by and antifungal susceptibility of *Candida* isolates from urine. *Appl. Environ. Microbiol.* 73, 1697–1703

60   Nobile C J and Mitchell A P (2006) Genetics and genomics of *Candida albicans* biofilm formation. *Cell. Microbiol.* 8, 1382–1391

61   Silva-Dias A, Palmeira-de-Oliveira A, Miranda I M, et al (2014) Anti-biofilm activity of low-molecular weight chitosan hydrogel against *Candida* species. *Med. Microbiol. Immunol.* 203, 25–33

62   Nobile C J, Fox E P, Nett J, et al (2011) A recently evolved transcriptional network controls biofilm development in *Candida albicans*. *Cell* 148, 126–138

63   Finkel J S and Mitchell A P (2011) Genetic control of *Candida albicans* biofilm development. *Nat. Rev. Microbiol.* 9, 109–118

64   Al-Fattani M A and Douglas L J (2006) Biofilm matrix of *Candida albicans* and *Candida tropicalis*: Chemical composition and role in drug resistance. *J. Med. Microbiol.* 55, 999–1008

65   Baillie G S and Douglas L J (2000) Matrix polymers of *Candida* biofilms and their possible role in biofilm resistance to antifungal agents. *J. Antimicrob. Chemother.* 46, 397–403

66   Chandra J, Kuhn D M, Mukherjee P K, et al (2001) Biofilm formation by the fungal pathogen *Candida albicans*: development, architecture, and drug resistance. *J. Bacteriol.* 183(18):53, 5385–5394

67   Donlan R M E and Costerton J W (2002) Biofilms: survival mechanisms of clinically relevant microorganisms. *Clin. Microbiol. Rev.* 15, 167–193

68   Connolly L, Riccombeni A, Grózer Z, et al (2013) The APSES transcription factor Efg1 is a global regulator that controls morphogenesis and biofilm formation in *Candida parapsilosis*. *Mol. Microbiol.* 90, 36–53

69   Holland L M, Schröder M S, Turner S A, et al (2014) Comparative phenotypic analysis of the major fungal pathogens *Candida parapsilosis* and *Candida albicans*. *PLoS Pathog.* 10, 1–18

70   Liu H (2001) Transcriptional control of dimorphism in *Candida albicans*. *Curr. Opin. Microbiol.* 4, 728–735

71   Schweizer A, Rupp S, Taylor B N, et al (2000) The TEA/ATTS transcription factor CaTec1p regulates hyphal development and virulence in *Candida albicans*. *Mol. Microbiol.* 38, 435–445

72   Nett J, Lincoln L, Marchillo K, et al (2007) Putative role of β-1,3 glucans in *Candida albicans* biofilm resistance. *Antimicrob. Agents Chemother.* 51, 510–520

73   Zarnowski R, Westler W, Lacmbouh G A, et al (2014) Novel entries in a fungal biofilm matrix encyclopedia. *MBio* 5(4), e01333–e01314

74   Nett J E, Crawford K, Marchillo K, et al 2010) Role of Fks1p and matrix glucan in *Candida albicans* biofilm resistance to an echinocandin, pyrimidine, and polyene. *Antimicrob. Agents Chemother.* 54, 3505–3508

75   Taff H T, Nett J, Zarnowski R, et al (2012) A *Candida* biofilm-induced pathway for matrix glucan delivery: implications for drug resistance. *PLoS Pathog.* 8, 1–13

76   Nobile C J, Nett J, Hernday A, et al (2009) Biofilm matrix regulation by *Candida albicans* Zap1. *PLoS Biol.* 7, 1–15

77   Nett J E, Sanchez H, Cain M T, et al (2011) Interface of *Candida albicans* biofilm matrix-associated drug resistance and cell wall integrity regulation. *Eukaryot. Cell* 10, 1660–1669

78   González M, Díez-Orejas R, Molero G, et al (1997) Phenotypic characterization of a *Candida albicans* strain deficient in its major exoglucanase. *Microbiology* 143, 3023–3032

79   Fonzi W A (1999) *PHR1* and *PHR2* of *Candida albicans* encode putative glycosidases required for proper cross-linking of β-1,3- and β-1,6-glucans. *J. Bacteriol.* 181, 7070–7079

80   Sarthy A V, McGonigal T, Coen M, et al (1997) Phenotype in *Candida albicans* of a disruption of the BGL2 gene encoding a 1,3-β-glucosyltransf erase. *Microbiology* 143, 367–376

81   Uppuluri P, Chaturvedi A, Srinivasan A, et al (2010) Dispersion as an important step in the *Candida albicans* biofilm developmental cycle. *PLoS Pathog.* 6, 1–13

82   Shen J, Cowen L, Griffin A, et al (2008) The *Candida albicans* pescadillo homolog is required for normal hypha-to-yeast morphogenesis and yeast proliferation. *Proc. Natl. Acad. Sci. U. S. A.* 105, 20918–23

83   Uppuluri P, Pierce C, Thomas D, et al (2010) The transcriptional regulator Nrg1p controls *Candida albicans* biofilm formation and dispersion. *Eukaryot. Cell* 9, 1531–1537

84   Braun B R, Kadosh D and Johnson A (2001) *NRG1*, a repressor of filamentous growth in *C.albicans*, is down-regulated during filament induction. *EMBO J.* 20, 4753–4761

85   Murad A M A, Leng P, Straffon M, et al (2001) *NRG1* represses yeast hypha morphogenesis and hypha-specific gene expression in *Candida albicans*. *EMBO J.* 20, 4742–4752

86   Bar-Yosef H, Gonzalez N V, Ben-Aroya S, et al (2017) Chemical inhibitors of *Candida albicans* hyphal morphogenesis target endocytosis. *Sci. Rep.* 7, 1–12

87   Davis D (2003) Adaptation to environmental pH in *Candida albicans* and its relation to pathogenesis. *Current Genetics*, 44(1), 1–7

88   Biswas S, Dijck P V and Datta A (2007) Environmental sensing and signal transduction pathways regulating morphopathogenic determinants of *Candida albicans*. *Microbiol. Mol. Biol. Rev.* 71, 348–376

89   Lu Q, Jayatilake J, Samaranayake L, et al (2006) Hyphal invasion of *Candida albicans* inhibits the expression of human β-defensins in experimental oral candidiasis. *J. Invest. Dermatol.* 126, 2049–2056

90   Lo H J, Köhler J R, DiDomenico B, et al (1997) Nonfilamentous *C. albicans* mutants are avirulent. *Cell* 90, 939–949

91   Alves C, Wei X, Silva S, et al (2014) *Candida albicans* promotes invasion and colonisation of *Candida glabrata* in a reconstituted human vaginal epithelium. *J. Infect.* 69, 396–407

92   Liu H, Kohler J and Fink G R (1994) Suppression of hyphal formation in *Candida albicans* by mutation of a *STE12* homolog. *Science* 266(5191), 1723–1726

93   Casadevall A and Pirofski L (2001) Host-pathogen interactions: the attributes of virulence. *J. Infect. Dis.* 184, 337–344

94   Rocha C R C, Schröppel K, Harcus D, et al (2001) Signaling through adenylyl cyclase is essential for hyphal growth and virulence in the pathogenic fungus *Candida albicans*. *Mol. Biol. Cell* 12, 3631–3643

95   Saputo S, Kumar A and Krysan D (2014) Efg1 directly regulates *ACE2* expression to mediate cross talk between the cAMP/PKA and RAM pathways during *Candida albicans* morphogenesis. *Eukaryot. Cell* 13, 1169–1180

96   Fonzi W a (2002) Role of pH response in *Candida albicans* virulence. *Mycoses* 45 Suppl 1, 16–21

97   Du H and Huang G (2016) Environmental pH adaption and morphological transitions in *Candida albicans*. *Curr. Genet.* 62, 283–286

98   Lotz H, Sohn K, Brunner H, et al (2004) *RBR1*, a novel pH-regulated cell wall gene of *Candida albicans,* is repressed by *RIM101* and activated by *NRG1*. *Eukaryot Cell* 3, 776–784

99   Basso V, d'Enfert C, Znaidi S, et al (2018) From genes to networks: The regulatory circuitry controlling *Candida albicans* morphogenesis. *Curr. Top. Microbiol. Immunol.* DOI: 10.1007/82

100   Stoldt V R, Sonneborn A, Leuker C E, et al (1997) Efg1p, an essential regulator of morphogenesis of the human pathogen *Candida albicans*, is a member of a conserved class of bHLH proteins regulating morphogenetic processes in fungi. *EMBO J.* 16, 1982–1991

101   Setiadi E R, Doedt T, Cottier F, et al (2006) Transcriptional response of *Candida albicans* to hypoxia: linkage of oxygen sensing and Efg1p-regulatory networks. *J. Mol. Biol.* 361, 399–411

102   Desai P R, Wijlick L, Kurtz D, et al (2015) Hypoxia and temperature regulated morphogenesis in *Candida albicans*. *PLoS Genet.* 11, 1–31

103   Dwivedi P, Thompson A, Xie Z, et al (2011) Role of Bcr1-activated genes Hwp1 and Hyr1 in *Candida albicans* oral mucosal biofilms and neutrophil evasion. *PLoS One* 6, e16218

104   Lane S, Zhou S, Pan T, et al (2001) The basic helix-loop-helix transcription factor Cph2 regulates hyphal

development in *Candida albicans* partly via *TEC1*. *Mol. Cell. Biol.* 21, 6418–28

105   Sohn K, Urban C, Brunner H, et al (2003) *EFG1* is a major regulator of cell wall dynamics in *Candida albicans* as revealed by DNA microarrays. *Mol Microbiol* 47, 89–102

106   Sharkey L L, McNemar M D, Saporito-Irwin S M, et al (1999) *HWP1* functions in the morphological development of *Candida albicans* downstream of *EFG1*, *TUP1*, and *RBF1*. *J. Bacteriol.* 181, 5273–5279

107   Dünkler A, Walther A, Specht C A, et al (2005) *Candida albicans CHT3* encodes the functional homolog of the Cts1 chitinase of Saccharomyces cerevisiae. *Fungal Genet. Biol.* 42, 935–947

108   Heilmann C J, Sorgo A G, Siliakus A R, et al (2011) Hyphal induction in the human fungal pathogen *Candida albicans* reveals a characteristic wall protein profile. *Microbiology* 157, 2297–2307

109   Ghosh A K, Wangsanut T, Fonzi W, et al (2015) The *GRF10* homeobox gene regulates filamentous growth in the human fungal pathogen *Candida albicans*. *FEMS Yeast Res.* 15, 1–11

110   Chauvel M, Nesseir A, Cabral V, et al (2012) A versatile overexpression strategy in the pathogenic yeast *Candida albicans*: Identification of regulators of morphogenesis and fitness. *PLoS One* 7, e45912

111   Birse C E, Irwin M Y, Fonzi W, et al (1993) Cloning and characterization of *ECE1*, a gene expressed in association with cell elongation of the dimorphic pathogen *Candida albicans*. *Infect. Immun.* 61, 3648–3655

112   Hayek P, Dib L, Yazbeck P, et al (2010) Characterization of Hwp2, a *Candida albicans* putative GPI-anchored cell wall protein necessary for invasive growth. *Microbiol. Res.* 165, 250–258

113   Zakikhany K, Naglik J, Schmidt-Westhausen A, Holland G, et al (2007) *In vivo* transcript profiling of *Candida albicans* identifies a gene essential for interepithelial dissemination. *Cell. Microbiol.* 9, 2938–2954

114   Martin R, Moran G P, Jacobsen I, et al (2011) The *Candida albicans*-specific gene *EED1* encodes a key regulator of hyphal extension. *PLoS One* 6, e18394 (1-13)

115   Polke M, Sprenger M, Scherlach K, et al (2017) A functional link between hyphal maintenance and quorum sensing in *Candida albicans*. *Mol. Microbiol.* 103, 595–617

116   Leng P, Lee P, Wu H, et al (2001) Efg1, a morphogenetic regulator in *Candida albicans*, is a sequence-specific DNA binding protein. *J. Bacteriol.* 183, 4090–3

117   Banerjee M, Thompson D S, Lazzell A, et al (2008) *UME6*, a novel filament-specific regulator of *Candida albicans* hyphal extension and virulence. *Mol. Biol. Cell* 19, 308–317

118   Zeidler U, Lettner T, Lassnig C, et al (2009) *UME6* is a crucial downstream target of other transcriptional regulators of true hyphal development in *Candida albicans*. *FEMS Yeast Res.* 9, 126–142

119   Arendrup M C (2010) Epidemiology of invasive candidiasis. *Curr. Opin. Crit. Care* 16, 445–452

120   Mikolajewska A, Schwartz S and Ruhnke M (2012) Antifungal treatment strategies in patients with haematological diseases or cancer: From prophylaxis to empirical, pre-emptive and targeted therapy. *Mycoses* 55, 2–16

121   Cowen L E (2008) The evolution of fungal drug resistance: modulating the trajectory from genotype to phenotype. *Nat. Rev. Microbiol.* 6, 187–198

122   Chen S, Slavin M and Sorrell T (2011) Echinocandin antifungal drugs in fungal infections. *Drugs* 71, 11–41

123   Silva S, Rodrigues C, Araújo D, et al (2017) *Candida* species biofilms' antifungal resistance. *J. Fungi* 3, 8

124   Taff H T, Mitchell K, Edward J, et al (2013) Mechanisms of *Candida* biofilm drug resistance. 8, 1–19

125   Prasad R, Nair R and Banerjee A (2019) Emerging mechanisms of drug resistance in *Candida albicans*. In *Yeasts in Biotechnology and Human Health* 58, 135–153

126   Chan J H P, Lim S and Wong W S F (2006) Antisense Oligonucleotides: from design to therapeutic application. *Clin. Exp. Pharmacol. Physiol.* 33(5-6), 533-540

127   Crooke S T (2004) Progress in Antisense Technology. Annu Rev Med. 55, 61–95

128   Dias N and Stein C A (2002) Antisense oligonucleotides: basic concepts and mechanisms. *Mol. Cancer Ther.* 1, 347–355

129   Potaczek D P, Garn H, Unger S D, et al (2016) Antisense molecules: A new class of drugs. *J. Allergy Clin. Immunol.* 137, 1334–1346

130   DeVos S L and Miller T M (2013) Antisense oligonucleotides: treating neurodegeneration at the level of RNA. *Neurotherapeutics* 137(5), 1334-1346

131   Quemener A M, Bachelot L, Forestier A, et al (2020) The powerful world of antisense oligonucleotides: From bench to bedside. *Wiley Interdiscip Rev RNA* 11(5), e1594

132   Khvorova A and Watts J K (2017) The chemical evolution of oligonucleotide therapies of clinical utility. *Nat. Biotechnol.* 35, 238–248

133   Batista-duharte A, Sendra L, Herrero M J, et al (2020) Progress in the use of antisense oligonucleotides for vaccine improvement. *Biomolecules* 10(2), 316

134   Eckstein F (2000) Phosphorothioate oligodeoxynucleotides: what is their origin and what is unique about them? *Antisense Nucleic Acid Drug Dev.* 10, 117–21

135   Clercq E D, Eckstein E and Merigan T C (1969) Interferon induction increased through chemical modification of a synthetic polyribonucleotide. *Science* 165, 1137–1139

136   Campbell J M, Bacon T A and Wickstrom E (1990) Oligodeoxynucleoside phosphorothioate stability in subcellular extracts, culture media, sera and cerebrospinal fluid. *J. Biochem. Biophys. Methods* 20, 259–67

137   Brown D A, Kang S H, Gryaznov S M, et al (1994) Effect of phosphorothioate modification of oligodeoxynucleotides on specific protein binding. *J. Biol. Chem.* 269, 26801–26805

138   Robbins M, Judge A, Liang L, et al (2007) 2'-O-methyl-modified RNAs act as TLR7 antagonists. *Mol. Ther.* 15, 1663–1669

139   Altmann K H, Fabbro D, Dean N M, et al (1996) Second-generation antisense oligonucleotides: structure-activity relationships and the design of improved signal-transduction inhibitors. *Biochem. Soc. Trans.* 24, 630–7

140   Cummins L L, Owens S R, Risen L M, et al (1995) Characterization of fully 2'-modified oligoribonucleotide hetero-and homoduplex hybridization and nuclease sensitivity. *Nucleic Acids Res.* 23(11), 2019-2024

141   Monia B P, Johnston J F, Sasmor H, et al (1996) Nuclease resistance and antisense activity of modified oligonucleotides targeted to Ha-ras. *J. Biol. Chem.* 271, 14533–14540

142   Choung S, Kim Y J, Kim S, et al (2006) Chemical modification of siRNAs to improve serum stability without loss of efficacy. *Biochem. Biophys. Res. Commun.* 342, 919–927

143   Evers M M, Toonen L and van Roon-Mom W (2015) Antisense oligonucleotides in therapy for neurodegenerative disorders. *Adv. Drug Deliv. Rev.* 87, 90–103

144   Liebsch G, Landgraf R, Engelmann M, et al (1999) Differential behavioural effects of chronic infusion of CRH 1 and CRH 2 receptor antisense oligonucleotides into the rat brain. *J. Psychiatr. Res.* 33, 153–163

145   Kurreck J (2003) Antisense technologies: Improvement through novel chemical modifications. *Eur. J. Biochem.* 270, 1628–1644

146   Koshkin A A, Singh S K, Nielsen P, et al (1998) LNA (Locked Nucleic Acids): Synthesis of the adenine, cytosine, guanine, 5-methylcytosine, thymine and uracil bicyclonucleoside monomers, oligomerisation, and unprecedented nucleic acid recognition. *Tetrahedron* 54(14), 3607–3630

147   Swayze E E, Siwkowski A M, Wancewicz E V, et al (2007) Antisense oligonucleotides containing locked nucleic acid improve potency but cause significant hepatotoxicity in animals. *Nucleic Acids Res.* 35, 687–700

148   Grünweller A and Hartmann R K (2007) Locked nucleic acid oligonucleotides: the next generation of antisense agents? *BioDrugs* 21, 235–43

149   Vester B and Wengel J (2004) LNA (locked nucleic acid): high-affinity targeting of complementary RNA and DNA. *Biochemistry* 43, 13233–41

150   Zhang Y, Qu Z, Kim S, et al (2011) Down-modulation of cancer targets using locked nucleic acid (LNA)-based antisense oligonucleotides without transfection. *Gene Ther.* 18, 326–333

151   Renneberg D and Leumann C J (2002) Watson-Crick base-pairing properties of tricyclo-DNA. *J Am Chem Soc* 124, 5993–6002

152   Goyenvalle A, Griffith G, Babbs A, et al (2015) Functional correction in mouse models of muscular dystrophy using exon-skipping tricyclo-DNA oligomers. *Nat. Med.* 21, 270–275

153   Nielsen P, Egholm M, Berg R H, et al (1991) Sequence-selective recognition of DNA by strand displacement with a thymine-substituted polyamide. *Science* 254, 1497–1500

154   Egholm M, Buchardt O, Christensen L, et al (1993) PNA hybridizes to complementary oligonucleotides obeying the Watson-Crick hydrogen-bonding rules. *Nature* 365, 566–8

155   Amantana A and Iversen P L (2005) Pharmacokinetics and biodistribution of phosphorodiamidate morpholino antisense oligomers. *Curr. Opin. Pharmacol.* 5, 550–5

156   Nelson M, Stein D, Kroeber A, et al (2005) Arginine-rich peptide conjugation to morpholino oligomers:

effects on antisense activity and specificity. *Bioconjug. Chem.* 16, 959–66

157   Crooke S T (2017) Molecular Mechanisms of Antisense Oligonucleotides. *Nucleic Acid Ther.* 00, 1–8

158   Liang X H, Sun H, Shen W, et al (2015) Identification and characterization of intracellular proteins that bind oligonucleotides with phosphorothioate linkages. *Nucleic Acids Res.* 43, 2927–2945

159   Crooke S T (2008) Chapter 1 - Mechanisms of antisense drug action, an introduction. Antisense Drug Technology: Principles, Strategies, and Applications. 2nd edition, Taylor & Francis

160   Cerritelli S M and Crouch R J (2009) Ribonuclease H: The enzymes in eukaryotes. *FEBS J.* 276, 1494–1505

161   Vickers T A and Crooke S T (2015) The rates of the major steps in the molecular mechanism of RNase H1-dependent antisense oligonucleotide induced degradation of RNA. *Nucleic Acids Res.* 43, 8955–8963

162   Monia B P, Johnston J F, Ecker D J, et al (1992) Selective inhibition of mutant Ha-ras mRNA expression by antisense oligonucleotides. *J. Biol. Chem.* 267, 19954–19962

163   Peacey E, Rodriguez L, Liu Y, et al (2012) Targeting a pre-mRNA structure with bipartite antisense molecules modulates tau alternative splicing. *Nucleic Acids Res.* 40, 9836–9849

164   Kouer E and Dean N M (2006) Restoration of correct splicing in thalassemic pre-mRNA by antisense oligonucleotides. *Biochemistry* 90, 8673–8677

165   Krol J, Loedige I and Filipowicz W (2010) The widespread regulation of microRNA biogenesis, function and decay. *Nat. Rev. Genet.* 11, 597–610

166   Huntzinger E and Izaurralde E (2011) Gene silencing by microRNAs: contributions of translational repression and mRNA decay. *Nat. Rev. Genet.* 12, 99–110

167   Esau C, Davis S, Murray S F, et al (2006) miR-122 regulation of lipid metabolism revealed by in vivo antisense targeting. *Cell Metab.* 3(2), 87-98

168   Davis S, Propp S, Freier S, et al (2009) Potent inhibition of microRNA *in vivo* without degradation. *Nucleic Acids Res* 37, 70–77

169   Fabani M M and Gait M J (2008) miR-122 targeting with LNA / 2'-O-methyl oligonucleotide mixmers , peptide nucleic acids (PNA), and PNA – peptide conjugates. *RNA* 14(2), 336-346

170   Lanford R E, Hidevrandt-Eriksen E, Petri A, et al (2012) Therapeutic silencing of microRNA-122 in primates with chronic hepatitis C virus infection. *Science* 327, 198–201

171   Janssen H, Reesink H, Lawitz E, et al (2013) Treatment of HCV Infection by Targeting MicroRNA. *N. Engl. J. Med.* 368, 1685-1694

172   Juliano R L (2016) The delivery of therapeutic oligonucleotides. *Nucleic Acids Res.* 44, 6518–6548

173   Loke S L, Stein C A, Zhang X H, et al (1989) Characterization of oligonucleotide transport into living cells. *Proc. Natl. Acad. Sci. U. S. A.* 86, 3474–8

174   Yakubov L, Deeva E, Zarytova V, et al (1989) Mechanism of oligonucleotide uptake by cells: involvement of specific receptors? *Proc. Natl. Acad. Sci. U. S. A.* 86, 6454–6458

175   Vlassov V V, Balakireva L A and Yakubov L A (1994) Transport of oligonucleotides across natural and model membranes. *BBA - Rev. Biomembr.* 1197, 95–108

176   Glover D J, Lipps H J and Jans D A (2005) Towards safe, non-viral therapeutic gene expression in humans. , *Nature Reviews Genetics*, 6(4), 299–310

177   Zhang S, Zhi D and Huang L (2012) Lipid-based vectors for siRNA delivery. *J Drug Target* 20, 724–735

178   Yin H, Kanasty R, Eltoukhy A, et al (2014) Non-viral vectors for gene-based therapy. *Nature Reviews Genetics* 15, 541–555

179   Hattori Y (2017) Progress in the development of lipoplex and polyplex modified with anionic polymer for efficient gene delivery. *J. Genet. Med. Gene Ther.* 1, 003–018

180   Barba A A, Bochicchio S, Dalmoro A, et al (2019) Lipid delivery systems for nucleic-acid-based-drugs: From production to clinical applications. *Pharmaceutics* 11, 5–7

181   Asami Y, Yoshioka K, Nishina K, et al (2016) Drug delivery system of therapeutic oligonucleotides. *Drug Discov. Ther.* 10, 256–262

182   Hong C A and Nam Y S (2014) Functional nanostructures for effective delivery of small interfering RNA therapeutics. *Theranostics* 4, 1211–1232

183   Zhou J, Shum K, Burnett J, et al (2013) Nanoparticle-Based Delivery of RNAi Therapeutics: Progress and Challenges. *Pharmaceuticals* 6, 85–107

184   Dencheva N, Denchev Z, Lanceros-Méndez S, et al (2016) One-step in situ synthesis of polyamide

microcapsules with inorganic payload and their transformation into responsive thermoplastic composite materials. *Macromol. Mater. Eng.* 301, 119–124

185   Dencheva N, Braz J, Nunes T, et al (2018) One-pot low temperature synthesis and characterization of hybrid poly(2-pyrrolidone) microparticles suitable for protein immobilization. *Polymer* 145, 402–415

186   Dencheva N, Oliveira F, Braz J, et al (2020) Bovine serum albumin-imprinted magnetic poly(2-pyrrolidone) microparticles for protein recognition. *Eur. Polym. J.* 122, 109375

187   Dencheva N, Braz J, Scheibel D, et al (2020) Polymer-assisted biocatalysis: polyamide 4 microparticles as promising carriers of enzymatic function. *Catalysts* 10, 767

188   Wu G Y and Wu C H (1988) Receptor-mediated gene delivery and expression *in vivo. J. Biol. Chem.* 263, 14621–14624

189   Wu G Y and Wu C H (1987) Receptor-mediated in vitro gene transformation by a soluble DNA carrier system. *J. Biol. Chem.* 262, 4429–4432

190   Alexis F, Pridgen E, Molnar L, et al (2008) Factors Affecting the Clearance and Biodistribution of Polymeric Nanoparticles. *Mol. Pharm.* 5, 505–515

191   Bazile D, Prud'homme C, Bassoullet M T, et al (1995) PEG-PLA nanoparticles avoid uptake by the mononuclear phagocytes system. *J. Pharm. Sci.* 84, 493–498

192   Boussif O, Lezoualc'h F, Zanta M A, et al (1995) A versatile vector for gene and oligonucleotide transfer into cells in culture and *in vivo*: Polyethylenimine. Proc Natl Acad Sci U S A 92(16), 7297-7301

193   Bozzuto G and Molinari A (2015) Liposomes as nanomedical devices. *Int. J. Nanomedicine Dovepress* 10, 975–999

194   Torchilin V P (2005) Recent advances with liposomes as pharmaceutical carriers. *Nature Reviews Drug Discovery* 4, 145–160

195   Bochicchio S, Dalmoro A, Barba A A, et al (2014) Liposomes as siRNA Delivery Vectors. *Curr. Drug Metab.* 15, 882–892

196   Zhang Y, Wang Z and Gemeinhart R A (2013) Progress in MicroRNA Delivery. *J Control Release* 172, 962–974

197   Koltover I, Salditt T, Rädler J O, et al (1998) An inverted hexagonal phase of cationic liposome-DNA complexes related to DNA release and delivery. *Science* 281, 78–81

198   Ahmad A, Evans H, Ewert K, et al (2005) New multivalent cationic lipids reveal bell curve for transfection efficiency versus membrane charge density: Lipid - DNA complexes for gene delivery. *J. Gene Med.* 7, 739–748

199   Bennett C F, Baker B, Pham N, et al (2017) Pharmacology of Antisense Drugs. *Annu. Rev. Pharmacol. Toxicol* 57, 81–105

200   Bennett C F (2019) Therapeutic antisense oligonucleotides are coming of age. *Annu Rev Med.* 70, 307-321

201   Geary R S, Norris D, Yu R, et al (2015) Pharmacokinetics, biodistribution and cell uptake of antisense oligonucleotides. *Adv. Drug Deliv. Rev.* 87, 46–51

202   Yu R Z, Grundy J S and Geary R S (2013) Clinical pharmacokinetics of second generation antisense oligonucleotides. *Expert Opin. Drug Metab. Toxicol.* 9, 169–182

203   Geary R S (2009) Antisense oligonucleotide pharmacokinetics and metabolism. *Expert Opin. Drug Metab. Toxicol.* 5, 381–391

204   Levin A A, Yu R Z and Geary R S (2007) Basic Principles of the Pharmacokinetics of Antisense Oligonucleotide Drugs. In *Antisense Drug Technology: Principles, Strategies, and Applications* Crooke S T, editor, pp. 183–215

205   Stein C A, Hansen J, Lai J, et al (2009) Efficient gene silencing by delivery of locked nucleic acid antisense oligonucleotides, unassisted by transfection reagents. *Nucleic Acids Res.* 38, 1–8

206   Hagedorn P H, Persson R, Funder E D, et al (2018) Locked nucleic acid: modality, diversity, and drug discovery. *Drug Discov. Today* 23, 101–114

207   Cantafio M, Nielsen B, Mignogna C, et al (2016) Pharmacokinetics and pharmacodynamics of a 13-mer LNA-inhibitor-miR-221 in mice and non-human primates. *Mol. Ther. - Nucleic Acids* 5(6)

208   Di Martino M T, Arbitrio M, Fonsi M, et al (2020) Allometric scaling approaches for predicting human pharmacokinetic of a locked nucleic acid oligonucleotide targeting cancer-associated miR-221. *Cancers*

(Basel). 12, 1–15

209   Geary R S, Yu R Z, Siwkowski A, et al (2008) Toxicologic Properties of 2'-O-MethoxyethylChimeric Antisense Inhibitors in Animals and Man. In *Antisense Drug Technology: Principles, Strategies and Applications*, Crooke S T, editor pp. 327-363

210   Burel S A, Hart C E, Cauntay, P, et al (2015) Hepatotoxicity of high affinity gapmer antisense oligonucleotides is mediated by RNase H1 dependent promiscuous reduction of very long pre-mRNA transcripts. *Nucleic Acids Res.* 44, 2093–2109

211   Henry S P, Seguin R, Cavagnaro J, et al (2016) Considerations for the characterization and interpretation of results related to alternative complement activation in monkeys associated with oligonucleotide-based therapeutics. *Nucleic Acid Ther.* 26, 210–215

212   Henry S P, Giclas P C, Leeds J, et al (1997) Activation of the alternative pathway of complement by a phosphorothioate oligonucleotide: potential mechanism of action. *J. Pharmacol. Exp. Ther.* 281, 810–816

213   Jason T L H, Koropatnick J and Berg R W (2004) Toxicology of antisense therapeutics. *Toxicol. Appl. Pharmacol.* 201, 66–83

214   Boye S, Pradhan A, Grant R, et al (2002) Evidence for sequence-dependent and reversible nonspecific effects of PS-capped antisense treatment after intracerebral administration. *Antisense Nucleic Acid Drug Dev.* 12, 95–102

215   Cotter F E, Waters J and Cunningham D (1999) Human Bcl-2 antisense therapy for lymphomas. *Biochim. Biophys. Acta - Gene Struct. Expr.* 1489(1), 97–106

216   Crooke S T, Baker B, Kwoh T J, et al (2016) Integrated safety assessment of 2′-O-Methoxyethyl Chimeric Antisense Oligonucleotides in NonHuman primates and healthy human volunteers. *Mol. Ther.* 24, 1771–1782

217   Frazier K S (2015) Antisense oligonucleotide therapies: the promise and the challenges from a toxicologic pathologist's perspective. *Toxicol. Pathol.* 43, 78–89

218   Henry S P, Geary R S, Yu R, et al (2001) Drug properties of second-generation antisense oligonucleotides: How do they measure up to their predecessors? *Current Opinion in Investigational Drugs*, 2(10), 1444–1449

219   Chi X, Gatti P and Papoian T (2017) Safety of antisense oligonucleotide and siRNA-based therapeutics. *Drug Discovery* 22(5), 823–833

220   Sewell K, Geary R, Baker B, et al (2002) Phase I Trial of ISIS 104838, a 2'-Methoxyethyl Modified Antisense Oligonucleotide Targeting Tumor Necrosis Factor-alfa. *J. Pharmacol. Exp. Ther.* 303(3), 1334–1343

221   Hong D S, Kurzrock R, Oh Y, et al (2011) A phase 1 dose-escalation, pharmacokinetic, and pharmacodynamic evaluation of eIF-4E antisense oligonucleotide LY2275796 in patients with advanced cancer. *Clin Cancer Res* 17(20), 6582–6591

222   Limmroth V, Barkhof F, Desem N, et al (2014) CD49d antisense drug ATL1102 reduces disease activity in patients with relapsing-remitting MS. *Neurology*, 83(20), 1780-1788

223   Jepsen J S, Sørensen M D, Wengel J (2004) Locked nucleic acid: A potent nucleic acid analog in therapeutics and biotechnology. , *Oligonucleotides*, 14(2), 130–146

224   Hagedorn P H, Yakimov V, Ottosen S, et al (2013) Hepatotoxic potential of therapeutic oligonucleotides can be predicted from their sequence and modification pattern. *Nucleic Acid Ther.* 23, 302–310

225   Kenney S P and Meng X J (2015) Therapeutic targets for the treatment of hepatitis E virus infection. *Expert Opin. Ther. Targets* 19, 1245–60

226   Stein C A and Castanotto D (2017) FDA-Approved Oligonucleotide Therapies in 2017. *Mol. Ther.* 25, 1069–1075

227   Kilanowska A and Studzí S (2020) In vivo and in vitro studies of antisense oligonucleotides-a review. *RSC Advances* 10, 34501

228   Goyon A, Fountain K, Budman Y, et al (2003) Characterization of therapeutic oligonucleotides by liquid chromatography. *Journal of Pharmaceutical and Biomedical Analysis*, 13(4), 229-243

229   Anderson K P, Fox M C, Brown-Driver V, et al (1996) Inhibition of human cytomegalovirus immediate-early gene expression by an antisense oligonucleotide complementary to immediate-early RNA. *Antimicrob Agents Chemother.* 40(9), 2004-2011

230   Mulamba G B, Hu A, Azad R F, et al (1998) Human cytomegalovirus mutant with sequence-dependent

resistance to the phosphorothioate oligonucleotide fomivirsen (ISIS 2922). *Antimicrob Agents Chemother.* 42(4), 971-973

231   Hong D, Kurzrock R, Kim Y, et al (2015) AZD9150, a next-generation antisense oligonucleotide inhibitor of STAT3 with early evidence of clinical activity in lymphoma and lung cancer. *Sci. Transl. Med.* 7(314), 314ra185

232   Reilley M J, McCoon P, Cook C, et al (2018) STAT3 antisense oligonucleotide AZD9150 in a subset of patients with heavily pretreated lymphoma: results of a phase 1b trial. *J. Immunother. Cancer* 6(1), 119

233   Shimojo M, Kasahara Y, Inoue M, et al (2019) A gapmer antisense oligonucleotide targeting SRRM4 is a novel therapeutic medicine for lung cancer. *Sci. Rep.* 9, 7618

234   Chi K N, Higano C S, Blumenstein B, et al (2017) Custirsen in combination with docetaxel and prednisone for patients with metastatic castration-resistant prostate cancer (SYNERGY trial): a phase 3, multicentre, open-label, randomised trial. *Lancet Oncol.* 18, 473–485

235   Keiser M S, Kordasiewicz H B and McBride J L (2016) Gene suppression strategies for dominantly inherited neurodegenerative diseases: lessons from Huntington's disease and spinocerebellar ataxia. *Hum. Mol. Genet.* 25, R53–R64

236   Good L and Nielsen P E (1998) Antisense inhibition of gene expression in bacteria by PNA targeted to mRNA. *Nat. Biotechnol.* 16, 355–358

237   Patenge N, Pappesch R, Krawack F, et al (2013) Inhibition of growth and gene expression by PNA-peptide conjugates in Streptococcus pyogenes. *Mol. Ther. - Nucleic Acids* 2(11), e132

238   Wesolowski D, Alonso D and Altman S (2013) Combined effect of a peptide-morpholino oligonucleotide conjugate and a cell-penetrating peptide as an antibiotic. *Pnas* 110(21), 8686–8689

239   Liang S, He Y, Xia Y, et al (2015) Inhibiting the growth of methicillin-resistant Staphylococcus aureus in vitro with antisense peptide nucleic acid conjugates targeting the ftsZ gene. *Int. J. Infect. Dis.* 30, e1–e6

240   Singh P and Panda D (2010) FtsZ inhibition: a promising approach for antistaphylococcal therapy. *Drug News Perspect.* 23, 295–304

241   Sully E K and Geller B L (2016) Antisense antimicrobial therapeutics. *Curr. Opin. Microbiol.* 33, 47–55

242   Testa S, Disney M, Gryaznov S, Turner D (2000) Methods and compositions for inhibition of rna splicing WO2000055374

Chapter II

Exploitation of the antisense oligonucleotides to control *Candida albicans* filamentation

Main goal

To explore the second (2'-*O*Methyl) and third (LNA) generation of antisense oligonucleotides modifications to control *Candida albicans* switch from yeast to filamentous forms.

Chapter II.1

Application of 2'-*O*MethylRNA antisense oligonucleotide to control *Candida albicans EFG1* virulence determinant

Main goal

To design an antisense oligonucleotide based on the second generation of antisense oligonucleotides targeting the *EFG1* mRNA of *Candida albicans* and to validate *in vitro* its applicability through filamentation enumeration, *EFG1* gene expression and Efg1p protein translation.

Conclusions

This study validated the possibility to use antisense oligonucleotides with 2'OMe chemical modifications to control *C. albicans* virulence determinants. The anti-*EFG1* 2'OMe ASO was able to significantly reduce *EFG1* gene expression and Efg1p protein translation, and effectively prevent *C. albicans* cell filamentation, even in different simulated human body fluids.

II.1.1 Introduction

As referred previously (Chapter I), candidiasis is the primary fungal disease, with a mortality rate of about 30-50 % and with costs associated with hospitalized patients that range from €5,700 to €85,000 (in U.S. dollars, approximately $6,286 to $93,752) per episode [1,2]. This important clinical, social and economic problem is due to the recognized phenomenon of *Candida* species antifungal resistance, associated with the indiscriminate use of traditional antifungal agents [1–3]. *Candida albicans* remains the most prevalent of all *Candida* species in Europe, with a range of incidence of around 40 % [2,4,5]. The pathogenicity of *C. albicans* is supported by a series of virulence factors, one of the most alarming being its ability to switch from yeast to filamentous forms, a tightly regulated process by a network of genes known as dimorphic switching [6]. This virulence factor requires *C. albicans* to sense and respond to the host environment and is essential for its pathogenicity [7–9]. *EFG1* is one of the most important and well-studied regulator genes involved in *C. albicans* filamentation [10–15].

As a consequence of the rising levels of *C. albicans* multi-resistance to the traditional antifungal treatments, new alternative therapies, with novel mechanisms of action, enhanced therapeutic potential, improved pharmacokinetics, and less toxicity, are urgently needed [16,17]. Antisense therapy (AST) holds great promise for the treatment of many human chronic non-infectious diseases; [18–24] however, for controlling *Candida* species growth, the knowledge is scarce [23,25]. Moreover, the control of yeast virulence determinants has never been exploited before with AST. The concept underlying AST is relatively straightforward: the use of a complementary sequence to a specific mRNA that can inhibit gene expression, inducing a blockage in the transfer of genetic information from DNA to protein [26].

Antisense oligonucleotides (ASOs) are simply short strands of nucleic acids that have a sequence that is complementary to the target mRNA, and that bind to this target by means of standard Watson-Crick base pairing [26]. Up to now, there have been three generations of ASOs [24-26] with several chemical modifications in order to increase its nuclease resistance, reduce its toxicity, and enhance its affinity and half-life [22]. The 2'-*O*MethylRNA (2'OMe) sugar modification belongs to the second generation of acid mimics; however, these do not support RNase H activity (a specific degradation mechanism cleaving the target mRNA) [27,28]. An insertion of a longer central unmodified region, known as *gapmers*, has been used as a popular strategy to allow that RNase to join and activate the degradation of the mRNA target [29,30].

Thus, this work is based on that if a pathogen's genetic sequence of a specific gene is a determinant of virulence, as is the case with the *EFG1* gene, it will be possible to synthesize a nucleic

acid mimic that will bind to the mRNA produced and degrade it, blocking its translation into protein and, consequently, reducing its virulent phenotype (which, in this case, would be the filaments development).

II.1.2 Materials and Methods

a. Microorganisms

A total of 11 clinical strains (Figure II.1.1 A), including *Candida albicans* (n=10) and *Saccharomyces cerevisiae* (n=1), recovered from different body sites, were used during this study. All isolates were recovered from vaginal, urinary, and oral tracts and were obtained from *Candida* collection of the Biofilm group of the Centre of Biological Engineering, University of Minho, Braga, Portugal. Four reference strains - *Candida albicans* (SC5314), *Candida parapsilosis* (ATCC 22019)*, Candida tropicalis* (ATCC 750) and *Candida glabrata* (ATCC 2001)- were included in this study. The mutant strain *C. albicans* ΔΔefg1 (HLC52) was also tested [31].

b. Growth conditions

For all experiments, yeast strains were subcultured on sabouraud dextrose agar (SDA; Merck, Darmstadt, Germany) and incubated for 24 h at 37 °C. Cells were then inoculated in sabouraud dextrose broth (SDB; Merck, Darmstadt, Germany) and incubated overnight at 37 °C, 120 rpm. After incubation, the cells' suspensions were centrifuged for 10 min at 3000 g at 4 °C and washed twice with phosphate-buffered saline (PBS, pH 7, 0.1 M). Pellets were suspended in 5 mL of Roswell Park memorial institute 1640 medium (RPMI, pH 7, Sigma-Aldrich, St Louis, USA), and the cellular density was adjusted for each experiment using a *Neubauer* chamber (Paul Marienfild, Lauda-Königshofen, Germany) to 1×10^5 or 1×10^6 cells mL^{-1}. All experiments of this work were performed in triplicate and in a minimum of three independent assays.

c. Design and synthesis

To design a specific ASO for *C. albicans EFG1*, the target region of the gene was selected based on a search conducted at the *Candida* Genome Database (CGD) (http://www.candidagenome.org/cgi-bin/compute/blast_clade.pl). Several *EFG1* gene sequences were aligned to make sure that conserved regions were used for the design. Also, a BLAST search was performed to ensure that the sequences were not targeting any sequence of the human genome or a similar region in another *C. albicans* gene. The *EFG1* sequence **5'-ACAATAACGGTATGCC-3'** was selected as the target, taking into account its

high specificity to the *C. albicans* genome, its non-binding against the *Homo sapiens* genome, and the number of nucleotides [26]. Specific ASOs were then designed for the use of 2' ribose modification. 2'OMe was selected, since it is one of the most used for antisense applications [28–30,32]. A gapmer was introduced to increase the odds of activating RNase H activity [33]. The calculator from Integrated DNA Technologies (IDT: http://eu.idtdna.com/calc/analyzer) was used to determine the theoretical Tm and the GC content of the possible ASO for that target region. The selected ASO was produced according to the user's own specifications at EXIQON and purified by high-pressure liquid chromatography (HPLC). The same ASO was synthetized with an orange-fluorescent fluorophore (TYE563). A scrambled ASO, similar to the *EFG1* ASO, was also synthesized to be used as negative control.

d. Sensitivity and specificity tests

The sensitivity and specificity of anti-*EFG1* 2'OMe ASO was determined against different yeast strains (Figure II.1.1 A) by fluorescence *in situ* hybridization (FISH) [34]. For that, 20 µL of an inoculum of *Candida* cells adjusted to 1 x 10^6 cells mL^{-1} were transferred to a slide and fixated with 30 µL 4 % (v/v) paraformaldehyde (Sigma-Aldrich) for 10 min, and the excess was removed. After that, cells were permeabilized with 30 µL 50 % (v/v) ethanol for an additional 10 min and allowed to air dry. The hybridization step was performed with 20 µL ASO (200 nM) coupled with orange-fluorescent fluorophore diluted in hybridization solution (900 nM NaCl [Panreac Applichem, Barcelona, Spain], 30 % formamide [Sigma-Aldrich, Sintra, Portugal], 20 mM Tris-HCl [Sigma-Aldrich, Sintra, Portugal], and 0.01 % SDS (Sigma-Aldrich, Sintra, Portugal]). Negative controls were prepared only with 20 µL hybridization solution without probe. Samples were then covered with coverslips and incubated at 37 °C for 3 h in dark conditions. After hybridization, slides were submerged in wash solution (20 mM Tris-HCl, 0.01 % SDS, and 900 mM NaCl) and incubated for 30 min at the same temperature.

The images from cells were acquired with an epifluorescence microscope (Olympus Portugal, Porto, Portugal). Cells were observed using a 40x objective. The exposure time, gain, and saturation values were fixed for each sample. The TRITC filter (530-550/591) was used for images acquisition.

e. Cytotoxicity

In order to select the concentration of anti-*EFG1* 2'OMe without cytotoxicity to be used during this study, the ASO cytotoxicity was determined against 3T3 cell line (fibroblast cells, embryonic tissue, mice from the CCL 163 line, American Type Culture Collection). For that, 3T3 cells were grown in Dulbecco's modified eagle medium (DMEM, Biochrom, Berlin, Germany) supplied by 10 % fetal bovine serum (FBS;

Sigma-Aldrich) and 1 % antibiotic containing P/S (penicillin and streptomycin; Biochrom, Berlin, Germany). After detachment, a suspension with 1×10^5 cells mL^{-1} was added to a 96-well plate, and cells grew until attaining 80 % confluence. Prior to the cytotoxicity assay, the wells were washed twice with PBS. Different concentrations of ASO (10, 20, 40 and 60 nM) were prepared in DMEM, and 50 µL of each concentration was added to each well. Negative control was performed by adding 50 µL of DMSO to the cells, and positive control was performed by adding 50 µL of DMEM. The plates were incubated for 24 h at 37 °C and 5 %CO_2.

After incubation, 10 µL of 3-(4,5-dimethylthiazol-2-yl)-5-(3-carboxymethoxyphenyl)-2-(4-sulfophenyl)-2H-tetrazolium solution (MTS, CellTiter 96 Aqueous One Solution Cell Proliferation Assay, Promega) and 1 % DMEM without phenol was added to each well and incubated during 1 h. Lastly, the absorbance was measured at 490 nm in a microplate reader (Biochrom EZ Reader 800 Plus, Biochrom, Cambridge, England). The cytotoxicity results were expressed as the percentage of viable cells corresponding the optical density 490 (OD$_{490}$) of cells grown without ASO as 100 % cell viability.

f. Effect on *C. albicans* filamentation

In parallel, to determine the effect on *C. albicans* filamentation, the similar concentrations of the ASO (10, 20 and 40 nM) were incubated with *C. albicans* SC5314, and the effects were evaluated in terms of filaments number. For this, 100 µL of ASO at the different concentrations prepared in RPMI medium were added to each well of a 96-well plate (Orange Scientific, Braine-l'Alleud, Belgium) together with 100 µL of 1×10^6 cells mL^{-1} of *Candida* cell suspensions. The positive controls were prepared with 200 µL of cells in RPMI medium without the addition of ASO, and the negative controls were prepared only with RPMI medium. In addition, the scrambled ASO was used as control. The ASO effects were evaluated at 4, 6 and 8 h of incubation.

To determine the percentage of filamentation, *Candida* cells were scraped from each well, and the filaments were enumerated using a Neubauer chamber by optic microscopy. The results were presented as percentage of filamentation reduction through the following formula:

$$\% \text{ of filamentation inhibition} = \frac{\% \text{ filament cells (control)} - \% \text{ filament cells (ASO)}}{\% \text{ filaments cells (control)}}$$

g. Effect on *EFG1* gene expression

Reverse transcription-qPCR studies were performed to determine the effect of 40 nM ASO on *EFG1* gene expression. For that, in 24-well plates (Orange Scientific, Braine-l'Alleud, Belgium), 500 µL *C.*

albicans cells at 1 x 10⁶ cells mL⁻¹ were incubated with 500 µL ASO for the same periods of time. After each time point, the cells were collected from each well, recovered by centrifugation for 5 min at 7000 g and 4 °C, and washed once with sterile water. RNA extraction was performed using the PureLink RNA Mini Kit (Invitrogen, Carlsbad, CA, USA) [35,36]. Then, to avoid potential DNA contamination, samples were treated with DNase I treatment (DNase I, Amplification Grade, Invitrogen), and RNA concentration was determined by optical density measurement with the NanoDrop 1000 Spectrophotometer (Thermo Fisher Scientific). The complementary DNA (cDNA) was synthetized using the iScript Reverse Transcriptase (Bio-rad) in accordance with the manufacturer's instructions. qRT-PCR (CFX96, Biorad) was performed on a 96-well microtiter plate using EvaGreen Supermix (Bio-rad, Berkeley, CA, USA). The expression of the *EFG1* gene was normalized with the *ACT1 Candida* reference gene [37]. No-reverse transcriptase (NRTs) controls and no-template controls (NTC) were included in each run. Each reaction was performed in triplicate, and mean values of relative expression were determined for each gene. The primers were designed using the Primer 3 web-based software (http://www.bioinformatics.nl/cgi-bin/primer3plus/primer3plus.cgi) and are described in Table II.1.1.

Table II.1.1 Primers used for qRT-PCR, with the respective theoretical Tm obtained from the calculator from IDT and amplification product

Candida albicans Gene	Systematic Name	Sequence (5'-3')	Primer	Tm (°C)	AP (BP)
EFG1	CR_07890W_A / Orf19.610	5'-TTCTGGTGCAGGTTCCAC-3'	Forward	57	168
		5'-CCTGGTTGTGATGCAGGT-3'	Reverse		
ACT1	C1_13700W_A / Orf19.5007	5'-AATGGGTAGGGTGGGAAAAC-3'	Forward	57	150
		5'-AGCCATTTCCATTGATCGTC-3'	Reverse		

AP, amplification product; **BP**, base pairs.

h. Performance

In order to evaluate the performance of the anti-*EFG1* 2'OMe throughout the study, *C. albicans* SC5314 was incubated with 40 nM of ASO for 24 h. For that, 5 mL of anti-*EFG1* 2'OMe at 40 nM prepared in RPMI medium was added to 5 mL of a *C. albicans* SC5314 suspension at 1 x 10⁵ cells mL⁻¹ and incubated at 37 °C under gentle agitation (120 rpm). The positive control was prepared only with 10 mL of the same concentration of cells. At pre-determined time points (6, 8, 10 and 24 h) aliquots were

recovered, and three complementary criteria were evaluated: percentage of filamentation reduction at 6, 8, 10 and 24 h; levels of *EFG1* expression and Efg1 protein translation at 24 h of incubation.

The ASO effect on *C. albicans* filamentation and on levels of *EFG1* gene expression were evaluated as described previously. For that, the number of filaments of cells grown in the presence and absence of ASO was enumerated, and RNA was extracted from those cells to quantify the levels of *EFG1* gene expression. Epifluorescence microscopy images were used to confirm the levels of filamentation and to determine the length of the filaments. *C. albicans* cells grown in the presence and absence of ASO were stained 1 % (v/v) of calcofluor (Sigma-Aldrich, St. Louis, MO, EUA) for 15 min in dark conditions. Consequently, the cells were centrifuged for 5 min and washed twice with ultra-pure water. All samples were observed with an Olympus BX51 microscope (Olympus Portugal, Porto, Portugal) coupled with a DP71 digital camera. A specific filter 360-370/421 (blue channel) was used, and the images were acquired with the program FluoView FV100 (Olympus). The length of the filaments was determined using ImageJ plug-in (Maryland, USA) software.

i.   Effect on Efg1p translation

Liquid chromatography (LC)-MALDI-TOF-mass spectrometry (MS) (Q-Exactive Orbitrap, Thermo Fisher Scientific) was used to infer about the effect of ASO in the translation of respective genes into a protein (Efg1p) [38]. For that, the proteome of *C. albicans* cells grown in the presence and absence of the ASO was obtained as described previously [39], with some modifications. Cells were obtained by centrifugation for 5 min, at 8000 g and 4 °C, and washed twice with sterile ice-cold ultrapure water. Then, cells were washed with lysis buffer (10 mM Tris-HCl [pH 7.4], 1 mM phenylmethylsulfonyl fluoride [PMSF]) and resuspended in ice-cold lysis buffer in order to lyse mechanically, with an equal volume of glass beads in a cell homogenizer (FastPrep, MP biomedicals), four times. Lysed cells were separated by centrifugation at 1000 g for 10 min at 4 °C, and the pellet was washed twice with each of the following ice-cold solutions: 1 mM PMSF and 5 % NaCl (Thermo Fisher Scientific, Waltham, MA, USA) and 1 mM PMSF in ultrapure water. Then, it was resuspended in washing buffer (50 mM Tris HCl (pH 8), 1 mM PMSF) and extracted by boiling with SDS extraction buffer (50 mM Tris-HCl (pH 8.0), 0.1 M EDTA, 2 % SDS, 10 mM DTT) for 10 min. Finally, the supernatant was transferred to fresh tubes, and the protein concentration was determined using the Pierce BCA Protein Assay Kit (Thermo Fisher Scientific).

Proteins samples were analysed by nano-LC-MS/MS (tandem MS) in order to identify and quantify Efg1p and Act1p. Firstly, protein sample were digested based on the filter-aided sample preparation (FASP) procedure described by Wiśniewski and colleagues [40], with some modifications. Protein

digestion with trypsin/Lys-C mix was performed overnight at 37 °C (Promega, Madison, WI, USA), and each reaction was stopped with 1 % (w/v) trifluoroacetic acid (TFA). Peptides were then recovered by centrifugation, followed by an additional centrifugation step with 0.1 % TFA. Next, peptide samples were cleaned up and concentrated by SPE-C18 chromatography. Nano-LC-MS/MS equipment, composed by an Ultimate 3000 LC system coupled to a Q-Exactive Hybrid Quadrupole-Orbitrap mass spectrometer (Thermo Fisher Scientific, Bremen, Germany), was used to identify and quantify the proteins [41]. Samples were loaded onto a trapping cartridge (Acclaim PepMap 100 C18 [pore size, 100Å, 5 mm x 300 μm i.d.], catalog no. 160454, Thermo Fisher Scientific) in a mobile phase of 2 % acetonitrile (CAN), 0.1 % formic acid (FA) at 10 μL min^{-1}. Data acquisition was controlled by Xcalibur 4.0 and Tune 2.8 software (Thermo Fisher Scientific, Bremen, Germany).

The raw data was processed using Proteome Discoverer v2.2.0.388 software (Thermo Fisher Scientific) and searched against the UniProt database for the taxonomic selection *C. albicans* (November 2017 release). The Sequest HT search engine was used to identify tryptic peptides. The percentage of Efg1p translation was determined by the ratio of the media of the peptides area of Efg1p and the media of the peptides area corresponding to Act1p (used as reference protein).

j.   Performance on simulated human body fluids

To mimic the human body fluids, artificial saliva (AS), artificial urine (AU) and horse blood were used during this work. AU (pH 5.8) and AS (pH 6.8) were prepared with slight modifications to that previously described by Silva *et al.* in their 2010 and 2013 studies, respectively [42,43]. The composition of the AU was $CaCl_2$ (0.65 g/L), $MgCl_2$ (0.65 g/L), NaCl (4.6 g/L), Na_2SO_4 (2.3 g/L), $Na_3C_3H_5O (CO_2)_3$ (0.65 g/L), $Na_2C_2O_4$ (0.02 g/L), KH_2PO_4 (2.8 g/L), KCl (1.6 g/L), NH_4Cl (1.0 g/L), urea (25 g/L), creatinine (1.1 g/L) and glucose (3 g/L); and the composition of AS was peptone (5 g/L), glucose (2 g/L), mucin (1 g/L), NaCl (0.35 g/L), $CaCl_2$ (0.2 g/L) and KCl (0.2 g/L). The blood used was defibrinated horse blood (Probiológica-Empresa de Produtos Biológicos, Belas, Portugal) supplemented with 50 % of 0.9 % NaCl.

Pellets obtained as described earlier were resuspended in 10 mL of each body fluid after adjusting the cellular density to 1 x 10^6 cells mL^{-1}, using a Neubauer haemocytometer (Paul Marienfeld, Lauda-Königshofen, Germany) and incubated for 24 h (AS and AU) and 48 h (horse blood) at 37 °C in Erlenmeyer flasks, under gentle agitation (120 rpm). RPMI medium was used as positive control. All experiments were performed in triplicate and in a minimum of three independent assays.

To determine whether anti-*EFG1* 2'OMe maintains its performance on different simulated human body fluids, its ability to inhibit *C. albicans* filamentation and reduce *EFG1* expression was determined.

For that, at pre-determined time points (6, 8, 10 and 24 h for AS and AU and 48 h for horse blood), aliquots of each suspension were recovered, and the cells harvested by centrifugation at 3000 g for 10 min at 4°C and washed twice with PBS. To determine the percentage of filamentation, *Candida* cells that formed filaments were enumerated using a *Neubauer* chamber, as described earlier.

To determine the effect on *C. albicans EFG1* gene expression, qRT-PCR studies were evaluated at 24 h (for AS, AU and RPMI medium) and 48 h (for horse blood) of incubation. The extraction of RNA and qRT-PCR were performed as described earlier. Simultaneously, it was evaluated *C. albicans* capability for growing on the different simulated human body fluids by colony-forming unit (CFU) determination methodology. For that, 1 mL of each suspension was recovered, and cells were harvested by centrifugation at 3000 g for 10 min at 4 °C and washed twice with PBS. Serial dilutions were performed on PBS, inoculated onto SDA, and incubated for an additional 24 h at 37 °C. The results were presented as the log of CFUs cm^{-2}.

k. Statistical analysis

Data are expressed as the mean ± standard deviation of at least three independent experiments. The results were statistically analysed using GraphPad Prism® (GraphPad Software, San Diego, CA, USA). For that, the results obtained of filamentation inhibition and *EFG1* gene expression at 4, 6 and 8 h were compared using two-way ANOVA and Tukey and Sidak's multiple comparisons tests, respectively. The results obtained in the planktonic cells in RPMI were compared using one-way ANOVA and Sidak's multiple comparisons tests for the filamentation analysis and using t-test analysis for *EFG1* gene expression. The results obtained in the planktonic cells in simulated human body fluids were compared using two-way ANOVA and Tukey and Sidak's multiple comparisons tests for filamentation inhibition and *EFG1* gene expression, respectively. All tests were performed with a confidence level of 95 %.

II.1.3 Results and Discussion

Despite an increasing number of successful applications of AST for the treatment of human chronic non-infectious diseases [20–22,24,44–50], and, more recently, to manage infectious bacteria [44,51,52], this methodology was never exploited to control *Candida* species virulence factors. Moreover, *EFG1* has been reported as one of the most relevant virulence determinants involved in *C. albicans* filamentation and, consequently, in its pathogenicity [6,10–15]. This makes *EFG1* an ideal target for

validating an AST approach against *Candida*, not only because its role has been repeatedly proved but also because morphological changes can be easily examined.

Thus, based on the key hypothesis, it is intended with this work to validate *in vitro* the application of a 2'OMe ASO to control *C. albicans* switching from yeast to filamentous forms, reducing the mRNA produced by the *EFG1* gene, and inactivate its translation into Efg1p.

a. Anti-*EFG1* 2'OMe characterization

Nucleic acid mimics, in particular, the 2'OMe were the base for the design of the anti-*EFG1* ASO [26]. It has been described that the nucleic acid mimics must be designed with melting temperatures (Tm) around 39-42 °C and a guanine-cytosine (GC) content of approximately 50 % to 60 % in order to increase the binding affinity for target mRNA and stability in the human body [26,30]. Furthermore, several studies have shown that ASOs with sizes between 12 and 20 nt (nucleotides) usually present a good hybridization performance [53]. Taking account these features, the anti-*EFG1* 2'OMe sequence was the **5'-mG mG mC mA TACCGTTA mU mU mG mU-3'** (m – 2'OMe), with a theoretical Tm of 41.1 °C, 43.8 % of GC, and a total of 16 nt (Table II.1.2). Four 2'OMe chemical modifications were added to each end of the sequence to increase the stability of the ASO while maintaining the ability to recruit RNase H to degrade the mRNA [48]. Being a synthetic molecule, 2'OMe is not recognized by the RNase H, but a small DNA gap in the middle of the ASO ensures the enzyme binding. This way, the ASO will act not only by directly blocking the protein synthesis but also by promoting the degradation of the target mRNA.

Table II.1.2 Sequence of anti-*EFG1* 2'OMe (m) and scramble ASO, with the respective size, theoretical melting temperature (Tm) and GC content

ASO	Sequence (5'-3')	Size	Tm (°C)	% of GC
Anti-*EFG1* 2'OMe	5'-mG mG mC mA TACCGTTA mU mU mG mU-3'		41.1	
		16		43.8
Scramble ASO	5'-mG mG mC mA TTCCAGTA mU mU mG mU-3'		41	

A scramble ASO with the same number of nucleotides and chemical modifications (**5'-mG mG mC mA TTCCAGTA mU mU mG mU-3'**) was also synthetized with three mismatches, resulting in a theoretical Tm of 41 °C and 43.8 % of GC (Table II.1.2). Furthermore, the anti-*EFG1* 2'OMe was labelled with TYE563 at the 5' end to investigate its cellular uptake, sensitivity, and specificity.

b. Anti-*EFG1* 2'OMe cellular uptake, sensitivity and specificity

Sensitivity and specificity of the nucleic acid mimics are two important factors to the success of the ASO applicability [54–56]. In this study it was used the FISH test, a standard methodology used to identify microorganisms that makes use of nucleic acid coupled with fluorochromes [57–60], and epifluorescence analysis to evaluate the anti-*EFG1* 2'OMe cellular uptake, sensitivity and specificity against *C. albicans* cells.

The anti-*EFG1* 2'OMe specificity was tested against 10 strains of *C. albicans* and other 4 strains of other fungi (Figure II.1.1). Anti-*EFG1* 2'OMe binding in *C. albicans* was confirmed by the positive signal (presence of fluorescence) observed for all *C. albicans* strains tested (n = 10) (Figure II.1.1 A and II.1.1 B; Figure AI.1). The negative signal (absence of fluorescence) obtained for the other fungi tested and for *C. albicans ΔΔefg1* reinforces ASO specificity for *C. albicans* cells (Figure II.1.1).

A

Species	Strains	Origin	FISH results
	SC5314	Reference	+
	324LA/94	Oral cavity	+
	569322	Vaginal	+
	541863	Urinary tract	+
	557834	Vaginal	+
Candida albicans	545547	Urinary tract	+
	547096	Urinary tract	+
	552401	Urinary tract	+
	575541	Urinary tract	+
	568426	Expectoration	+
	ΔΔefg1		-
Candida parapsilosis	ATCC 22019	Reference	-
Candida glabrata	ATCC 2001	Reference	-
Candida tropicalis	ATCC 750	Reference	-
Saccharomyces cerevisiae	BY4741	Reference	-

B

Figure II.1.1 Anti-*EFG1* 2'OMe sensitivity and specificity obtained by FISH. (A) List of strains and species used and their origin, as well as the respective results obtained by FISH at 37 °C, during 3 h. **(B)** Illustrative images obtained by epifluorescence microscopy. The exposure time was the same for each strain: *Candida albicans* SC5314 were obtained with 218.7 ms; *Candida albicans* HLC52 (ΔΔefg1 mutant strain) with 713.2 ms, and *Candida tropicalis* ATCC750 with 293.9 ms of exposure. Negative controls were prepared only with 20 μL of hybridization solution without probe.

These studies demonstrate the anti-*EFG1* 2'OMe *Candida* cellular uptake without carriers or transfection agents for instance, by adsorptive endocytosis as in other microorganisms [61–63], and its ability to hybridize with the respective target with high specificity for *C. albicans* cells.

c. Anti-*EFG1* 2'OMe ASO behaviour

In order to determine the concentration of anti-*EFG1* 2'OMe to be used *in vitro* validation studies, *C. albicans* SC5314 was incubated with different concentrations of ASO (10-60 nM) (Figure II.1.2). Additionally, the same was applied to investigate the cytotoxic effect of the ASO on 3T3 cell line (Figure II.1.2 A).
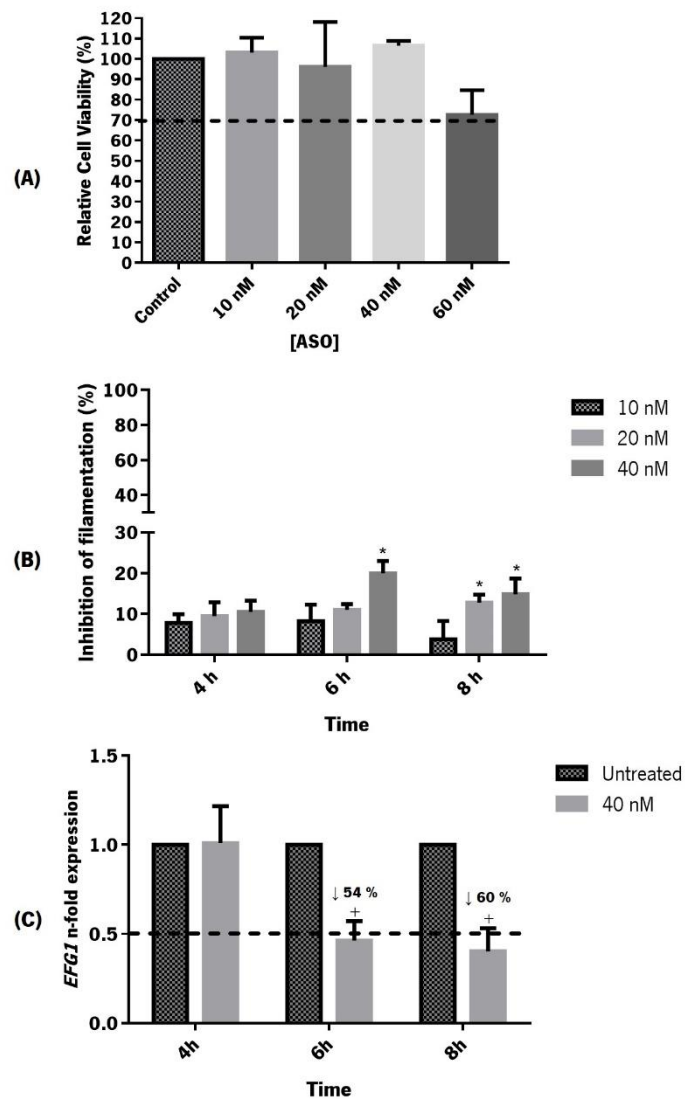
Figure II.1.2 Anti-*EFG1* 2'OMe effect on *Candida albicans* filamentation. (A) Relative cell viability (%) determined by the absorbance values (Abs; 490 nm cm^{-2}) of formazan product obtained from 3T3 cells treated with different concentrations of ASO (10, 20, 40, and 60 nM). The control is related to the cells without ASO treatment.

(B) Percentage of inhibition (%) of filamentous forms, after treatment with different concentration of ASO (10, 20, and 40 nM). **(C)** Levels of *EFG1* gene expression obtained by Pfaffl method, after application of 40 nM ASO, at different time points (4, 6 and 8 h) in RPMI. Error bars represent standard deviation. *Significant differences among 10 nM and the other concentrations of ASO tested (P-value< 0.05). +Significant differences between untreated and treated cells (P-value< 0.05).

Cytotoxicity evaluation

Figure II.1.2 A presents the results of ASO cytotoxicity on the 3T3 cell line for the determination of the minimal ASO concentration capable to inhibit *C. albicans* filamentation and *EFG1* gene expression.

MTS assays were performed to infer about the anti-*EFG1* 2'OMe cytotoxicity against 3T3 cells. The results demonstrated that the ASO concentrations of 10, 20, and 40 nM tested were not cytotoxic, since the relative cell viability is higher than 70 % of the control (absence of ASO) (Figure II.1.2 A) [64]. However, the relative cell viability for 60 nM is approximately 70 %, so it could be considered a cytotoxic concentration. Therefore, it was decided to use 40 nM of ASO for the next experimental assays.

Effect on filamentation and gene expression

Concerning the anti-*EFG1* 2'OMe effect on *C. albicans* filamentation, it was possible to verify a reduction for all the concentrations tested (Figure II.1.2 B). As expected, the percentage of filamentation of *C. albicans* without ASO increased from 4 h to 8 h, reaching 80% filamentation (Figure AI.2 A). In the presence of ASO, after 4 h of incubation, approximately 10% reduction was observed (Figure II.1.2 B) without statistically differences among the ASO concentrations tested (P-value>0.05). Additionally, the results revealed a more pronounced effected after 6 h, specifically with 40 nM ASO, with approximately 20 % reduction (P-value<0.05). After 8 h of incubation, a similar performance was observed with 15 % of reduction, even for the lower concentration (20 nM) of ASO. Additionally, the ASO scramble was unable to reduce *C. albicans* filamentation (Figure AI.3).

The *EFG1* expression levels were determined for *C. albicans* SC5314 cells growing in the presence and the absence of 40 nM of ASO in order to evaluate the effect of anti-*EFG1* 2'OMe in the blockage of the expression of the respective gene. As expected, this strain expresses the *EFG1* gene and a 3-fold increase on its expression levels was noticed from 4 h to 8 h (Figure AI.2 B). Regarding ASO treatment, qRT-PCR studies revealed a decrease on the levels of *EFG1* expression after 6 h and 8 h (P-value<0.05) (Figure II.1.2 C). Indeed, a reduction of 54 % at 6 h and 60 % at 8 h on the *EFG1* levels of expression was demonstrated (P-value<0.05).

After defining the most appropriate concentration of anti-*EFG1* 2'OMe to be used (40 nM), it was evaluated the performance of the ASO on longer periods (Figure II.1.3). In terms of *C. albicans* filamentation reduction (Figure II.1.3 A), the results showed an increase on inhibition over time, reaching 80 % after 24 h of treatment (P-value<0.05) compared to the absence of ASO. It is important to address that the dimorphic switching in *C. albicans* is dependent on a network of genes [12,14,65–68]. Thus, it was not expected a total reduction on *C. albicans* filamentation. Subsequent examination of epifluorescence microscopy images confirms these results and also revealed a significant and relevant decrease in terms of the filaments' length (74 μm to 34 μm at 6 h, 81 μm to 54 μm at 8 h, 68 μm to 37 μm at 10 h and 143 μm to 56 μm at 24 h of treatment) (Figure II.1.3 D). This is an important result once *C. albicans* filamentation is considered one of the most problematic virulence factors, increasing its capability to invade human cells and causing tissue damage [69,70].
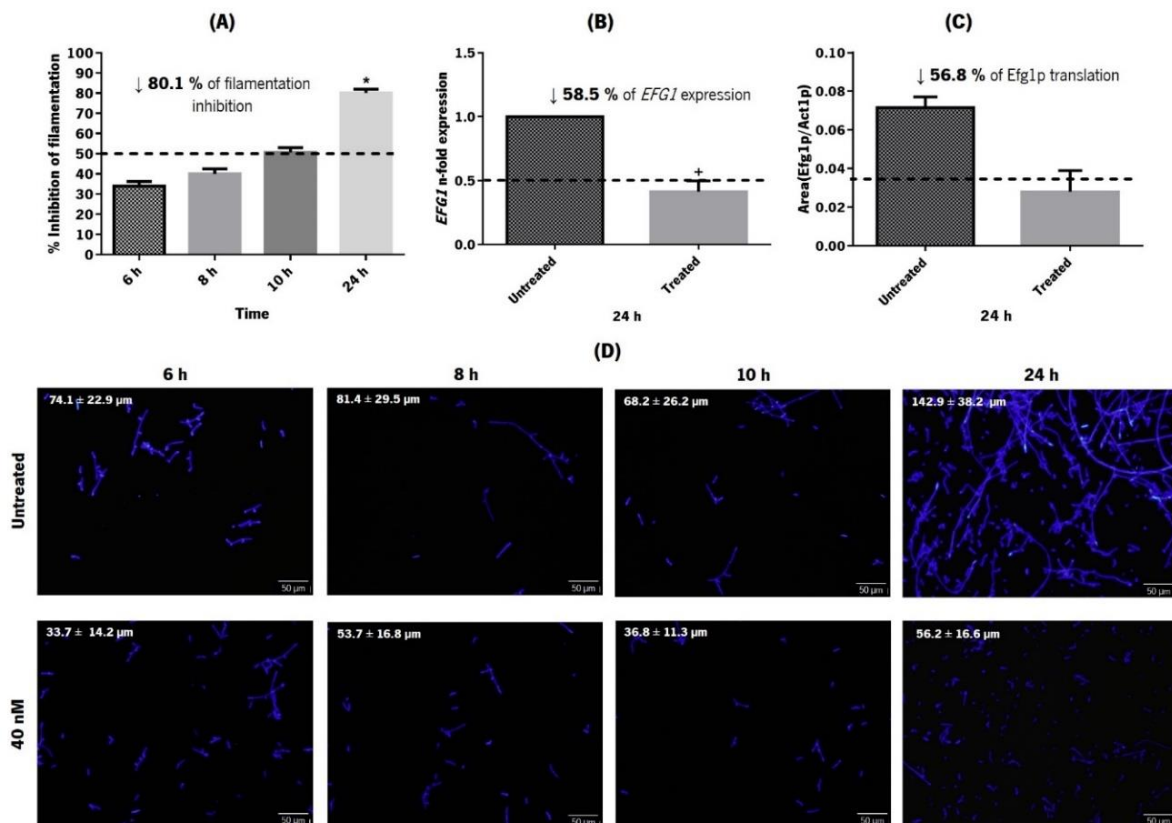
Figure II.1.3 Anti-*EFG1* 2'OMe effect on Efg1p translation. **(A)** Percentage inhibition (%) of filamentous forms at different time points (6, 8, 10, and 24 h). **(B)** Levels of *EFG1* gene expression obtained by the Pfaffl method at 24 h. **(C)** Levels of Efg1p translation normalized with the translation of Act1p at 24 h. **(D)** Epifluorescence microscopy images of *Candida* cells stained with Calcofluor after treatment with 40 nM ASO (control was prepared only with cells in RPMI; without ASO). The assays were performed for *C. albicans* SC5314. Error bars represent standard deviation. *****Significant differences between 6 h and the other times tested (P-value<0.05). +Significant differences between untreated and treated cells (P-value<0.05).

As mentioned earlier, ASOs affect cellular functions through transcription attenuation and protein translation inhibition [71–74]. The effect of anti-*EFG1* 2'OMe on *EFG1* gene expression and Efg1 protein translation were determined at 24 h of treatment (Figure II.1.3 B and II.1.3 C), as data from filamentation indicated this treatment time as quite effective. The results obtained showed a significant reduction in levels of *EFG1* expression (around 59%) (Figure II.1.3 B) and in Efg1p protein translation (around 57 %) (Figure II.1.3 C), corroborating the morphological data (Figure II.1.3 A and II.1.3 D).

Performance on simulated human body fluids

To mimic human body environments, the performance of anti-*EFG1* 2'OMe was also evaluated on different simulated human body fluids (AS and AU) and horse blood (Figure II.1.4). It is important to highlight that *C. albicans* was able to grow and filament in all simulated human body fluids tested, but in a time- and fluid-dependent manner (Figure AI.4 A and AI.4 B).
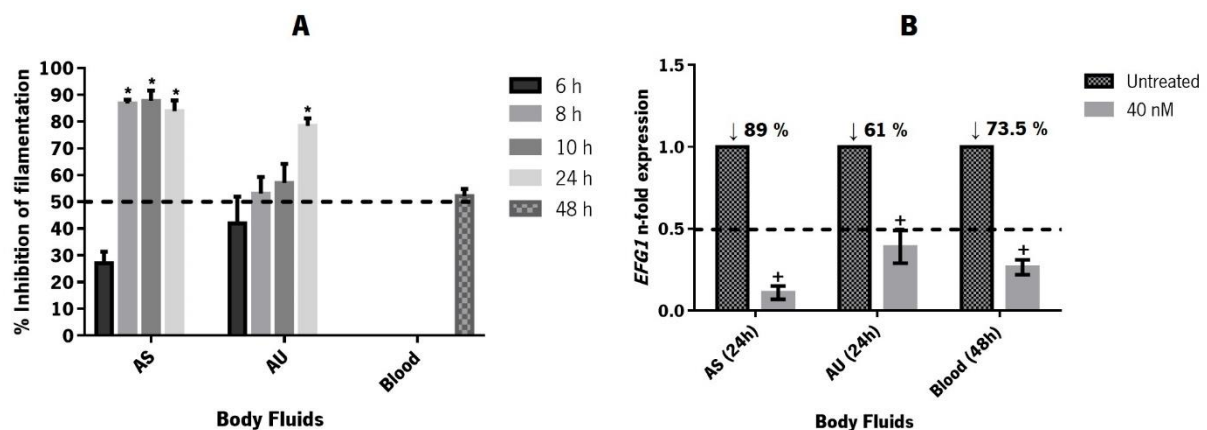
Figure II.1.4 Anti-*EFG1* 2'OMe effect on simulated human body fluids (AS, AU and horse blood). (A) Percentage of inhibition of filamentous forms (%) at different time points (6, 8, 10 and 24 h for AS and AU; 48 h for horse blood) and **(B)** Levels of *EFG1* gene expression for *C. albicans* SC5314 obtained by Pfaffl method, after treatment with 40 nM of ASO in the presence of different simulated human body fluids (AS and AU at 24 h and horse blood at 48 h). Error bars represent standard deviation. ***** Significantly differences between 6 h and the other times tested (P-value<0.05). ⁺Significantly differences between untreated and treated cells (P-value<0.05).

Interestingly, it can be noticed that anti-*EFG1* 2'OMe maintains its performance in simulated human body fluids, reducing *C. albicans* filamentation and *EFG1* gene expression. In fact, it was verified that the ASO was able to reduce 90 % and 80 % of *C. albicans* filamentation after 24 h of incubation in AS and AU (P-value<0.05) respectively, and 50 % after 48 h of incubation in horse blood (Figure II.1.4 A).

Figure II.1.4 B shows the levels of *EFG1* gene expression and demonstrates a decrease in the levels of expression of 89 % in AS, 61 % in AU and, 74 % in horse blood (P-value<0.05). It is important to highlight that the levels of *EFG1* expression in the absence of ASO were different in all simulated human body fluids tested (Figure AI.4 C), which justifies the different levels of reduction observed.

Considering any possible future clinical applications of the anti-*EFG1* 2'OMe in the control of local candidiasis (oral and urinary), as well as of systemic infections (blood), these are important results once the ASO maintains its performance in human fluids, inhibiting *C. albicans* filamentation and the *EFG1* gene expression.

This data demonstrates, for the first time, that it is possible to use antisense oligonucleotides with 2'OMe chemical modifications to control virulence determinants of *C. albicans.* The anti-*EFG1* 2'OMe that it was projected has significantly reduced *EFG1* gene expression and effectively prevented *C. albicans* cell filamentation in different simulated human body fluids. Undeniably, this work provides potentially valuable information for future research into the management of *Candida* infections. Thus, in the future, it will be possible to develop a credible and alternative method to control oral and urinary candidiasis, as well as systemic infections, based on AST methodology.

References

1   Quindós G (2018) Epidemiology of invasive mycoses: A landscape in continuous change. *Rev. Iberoam. Micol.* 35, 171–178

2   Koehler P, Stecher M, Cornely O A et al (2019) Morbidity and mortality of candidaemia in Europe: an epidemiologic meta-analysis. *Clin. Microbiol. Infect.* 25(10), 1200-1212

3   Negri M, Henriques M, Svidzinski T I *et al.* (2009) Correlation between Etest®, disk diffusion, and microdilution methods for antifungal susceptibility testing of *Candida* species from infection and colonization. *J. Clin. Lab. Anal.* 23, 324–330

4   Yapar N (2014) Epidemiology and risk factors for invasive candidiasis. *Ther. Clin. Risk Manag.* 10, 95–105

5   Gonçalves B, Ferreira C Alves C T *et al.* (2016) Vulvovaginal candidiasis: Epidemiology, microbiology and risk factors. *Crit. Rev. Microbiol.* 42, 905–927

6   Araújo D, Henriques M and Silva S (2017) Portrait of *Candida* species biofilm regulatory network genes. *Trends Microbiol.* 1, 62–75

7   Mayer F L Wilson D and Hube B (2013) *Candida albicans* pathogenicity mechanisms. *Virulence* 4, 119–28

8   Casadevall A and Pirofski L (2001) Host-pathogen interactions: the attributes of virulence. *J. Infect. Dis.* 184, 337–344

9   Saville S P, Lazzell A L, Monteagudo C and Lopez-Ribot J L (2003) Engineered control of cell morphology *in vivo* reveals distinct roles for yeast and filamentous forms of *Candida albicans* during infection. *Eukaryot. Cell* 2, 1053–60

10   Nobile C J, Fox E P, Nett J E *et al.* (2011) A recently evolved transcriptional network controls biofilm development in *Candida albicans*. *Cell* 148, 126–138

11   Nobile C J and Mitchell A P (2005) Regulation of cell-surface genes and biofilm formation by the *C. albicans*

transcription factor Bcr1p. *Curr. Biol.* 15, 1150–1155

12   Connolly L, Riccombeni A, Grózer Z *et al.* (2013) The APSES transcription factor Efg1 is a global regulator that controls morphogenesis and biofilm formation in *Candida parapsilosis*. *Mol. Microbiol.* 90, 36–53

13   Stoldt V R, Sonneborn A, Leuker C E and Ernst J F (1997) Efg1p, an essential regulator of morphogenesis of the human pathogen *Candida albicans*, is a member of a conserved class of bHLH proteins regulating morphogenetic processes in fungi. *EMBO J.* 16, 1982–1991

14   Ernst J F (2000) Transcription factors in *Candida albicans* - environmental control of morphogenesis. *Microbiology* 146, 1763–1774

15   Ramage G, VandeWalle K, López-Ribot J L and Wickes B L (2002) The filamentation pathway controlled by the Efg1 regulator protein is required for normal biofilm formation and development in *Candida albicans*. *FEMS Microbiol Lett* 214, 95–100

16   Eggimann P (2003) Epidemiology of *Candida* species infections in critically ill non-immunosuppressed patients. *lancet Infect. Dis.* 3(11), 685-702

17   Negri M, Silva S, Henriques M and Oliveira R (2012) Insights into *Candida tropicalis* nosocomial infections and virulence factors. *Eur. J. Clin. Microbiol. Infect. Dis.* 31, 1399–1412

18   Van Hauwermeiren F, Vandenbroucke R E, Grine L *et al.* (2014) Antisense oligonucleotides against TNFR1 prevent toxicity of TNF/IFNγ treatment in mouse tumor models. *Int. J. Cancer* 135, 742–750

19   Costerton W J, Montanaro L, Balaban N *et al.* (2009) Prospecting gene therapy of implant infections. *Int. J. Artif. Organs* 32, 689–95

20   Kenney S P and Meng X J (2015) Therapeutic targets for the treatment of hepatitis E virus infection. *Expert Opin. Ther. Targets* 19, 1245–60

21   Warren T K, Whitehouse C A, Wells J, *et al.* (2016) Delayed time-to-treatment of an antisense morpholino oligomer is effective against lethal marburg virus infection in Cynomolgus macaques. *PLoS Negl. Trop. Dis.* 10, 1–18

22   Deng Y, Nong L G, Huang W, *et al.* (2009) [Inhibition of hepatitis B virus (HBV) replication using antisense LNA targeting to both S and C genes in HBV]. *Zhonghua Gan Zang Bing Za Zhi* 17, 900–4

23   Testa S, Disney M, Gryaznov S, Turner D (2000) Methods and compositions for inhibition of rna splicing WO2000055374

24   Sully E K and Geller B L (2016) Antisense antimicrobial therapeutics. *Curr. Opin. Microbiol.* 33, 47–55

25   Disney M D, Haidaris C G, Turner D H, *et al.* (2003) Uptake and antifungal activity of oligonucleotides in *Candida albicans*. 100(4), 1530-1534

26   Chan J H, Lim S and Wong W S (2006) Antisense Oligonucleotides: from design to therapeutic application. *Clin. Exp. Pharmacol. Physiol.* 33(5-6), 533-540

27   Kurreck J (2003) Antisense technologies: Improvement through novel chemical modifications. *Eur. J. Biochem.* 270, 1628–1644

28   Khvorova A and Watts J K (2017) The chemical evolution of oligonucleotide therapies of clinical utility. *Nat. Biotechnol.* 35, 238–248

29   Dias N and Stein C A (2002) Antisense oligonucleotides: Basic concepts and mechanisms. *Mol. Cancer Ther.* 1, 347–355

30   DeVos S L and Miller T M (2013) Antisense oligonucleotides: treating neurodegeneration at the level of RNA. *Neurotherapeutics* 10(3), 486-497

31   Lo H J, Köhler J R, DiDomenico B, *et al.* (1997) Nonfilamentous *C. albicans* mutants are avirulent. *Cell* 90, 939–949

32   Altmann K H, Fabbro D, Dean N M, *et al.* (1996) Second-generation antisense oligonucleotides: structure-activity relationships and the design of improved signal-transduction inhibitors. *Biochem. Soc. Trans.* 24, 630–7

33   Vickers T A and Crooke S T (2015) The rates of the major steps in the molecular mechanism of RNase H1-dependent antisense oligonucleotide induced degradation of RNA. *Nucleic Acids Res.* 43, 8955–8963

34   Almeida C, Azevedo N F, Iversen C, *et al.* (2009) Development and application of a novel peptide nucleic acid probe for the specific detection of Cronobacter genomospecies (enterobacter sakazakii) in powdered infant formula. *Appl. Environ. Microbiol.* 75, 2925–2930

35   Fonseca E, Silva S, Rodrigues C F *et al.* (2014) Effects of fluconazole on *Candida glabrata* biofilms and its

relationship with ABC transporter gene expression. *Biofouling* 30, 447–57

36   Rodrigues C and Henriques M (2018) Portrait of matrix gene expression in *Candida glabrata* biofilms with stress induced by different drugs. *Genes (Basel).* 9, 205

37   Nailis H, Coenye T, Van Nieuwerburgh F, *et al.* (2006) Development and evaluation of different normalization strategies for gene expression studies in *Candida albicans* biofilms by real-time PCR. *BMC Mol. Biol.* 7, 1–9

38   Almeida A, Ferreira J A, Teixeira F, *et al.* (2013) Challenging the limits of detection of sialylated Thomsen-Friedenreich antigens by in-gel deglycosylation and nano-LC-MALDI-TOF-MS. *Electrophoresis* 34, 2337–2341

39   Pitarch A, Sánchez M, Nombela C and Gil C (2002) Sequential fractionation and two-dimensional gel analysis unravels the complexity of the dimorphic fungus *Candida albicans* cell wall proteome. *Mol. Cell. Proteomics* 1, 967–982

40   Wiśniewski J R, Zougman A, Nagarjuna N and Mann M (2009) Universal sample preparation method for proteome analysis. *Nat. Methods* 6, 359–362

41   Michalski A, Damoc E, Hauschild J P, *et al.* (2011) Mass spectrometry-based proteomics using Q Exactive, a high-performance benchtop quadrupole orbitrap mass spectrometer. *Mol. Cell. Proteomics* 10, M111.011015

42   Silva S, Negri M, Henriques M, *et al.* (2010) Silicone colonization by non-*Candida albicans Candida* species in the presence of urine. *J. Med. Microbiol.* 59, 747–754

43   Silva S, Pires P, Monteiro D R, *et al.* (2013) The effect of silver nanoparticles and nystatin on mixed biofilms of *Candida glabrata* and *Candida albicans* on acrylic. *Med. Mycol.* 51, 178–184

44   Deng Y B, Qin H J, Luo Y H, *et al.* (2015) Antiviral effect of hepatitis B virus S/C gene loci antisense locked nucleic acid on transgenic mice *in vivo. Genet. Mol. Res.* 14, 10087–95

45   Stein C A and Castanotto D (2017) FDA-Approved Oligonucleotide Therapies in 2017. *Mol. Ther.* 25, 1069–1075

46   Zamecnik P C and Stephenson M L (1978) Inhibition of Rous sarcoma virus replication and cell transformation by a specific oligodeoxynucleotide. *Proc. Natl. Acad. Sci. U. S. A.* 75, 280–4

47   Mizuta T, Fujiwara M, Hatta T, *et al.* (1999) Antisense oligonucleotides directed against the viral RNA polymerase gene enhance survival of mice infected with influenza A. *Nat. Biotechnol.* 17, 583–7

48   Hou J, Liu Z and Gu F (2005) Epidemiology and prevention of hepatitis B virus infection. *Int. J. Med. Sci.* 2, 50–57

49   Holden K L, Stein D A, Pierson T C, *et al.* (2006) Inhibition of dengue virus translation and RNA synthesis by a morpholino oligomer targeted to the top of the terminal 3′ stem-loop structure. *Virology* 344, 439–452

50   Warren T K, Warfield K L, Wells J, *et al.* (2010) Advanced antisense therapies for postexposure protection against lethal filovirus infections. *Nat. Med.* 16, 991–994

51   Singh P and Panda D (2010) FtsZ inhibition: a promising approach for antistaphylococcal therapy. *Drug News Perspect.* 23, 295–304

52   Sawyer A J, Wesolowski D, Gandotra N, *et al.* (2013) A peptide-morpholino oligomer conjugate targeting Staphylococcus aureus gyrA mRNA improves healing in an infected mouse cutaneous wound model. *Int. J. Pharm.* 453, 651–655

53   Stein C A (2001) The experimental use of antisense oligonucleotides: a guide for the perplexed. *J. Clin. Invest.* 108, 641–644

54   Kawasaki A M, Casper M D, Freier S M, *et al.* (1993) Uniformly modified 2′-Deoxy-2′-fluoro phosphorothioate oligonucleotides as nuclease-resistant antisense compounds with high affinity and specificity for RNA targets. *J. Med. Chem.* 36, 831–841

55   Partridge M, Vincent A, Matthews P, *et al.* (1996) A simple method for delivering morpholino antisense oligos into the cytoplasm of cells. *Antisense Nucleic Acid Drug Dev.* 6, 169–175

56   Behlke M, Devor E and Goodchild J (1989) Designing antisense oligonucleotides. *Trends Pharmacol. Sci.* 10, 435–437

57   Almeida C, Azevedo N F, Santos S, *et al.* (2011) Discriminating multi-species populations in biofilms with peptide nucleic acid fluorescence in situ hybridization (PNA FISH). *PLoS One* 6, 6(3), e14786

58   Rocha R, Santos R S, Madureira P, *et al.* (2016) Optimization of peptide nucleic acid fluorescence in situ

hybridization (PNA-FISH) for the detection of bacteria: The effect of pH, dextran sulfate and probe concentration. *J. Biotechnol.* 226, 1–7

59   Vilas Boas D, Almeida C, Sillankorva S, *et al.* (2016) Discrimination of bacteriophage infected cells using locked nucleic acid fluorescent *in situ* hybridization (LNA-FISH). *Biofouling* 32, 179–190

60   Ferreira A M, Cruz-Moreira D, Cerqueira L, *et al.* (2017) Yeasts identification in microfluidic devices using peptide nucleic acid fluorescence in situ hybridization (PNA-FISH). *Biomed. Microdevices* 19, 11

61   Asami Y, Yoshioka K, Nishina K, *et al.* (2016) Drug delivery system of therapeutic oligonucleotides. *Drug Discov. Ther.* 10, 256–262

62   Juliano R L (2018) Intracellular trafficking and endosomal release of oligonucleotides: What we know and what we don't. *Nucleic Acid Ther.* 28, 166–177

63   Chen C, Yang Z and Tang X (2018) Chemical modifications of nucleic acid drugs and their delivery systems for gene-based therapy. *Med. Res. Rev.* 38, 829–869

64   International Organization for Standardization. ISO10993-5:2009. Biological evaluation of medical devices. Part 5: Tests for *in vitro* cytotoxicity. Third edition, 2009.

65   Liu H, Köhler J and Fink G R (1994) Suppression of hyphal formation in *Candida albicans* by mutation of a *STE12* homolog. *Science* 266, 1723–1726

66   Nobile C J, Andes D R, Nett J E, *et al.* (2006) Critical role of Bcr1-dependent adhesins in *C. albicans* biofilm formation *in vitro* and *in vivo*. *PLoS Pathog.* 2, 0636–0649

67   Wan Harun W H, Jamil N A, Jamaludin N H *et al.* (2013) Effect of piper betle and Brucea javanica on the differential expression of Hyphal Wall Protein (*HWP1*) in non-*Candida albicans Candida* (NCAC) species. *Evid. Based. Complement. Alternat. Med.* 2013, 1–6

68   Orsi C F, Borghi E, Colombari B, *et al.* (2014) Impact of *Candida albicans* hyphal wall protein 1 (*HWP1*) genotype on biofilm production and fungal susceptibility to microglial cells. *Microb. Pathog.* 69-70C, 20–27

69   Biswas S, Van Dijck P and Datta A (2007) Environmental sensing and signal transduction pathways regulating morphopathogenic determinants of *Candida albicans*. *Microbiol. Mol. Biol. Rev.* 71, 348–376

70   Sudbery P E (2011) Growth of *Candida albicans* hyphae. *Nat. Rev. Microbiol.* 9, 737–748

71   Smith R A, Miller T M, Yamanaka K, *et al.* (2006) Antisense oligonucleotide therapy for neurodegenerative disease. *J Clin Invest* 116, 2290–2296

72   Keiser M S, Kordasiewicz H B and McBride J L (2016) Gene suppression strategies for dominantly inherited neurodegenerative diseases: lessons from Huntington's disease and spinocerebellar ataxia. *Hum. Mol. Genet.* 25, R53–R64

73   Harada T, Matsumoto S, Hirota S, et al (2019) Chemically modified antisense oligonucleotide against ARL4C inhibits primary and metastatic liver tumor growth. *Mol. Cancer Ther.* 18(3), 602-612

74   Luna Velez M V, Verhaegh G W, Smit F, *et al.* (2019) Suppression of prostate tumor cell survival by antisense oligonucleotide-mediated inhibition of AR-V7 mRNA synthesis. *Oncogene* 38(19), 3696-3709

Chapter II.2

Anti-*EFG1* 2'-*O*MethylRNA antisense oligonucleotide inhibits *Candida albicans* filamentation and attenuates candidiasis in *Galleria mellonella*

Main goal

To validate *in vivo* the applicability of anti-*EFG1* 2'OMe antisense oligonucleotide for inhibiting *Candida albicans* filamentation and to attenuate candidiasis.

Conclusions

This work confirmed that the anti-*EFG1* 2'OMe ASO was able to inhibit *C. albicans* filamentation and to attenuate the *C. albicans* virulence on a *G. mellonella* model.

II.2.1 Introduction

Given the *in vitro* findings described on Chapter II.1, the anti-*EFG1* 2'OMe ASO's *in vivo* validation is crucial. Among the *in vivo* models available, invertebrate models as *Galleria mellonella* have been emerged at the forefront to study fungal pathogenesis [1,2]. The possibilities of pathogens delivery into the larvae, by topical, oral and injection application are suited to study pathogens at human body temperature, making it a desirable model for the study of fungal pathogenesis [2,3].

Thus, the main goal of this part of the work was to validate *in vivo* the applicability of anti-*EFG1* 2'OMe ASO for inhibiting *Candida albicans* filamentation and to attenuate candidiasis.

II.2.2 Materials and methods

a. Anti-*EFG1* 2'OMe ASO preparation

The anti-*EFG1* 2'OMe ASO was designed and synthesized based on the 2nd generation of chemical modifications of nucleic acid mimics as described in the previous Chapter II.1. Aliquots of anti-*EFG1* 2'OMe ASO were prepared in sterile ultrapure water to 4 µM and stored a -20 °C for later use. Whenever necessary, ASO molecules were diluted in PBS to a final concentration of 40 and 100 nM.

b. *Candida albicans* cells and growth conditions

The *Candida albicans* SC5314, belonging to *Candida* strains collection of the Biofilm group of the Centre of Biological Engineering, was used during these studies. For all experiments, the yeast strain was subcultured on sabouraud dextrose agar (SDA; Merck, Germany) and incubated for 24 h at 37 °C. Cells were then inoculated in sabouraud dextrose broth (SDB; Merck, Germany) and incubated overnight at 37 °C, 120 rpm. After incubation, the cells' suspensions were centrifuged for 10 min, at 3000 g and 4 °C, and washed twice with phosphate-buffered saline (PBS; pH 7, 0.1 M). Pellets were suspended in 5 mL of PBS, and the cellular density was adjusted using a *Neubauer* chamber (Marienfild, Land-Konicshofem, Germany) to 7×10^7 cells mL^{-1}. The concentration of *C. albicans* cells used to infect larvae was selected based on a study of *G. mellonella* lethality as response to different concentrations of yeast (between 7×10^7 cells mL^{-1} and 2×10^8 cells mL^{-1}) (Figure AII.1).

c. *Galleria mellonella* larvae

Galleria mellonella larvae were reared on a pollen grain and bee wax diet at 25 °C in the darkness and used in a final stage of development with a weight of approximately 250 mg. The larvae were injected

into hemolymph via the hindmost left proleg, previously sanitized with 70 % (v/v) ethanol, using a micro syringe adapted in a micrometre to control the volume of injection [4]. All experiments were performed in triplicate and in a minimum of three independent assays.

d. *Galleria mellonella* toxicity assays

To test the *in vivo* toxicity of the anti-*EFG1* 2'OMe ASO, 10 larvae of *G. mellonella* were injected with 5 µL of 40 and 100 nM of ASO prepared in PBS. As control, a set of larvae were injected only with PBS. Larvae were placed in petri dishes and stored in the dark at 37 °C. Larvae's morphology and survival were followed over 4 days and the survival curves were constructed.

e. *Galleria mellonella* survival assays

To study the effect of the anti-*EFG1* 2'OMe ASO on the survival rate of *G. mellonella*, larvae were infected with 5 µL of a lethal dose of *C. albicans* cells ($7x10^7$ cells mL^{-1}) and randomly allocated to 5 different experimental groups (with a set of 10 larvae). Two sets of larvae were treated with a single-dose of 40 nM and 100 nM of ASO (0 h of post infection); two sets of larvae with a double-dose of 40 nM and 100 nM of ASO (0 h and 12 h of post infection); and a set only with PBS (control). After injections, the larvae were placed in petri dishes and stored in the dark at 37 °C, over 72 h, and consequently, survival curves were constructed. The larvae were considered dead when they displayed no movement in response to touch.

f. *Galleria mellonella* histological fat body analysis

The histological analysis of *G. mellonella* was performed to study the effect of anti-*EFG1* 2'OMe ASO on candidiasis progression and *C. albicans* morphology into the fat body of larvae. For that, one larva from each group were recovered at 24 h and 48 h, to be processed histologically. The fat body was removed, from each larva, through an incision in the midline of the ventral with a scalpel blade. The fat body was placed in 4 % (v/v) of paraformaldehyde and stored for 24 h at 4 °C to preserve the structures. The tissue was mounted in paraffin blocks and cut in sections of 4-5 µm, and the sections were stained with periodic acid Schiff (PAS) and haematoxylin-eosin (HE). Tissue sections were viewed and photographed with an OLYMPUS BX51 microscope coupled with a DP71 digital camera (Olympus Portugal SA, Porto, Portugal).

g. Statistical analysis

Data are expressed as the mean ± standard deviation of a least three independent experiments. Kaplan-Meier survival curves were plotted and differences in survival were calculated by using log-rank Mantel-Cox statistical test, all performed with GraphPad Prism 6® (GraphPad Software, San Diego, CA, USA).

II.2.3 Results

To assess of anti-*EFG1* 2'OMe ASO toxicity, *G. mellonella* larvae were infected with two different concentrations of ASO (40 nM and 100 nM). As shown, the anti-*EFG1* 2'OMe ASO did not reveal toxic effects on *G. mellonella* since no death was observed for both tested concentrations over 96 h (Figure II.2.1).
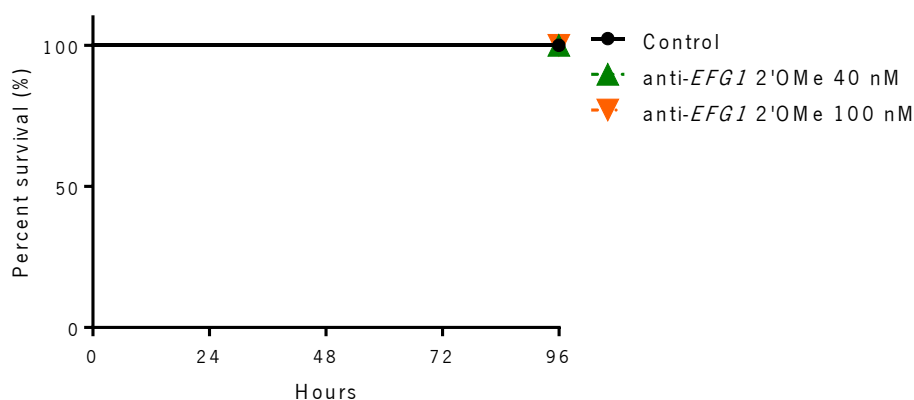
Figure II.2.1 Anti-*EFG1* 2'OMe ASO toxicity evaluation in *Galleria mellonella* model. For each condition, 10 larvae were injected with 40 nM and 100 nM of ASO, and their survival was monitored over 96 h. As control larvae were injected only with PBS.

To investigate the *in vivo* effects of anti-*EFG1* 2'OMe ASO on attenuation of *C. albicans* infections a *G. mellonella* larvae model was used, infected with a lethal dose of yeast cells (7×10^7 cells mL^{-1}). A first set of larvae was treated with a single-dose (0 h of post infection) of anti-*EFG1* 2'OMe ASO at 40 nM and 100 nM (Figure II.2.2 A). To note, the treatment of infected *G. mellonella* with a single-dose of anti-*EFG1* 2'OMe ASO enhances the survival of larvae over 24 h by 16 % with 40 nM (P-value>0.05) and by 30 % with 100 nM (P-value<0.05). Although, no effect was observed in larvae treated with 40 nM of anti-*EFG1* 2'OMe ASO at 48 h (P-value>0.05), the treatment with 100 nM intensified the larvae survival into 17 % (P-value>0.05). No significant effects were observed with a single-dose after 72 h of infection for both

concentrations tested (P-value>0.05). A second set of infected larvae were treated with a double-dose of anti-*EFG1* 2'OMe ASO (0 h and 12 h post infection) (Figure II.2.2 B). Results showed that a double-dose of anti-*EFG1* 2'OMe ASO significantly enhances the *G. mellonella* survival. To note, 90 % and 100 % of the larvae treated with 40 nM (P-value<0.05) and 100 nM (P-value<0.001), respectively, survived over the first 24 h of infection. An increase on *G. mellonella* survival was also evident at 48 h with a rate of 23 % for 40 nM (P-value<0.05) and of 50 % for 100 nM (P-value<0.001). Note that, the administration of a double-dose of anti-*EFG1* 2'OMe ASO not only was responsible by enhancing the larvae survival but also for prolonging the anti-*EFG1* 2'OMe ASO effects over 72 h, achieving 30 % more on the survival rate with 100 nM of ASO (P-value<0.001).
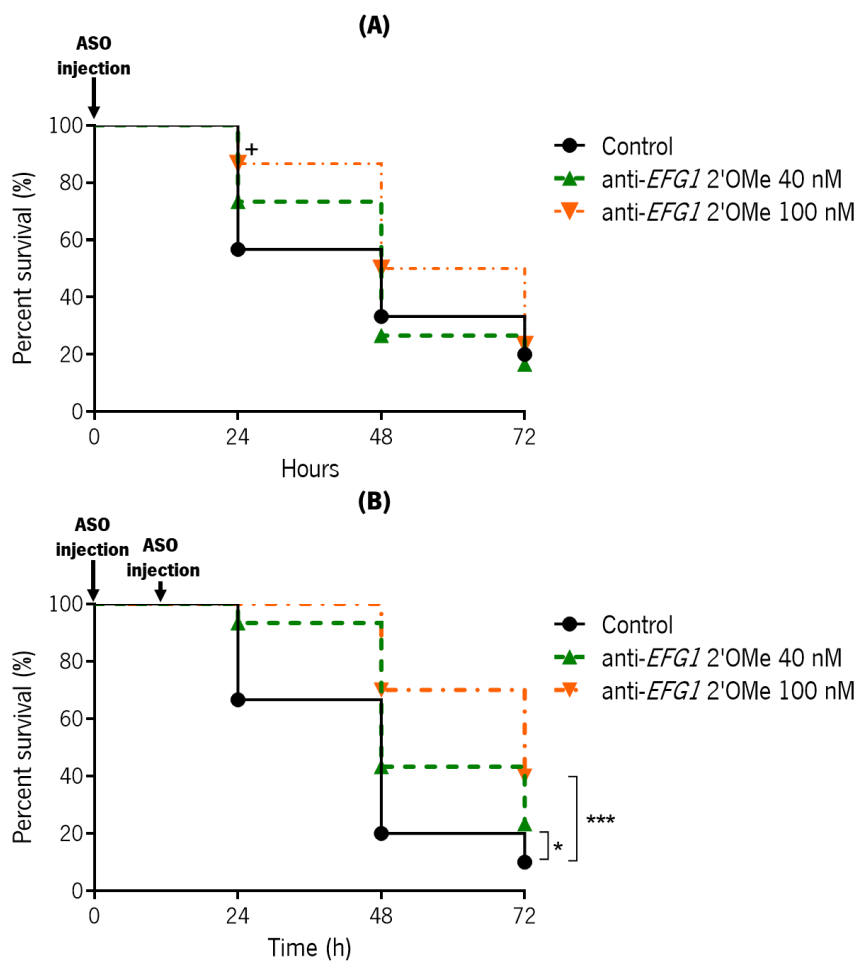
Figure II.2.2 Anti-*EFG1* 2'OMe ASO effect on the survival of *Galleria mellonella* larvae infected with *Candida albicans*. Survival curves of infected larvae were treated with: **(A)** a single-dose of anti-*EFG1* 2'OMe ASO (0 h post infection) and **(B)** a double-dose of anti-*EFG1* 2'OMe ASO (0 h and 12 h post infection). Larvae infected with *C. albicans* cells were treated with 40 nM and 100 nM of anti-*EFG1* 2'OMe ASO. As control larvae infected were injected only with PBS. [+]Significant difference among control and a single-dose of 100 nM of anti-*EFG1* 2'OMe ASO at 24 h (P-value<0.05). *****Significant difference among control and a double-dose of 40 nM of

anti-*EFG1* 2'OMe ASO for all times (P-value<0.05). ******* Significant difference among control and a double-dose of 100 nM of anti-*EFG1* 2'OMe ASO for all times (P-value<0.001).

To assess the effect of anti-*EFG1* 2'OMe ASO on candidiasis progression and *C. albicans* morphology, the fat body of larvae was fixed, sectioned, stained and evaluated (Figure II.2.3). Figure II.2.3 A reveals the quantity and invasiveness progression of *C. albicans* without treatment after 24 h and 48 h of infection. It is evident, that *C. albicans* cells are located mainly in digestive system, around the fat body and tend to organize into clusters with an extensive progression on quantity over the time. *Candida albicans* exhibits predominantly filamentous growth. The images highlight the contrast among the single-dose (Figure II.2.3 B) and double-dose (Figure II.2.3 C) treatments with the control, exhibiting both an expressive lower quantity of filaments with a significant decrease on fat body area occupied by *C. albicans* cells, with a more pronounced effect on sections of larvae treated with 100 nM of anti-*EFG1* 2'OMe ASO.
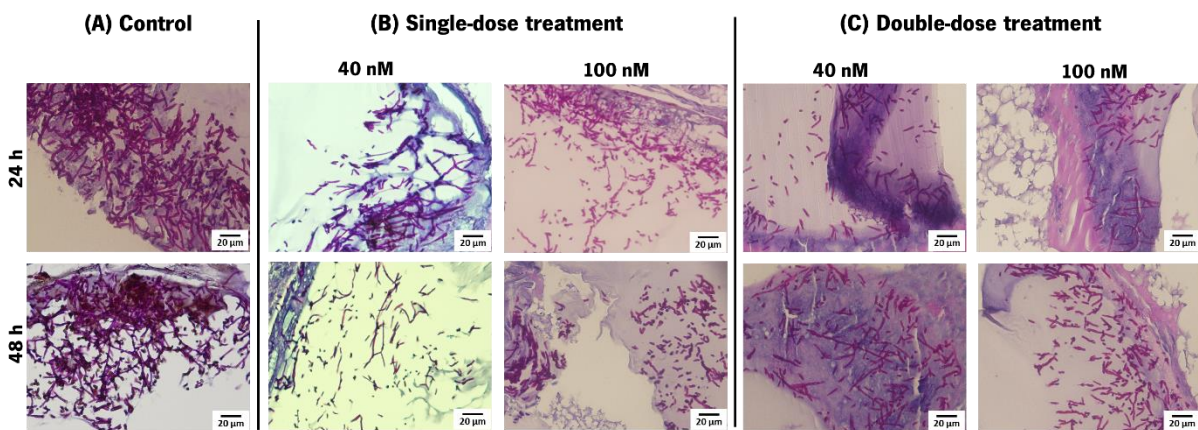
Figure II.2.3 Anti-*EFG1* 2'OMe ASO effect on *Candida albicans* cells morphology and progression into fat body of *Galleria mellonella*. Histological images of larvae infected **(A)** with *C. albicans* (at 24 h and 48 h) and treated **(B)** with a single-dose (0 h post infection) and **(C)** with a double-dose (0 h and 12 h post infection) of 40 nM and 100 nM of anti-*EFG1* 2'OMe ASO. The larvae sections were labelled with periodic acid Schiff coloration. The magnification images were at 400x.

II.2.4 Discussion

Taking in account the promising *in vitro* results obtained with the anti-*EFG1* 2'OMe ASO (Chapter II.1), the aim of this work was to validate *in vivo* its applicability for inhibiting *C. albicans* filamentation and to attenuate candidiasis, using the *G. mellonella* model. As in other microbiological relevant studies [4–6], it was opted to use the *G. mellonella* model to validate the *in vivo* performance of the anti-*EFG1*

2'OMe ASO since it is a model that provides a rapid, inexpensive and reliable way to evaluate the nano-drugs effects and toxicity *in vivo*.

No evidences of *in vivo* toxicity were observed using the *G. mellonella* model over 96 h (Figure II.2.1), as in the *in vitro* results (Chapter II.1). The infected *G. mellonella* larvae with $7x10^7$ cells mL^{-1} of *C. albicans* cells were treated with a single-dose (0 h post infection) of anti-*EFG1* 2'OMe ASO. It was clear, that the anti-*EFG1* 2'OMe ASO keeps its performance *in vivo*, once it was observed an increase on larvae survival comparing to untreated larvae. Moreover, with these results it is also clear that the *in vivo* anti-*EFG1* 2'OMe ASO efficacy is concentration dependent. In fact, the treatment of infected *G. mellonella* with a single-dose of anti-*EFG1* 2'OMe ASO enhances the survival of larvae over 24 h (16 %), being more pronounced with 100 nM of ASO (30 %) (Figure II.2.2 A). However, after 48 h of infection the anti-*EFG1* 2'OMe ASO loses its effectiveness. This result was expected, once in a clinical context, an infection is rarely controlled with a single-dose of antimicrobial and the treatments are not usually carried out over a precise time [7–10]. To mimic that, a double-dose of anti-*EFG1* 2'OMe ASO was administered (0 h and 12 h post infection) on *G. mellonella* larvae infected with *C. albicans* cells (Figure II.2.2 B). The results indicate that with a double-dose administration of anti-*EFG1* 2'OMe ASO it is possible to intensify the molecule efficacy and prolong its effect over the time. In fact, larvae treated with the double-dose of ASO survived around 90 % (with 40 nM) and 100 % (with 100 nM) over the first 24 h. Moreover, an increase on larvae survival was also evident at 48 h (by 50 %) and 72 h (by 30 %), with more pronounced effect in case of 100 nM of ASO. These findings corroborate with the observed on histological images of *G. mellonella* fat body, that evidences a strong decrease on the number of *C. albicans* as filaments and an evident reduction on the extension of area occupied by the *Candida* in tissues from larvae treated with anti-*EFG1* 2'OMe ASO (Figure II.2.3).

The results suggest that systemic delivery of anti-*EFG1* 2'OMe ASO is feasible, devoid of toxicity, and could be a promising treatment strategy for *C. albicans* infections. Therefore, it warrants further studies in other animal models.

Hereby, the present work confirms that the anti-*EFG1* 2'OMe ASO is able to inhibits *C. albicans* filamentation and attenuates the candidiasis on *G. mellonella* model. Undoubtedly, this work revealed the *in vivo* therapeutic potential of anti-*EFG1* 2'OMe ASO for controlling *C. albicans* infections.

References

1   Fedhila S, Buisson C, Dussurget O, et al. (2010) Comparative analysis of the virulence of invertebrate and mammalian pathogenic bacteria in the oral insect infection model *Galleria mellonella*. *J Invertebr Pathol* 103, 24–9.

2   Junqueira J C. (2012) *Galleria mellonella* as a model host for human pathogens. *Virulence* 3, 474–6.

3   Fuchs B B, O'Brien E, Khoury J B E and Mylonakis, E. (2010) Methods for using *Galleria mellonella* as a model host to study fungal pathogenesis. *Virulence* 1, 475–82.

4   Mil-Homens D, Ferreira-Dias S and Fialho A M. (2016) Fish oils against Burkholderia and *Pseudomonas aeruginosa*: *In vitro* efficacy and their therapeutic and prophylactic effects on infected *Galleria mellonella* larvae. *J Appl Microbiol* 120, 1509–19.

5   Vilela S F G, Barbosa J O, Rossoni R D, et al. (2015) *Lactobacillus acidophilus* ATCC 4356 inhibits biofilm formation by *C. albicans* and attenuates the experimental candidiasis in *Galleria mellonella*. *Virulence* 6, 29–39.

6   Rossoni R D, dos Santos Velloso M, Figueiredo L M A, et al. (2018) Clinical strains of *Lactobacillus* reduce the filamentation of *Candida albicans* and protect *Galleria mellonella* against experimental candidiasis. *Folia Microbiol (Praha)* 63, 307–14.

7   Straarup E M, Fisker N, Hedtjärn M, et al. (2010) Short locked nucleic acid antisense oligonucleotides potently reduce apolipoprotein B mRNA and serum cholesterol in mice and non-human primates. *Nucleic Acids Res* 38, 7100–11.

8   Torres A, Kozak J, Korolczuk A, et al. (2016) Locked nucleic acid-inhibitor of miR-205 decreases endometrial cancer cells proliferation *in vitro* and *in vivo*. *Oncotarget* 7, 73651–63.

9   Macedo D, Leonardelli F, Dudiuk C, et al. (2019) *In vitro* and *in vivo* evaluation of voriconazole-containing antifungal combinations against Mucorales using a *Galleria mellonella* model of mucormycosis. *J Fungi* 5, 5.

10   Kloezen W, Parel F, Brüggemann R, et al. (2018) Amphotericin B and terbinafine but not the azoles prolong survival in *Galleria mellonella* larvae infected with *Madurella mycetomatis*. *Med Mycol* 56, 469–78.

Chapter II.3

Antisense locked nucleic acid gapmers to control *Candida albicans* filamentation

Main goal

The main goal of this part of the work was to evaluate of a set of LNA-ASOs, in the so-called gapmer constitution, to control of *EFG1* gene expression and reduction of *in vitro* filamentation, also in the control *C. albicans* virulence in an *in vivo* model.

Conclusions

This work showed that LNA-type gapmer ASOs modifications with PS-linkages and palmitoyl-2'-amino-LNA monomers are very favorable for an *in vivo* application and therefore constitute promising lead structures for development of drugs against *Candida* species.

II.3.1 Introduction

As described on Chapter I, antisense oligonucleotides (ASOs) are short oligonucleotide sequences which are complementary to the target RNA which bind through standard Watson-Crick base pairing [1]. Normally, ASOs are chemically modified in order to protect them against the action of nucleases, to improve delivery and biodistribution and RNA-affinity and potency [2]. The phosphorothioate (PS) backbone was one of the early developed chemical modifications, and it is characterized by the substitution of one of the non-bridging phosphate oxygen atoms by sulphur [1,3,4]. To overcome some issues related to the chemical modifications, as in the case of PS and 2'OMethyl (as previously applied in Chapters II.1 and II.2), further chemical modifications were developed over the time. The third generation was, in fact, created to further enhance biostability and pharmacokinetics in addition to enhance nuclease resistance and the target affinity. The locked nucleic acid (LNA) is a sugar modification that belongs to the third generation, having, relative to native RNA, a methylene bridge between the 2'-oxygen and 4'-carbon atoms of the ribose sugar [5,6]. A derivative of LNA, named palmitoyl-2'-amino-LNA resulting from the inclusion of an N-palmitoylated nitrogen atom in the 2'-position of the ribose ring, has been developed [7,8] and shown to display similarly high-affinity binding as LNA to complementary RNA and DNA [2,7,9].

The main goal of this part of the work was to evaluate of a set of LNA-ASO, in the so-called gapmer constitution, to control of *EFG1* gene expression and reduction of *in vitro* filamentation, and also to control *C. albicans* virulence in an *in vivo* model of *G. mellonella*.

II.3.2 Methods

a. Design and synthesis of Anti-*EFG1* LNA-gapmer ASOs

Five LNA-gapmers were designed against the *C. albicans EFG1* (gene orf19.610) target using the sequence 5'-AATAACGGTATGCC-3' as starting point for introduction of LNA nucleotide modifications. Further, the LNA-gapmers were designed based on previous results. LNA-gapmer1 was the standard LNA-gapmer constitution one reference in this study, and four additional LNA-gapmers were subsequently designed by shortening the central DNA-nucleotide gap (LNA-gapmer2), adding PS-linkages (LNA-gapmer3 and LNA-gapmer5), and adding a palmitoyl-2'-amino-LNA modification (LNA-gapmer4 and LNA-gapmer5) (Table II.3.1). In all LNA-gapmers, chemical modifications were introduced distally within the sequences to increase the ASOs stability, whereas the central regions were constituted by DNA nucleotides in order to ensure compatibility with RNase H thus preserving a potential for RNA target cleavage upon hybridization between an ASO and its RNA target [10].

Table II.3.1 Sequence of anti-*EFG1* LNA-gapmer ASOs, with the respective size and GC content

ASO	Sequence	PO or PS	Size	% of GC
LNA-gapmer1		PO	14	42.9
LNA-gapmer2		PO	13	46.2
LNA-gapmer3		PS	14	42.9
LNA-gapmer4		PO	14	42.9
LNA-gapmer5		PS	14	42.9

◯ RNA   ● Locked Nucleic Acid (LNA)   ⬤ Palmitoyl-2'-amino-LNA
⌒ Phosphodiester (PO)   ⌒ Phosphorothioate (PS)

The LNA-gapmers were synthesized using the standard phosphoramidite method on an automated nucleic acid synthesizer (PerSpective Biosystems Expedite 8909 instrument). All standard oligonucleotides were purchased from IDT (Leuven, Belgium). LNA phosphoramidites were purchased from Qiagen and the synthesis was performed in 1.0 μmol scale using an LNA T 40 custom primer support (GE Healthcare). LNA phosphoramidites were incorporated following the following procedures: Trichloroacetic acid in CH_2Cl_2 as detritylation reagent; 0.25 M 4,5-dicyanoimidazole (DCI) in CH_3CN as an activator; acetic anhydride in THF (9:91; v/v) as capA solution; N-methylimidazole in THF (1:9; v/v) as capB solution; and a thiolation solution containing 0.2 M phenylacetyl disulfid (PADS) in 3-picoline/CH_3CN (1:1, v/v) for 180 sec. The coupling yields were based on the absorbance of the dimethoxytrityl cation (DMT$^+$) released after each coupling step. Palmitoyl-2'-amino-LNA phosphoramidite monomer was incorporated by manual-coupling [7] using 5-[3,5-bis(trifluoromethyl)phenyl]-*H*-tetrazole (0.25 M, in anhydrous acetonitrile) as an activator and extended coupling time (20 min). After the synthesis process, the LNA-gapmers were cleaved from the solid support and the protecting groups removed by treatment with a 1:1 mixture (v/v) of 98 % aqueous methanol (v/v) and a 7M solution of ammonia in methanol for 2 h at room temperature followed by treatment with 32 % aqueous ammonia (w/w) at 55 °C for 12 h. The ASOs were characterized by ion-exchange HPLC (IE-HPLC, Lachrom) and matrix-assisted laser desorption ionization time-to-flight mass spectrometry (MALDI-TOF, Microflex LT, Bruker, Daltonies). The purified ASOs were detrytilated by treatment with an 80 % (w/w) aqueous solution of acetic acid for 20

min at room temperature, precipitated by addition of ice-cold acetone, and characterized by IE-HPLC (purity >90 %) and MALDI-TOF mass spectrometry (confirmation of composition).

b.   Characterization of Anti-*EFG1* LNA-gapmer ASOs

Melting temperatures (T$_m$ values)

The T$_m$ values for duplexes involving RNA complementary strands were measured on a PerkinElmer Lambda 35 UV/VIS spectrometer equipment with Peltier Temperature Programmer (PTP6). The concentration of each oligonucleotide was determined optically at 260 nm using their molar extinction coefficients (134000 L M^{-1} cm^{-1} of strands). All measurements were performed in medium salt buffer with 220 mM Na$^+$ (composition: 200 mM NaCl, 20 mM NaH$_2$PO$_4$ and 0.1 mM EDTA, pH 7.0). The LNA-gapmer ASOs were mixed with the corresponding unmodified complementary strand at a 1:1 ratio (2.5 nmol of each strand). All melting curves for duplex denaturation were collected at a 260 nm wavelength as a function of temperature in the range from 8 to 80 °C (heating rate of 1 °C min^{-1}). The values for T$_m$ were determined as an average of two individual measurements.

Secondary structure

The secondary structure of the LNA-gapmer ASOs was determined by circular dichroism (CD) studies. The spectra were recovered on a JASCO DC 1500 spectrophotometer using cuvettes with 0.1 cm path length and averaged over three scans (320-200 nm, 50 nm min^{-1} intervals, 1 nm bandwidth, and 1 s response time) and with background corrected using the buffer applied (5 mM MgCl$_2$, 10 mM NaCl and 1 mM sodium phosphate). The LNA-gapmer ASOs were used in the following constitution, i.e., 50 μM RNA, 5 mM MgCl$_2$, 10 mM NaCl, and 1 mM sodium phosphate-pH 7.2. All other strands were prepared using 25 μM of each RNA using the same buffer. Hybridization step was performed by heating to 90 °C for 5 min followed by slow cooling to room temperature followed by spectral recording.

Surface charge

The surface charge of the LNA-gapmer ASOs was measured using t Malvern Zetasizer ZS (Malvern, CA). A dispersion of each LNA-gapmer ASOs (25 nM) in ultra-pure water was placed in a disposable cuvette and the zeta potential was measured at room temperature in triplicate.

c. Cytotoxicity

The cytotoxicity of the LNA-gapmer ASOs was determined using a 3T3 cell line (Fibroblasts, Embryonic tissue, Mouse from CCL3, American Type Culture Collection). For that, 3T3 cells were grown in DMEM (Biochrom, Germain) supplied by 10 % of FBS (Sigma Aldrich) and 1 % of antibiotic-containing P/S (Biochrom, Germain). After detachment, a suspension with 1×10^5 cells mL^{-1} was added to a 96-well plate and cells were allowed to grow until attaining 80 % confluence. Different concentrations of each LNA-gapmer (10, 40 and 100 nM) were prepared in DMEM medium and 50 µL of each concentration was added to each well. The positive control was prepared by adding 50 µL of DMEM medium and the negative control by adding 50 µL of DMSO to the cells. The plates were incubated for 24 h at 37 °C and 5 %CO_2. The MTS procedure was carried out as described in the previous Chapter II.1.

d. Anti-*EFG1* LNA-gapmer ASOs *in vitro*

<u>Microorganisms and growth conditions</u>

The *Candida* strain used in this study was *C. albicans* SC5314, which is a *Candida* collection reference strain from the Biofilm group of the Centre of Biological Engineering (Braga, Portugal). The strain identification was confirmed using a chromogenic medium, CHROMagar™ *Candida*, through the distinction of colony colours and by PCR-based sequencing with primers for ITS1 and ITS4 [11].

For all experiments, the yeast strain was subcultured on sabouraud dextrose agar (SDA; Merck, Germany) and incubated for 24 h at 37 °C. Cells were then inoculated in sabouraud dextrose broth (SDB; Merck, Germany) and incubated overnight at 37 °C, 120 rpm. After incubation, the cells' suspensions were centrifuged for 10 min, at 3000 g and 4 °C, and washed twice with phosphate-buffered saline (PBS; pH 7, 0.1 M). Pellets were suspended in 5 mL of RPMI (pH 7; Sigma, St Louis, USA), and the cellular density was adjusted for each experiment using a *Neubauer* chamber (Paul Marienfild, Lauda-Königshofen, Germany) to 1×10^6 cells mL^{-1}. All experiments were performed in triplicate and at least three independent assays were run.

<u>Effect on filamentation</u>

To evaluate the effect of the LNA-gapmer ASOs on *C. albicans* filamentation, yeast cells were incubated with each ASO during 24 h, in an Erlenmeyer flask. For that, 5 mL of each LNA-gapmer at 40 nM (prepared on RPMI) was added to 5 mL of *C. albicans* suspension at 1×10^6 cells mL^{-1} (prepared on RPMI). The suspensions were incubated at 37 °C under gentle agitation (120 rpm). The positive control was prepared with 10 mL of the same yeast cell concentration on RPMI. After 24 h, aliquots were

recovered, and filaments were counted using a Neubauer chamber. The results were presented as percentage (%) of filamentation reduction, as previously described in Chapter II.1. In addition to the filamentation inhibition studies, the length of the filaments was quantified through fluorescence microscopy analysis as previously described in Chapter II.1.

<u>Effect on *EFG1* gene expression</u>

Reverse transcription-qPCR (qRT-PCR) was used to determine the effect of LNA-gapmers on *EFG1* gene expression. After 24 h of incubation, 1 mL of each suspension was collected, subjected to centrifugation for 5 min at 6000 g and 4 °C, and then washed once with PBS. RNA extraction was performed using the PureLink RNA Mini Kit (Invitrogen, Carlsbad, CA, USA), as in previous Chapter II.1. To avoid potential DNA contamination, samples were treated with DNase I (Amplification Grade, Invitrogen) and the RNA concentration was determined by optical density measurement (NanoDrop 1000 Spectrophotometer Thermo Scientific®). The cDNA was synthesized using the Xpert cDNA Synthesis Mastermix (Grisp, Porto, Portugal) in accordance with the manufacturer's instructions, and qRT-PCR (CFX96, Biorad) was performed on a 96-well microtiter plate using Eva Green Supermix (Biorad, Berkeley, USA). Each reaction was performed in triplicate and mean values of relative expression were determined by the $2^{-\Delta\Delta Cq}$ method. The expression of the *EFG1* gene was normalized using the *ACT1 Candida* reference gene [12]. Non-transcriptase reverse (NRT) controls were included in each run. The primers were designed using the Primer 3 web-based (Table II.3.2).

Table II.3.2 Primers used for real time PCR, with the respective melting temperature (T_m) and amplification product (AP)

Candida albicans Gene	Systematic Name	Sequence (5'-3')	Primer	T_m (°C)	AP (BP)
EFG1	CR_07890W_A / Orf19.610	5'-TTCTGGTGCAGGTTCCAC-3'	Forward	57	168
		5'-CCTGGTTGTGATGCAGGT-3'	Reverse		
ACT1	C1_13700W_A / Orf19.5007	5'-AATGGGTAGGGTGGGAAAAC-3'	Forward	57	150
		5'-AGCCATTTCCATTGATCGTC-3'	Reverse		
AP, amplification product; BP, base pairs.					

e. Anti-*EFG1* LNA-gapmer ASOs *in vivo*

The *Galleria mellonella* caterpillar infection model was used for the *in vivo* studies as previously described by Mil-Homens *et al.* [13,14]. *Galleria mellonella* larvae were reared on a pollen grain and bee wax diet at 25 °C in the darkness, and a micro syringe was adapted into a micrometer range so as to control the injection volume into hemolymph of larvae.

<u>Toxicity evaluation</u>

To test toxicity of the anti-*EFG1* LNA-gapmer ASOs *in vivo*, 10 *G. mellonella* larvae were injected, via the hindmost left proleg previously sanitized with 70 % (v/v) ethanol, with 5 µL of two distinct concentrations (40 and 100 nM both prepared with PBS) of each LNA-gapmer. As control, a set of larvae were injected with the same volume of PBS. Larvae were placed in petri dishes, and stored in the dark at 37 °C. Larvae survival was recorded over 4 days and survival curves were constructed.

<u>*Galleria mellonella* survival</u>

To study the effect of the LNA-gapmer ASOs on *G. mellonella* survival rate, larvae were injected with *C. albicans* and each LNA-gapmer. The concentration of *C. albicans* to be injected (7×10^7 cells mL^{-1}) was selected based on the *G. mellonella* lethality, as described in previous Chapter II.2. Next, 10 larvae were injected with 5 µL of a suspension of *C. albicans* at 7×10^7 cells mL^{-1} mixed with 40 nM of each LNA-gapmer. Larvae were placed in petri dishes and stored in the dark at 37 °C for 3 days whereupon survival curves were constructed. Caterpillars were considered dead when they displayed no movement in response to a touch with tweezers.

Histological analysis of *G. mellonella* fat bodies were also performed to evaluate the effects of LNA-gapmers on *C. albicans* filamentation. For each condition, two larvae were recovered after pre-determined times (24 h, 48 h and 72 h) and their fat bodies were removed through an incision in the midline of the ventral with a scalpel blade. The fat bodies were stored in 4 % (v/v) paraformaldehyde at 4 °C to prepare for histological processing. The tissue was mounted in paraffin blocks and cut in sections of 4-5 µm which were stained with PAS and HE [15,16]. The yeast and hyphae of *C. albicans* were observed under a light microscope. For analysis of filamentation, all areas of the histological section stained with PAS that contained hyphae and yeast cells were photographed with an OLYMPUS BX51 microscope coupled with a DP71 digital camera (Olympus Portugal SA, Porto, Portugal).

f. Statistical analysis

Data are expressed as the mean ± standard deviation of a least three independent experiments. Results were compared using two-way ANOVA and Tukey's multiple comparisons tests. Kaplan-Meier survival curves were plotted and differences in survival were calculated by using log-rank Mantel-Cox statistical test. All performed with GraphPad Prism 6® (GraphPad Software, San Diego, CA, USA).

II.3.3 Results

a. Characterization of Anti-EFG1 LNA-gapmer ASOs

Figure II.3.1 A shows the values of T_m measured for all LNA-gapmer ASOs with RNA complement. The LNA-gapmer1 presented a T_m of 70 °C and similarly, the LNA-gapmer2 (exclusion of one nt) presented a Tm of 71.6 °C. In contrast, LNA-gapmer3 (addition of PS-linkages), LNA-gapmer4 (addition of the palmitoyl-2'-amino-LNA modification) and LNA-gapmer5 (addition of PS-linkages and the palmitoyl-2'-amino-LNA modification) showed a significant decrease in T_m (Figure II.3.1 A).

(A)

LNA-gapmer	Melting Temperatures (T_m, °C) Medium salt buffer	Superficial Charge (mV)
LNA-gapmer1	70.2	-28.9 ± 1.4
LNA-gapmer2	71.6	-31.9 ± 0.9
LNA-gapmer3	63.2	-35.1 ± 1.3
LNA-gapmer4	65.2	-43.7 ± 2.2
LNA-gapmer5	55.7	-54.1 ± 1.8

(B)
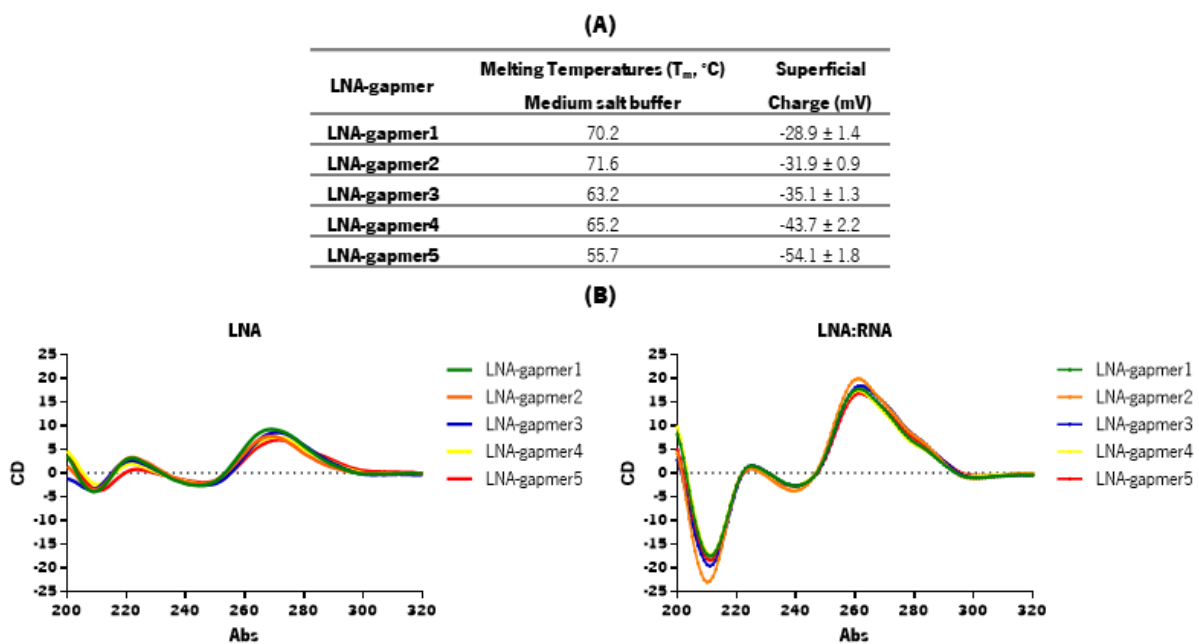
Figure II.3.1 Characterization of Anti-*EFG1* LNA-gapmer ASOs. (A) Thermal denaturation temperatures (T values, °C) determined in medium salt buffer with RNA complement, and evaluation of superficial charge by zeta potential determination. **(B)** Evaluation of overall conformation of the secondary structure by CD spectral analysis of single-stranded (ssLNA) and double-stranded complexes (dsLNA:RNA).

As expected, all LNA-gapmers showed a negative charge with the LNA-gapmer1 surface charge of approximately -30 mV (Figure II.3.1 A). All other LNA-gapmers showed a decrease on surface charge, with LNA-gapmer2 and LNA-gapmer3 presenting a little increase in the negative charge of the ASOs, with values of -31.9 mV and -35.1 mV, respectively. In contrast, the LNA-gapmer4 and LNA-gapmer5 showed a slight increase in ASO charge with values of -44 mV and -54 mV, respectively.

Figure II.3.1 B represents the results of the secondary structure for single-stranded (ss) and double-stranded(ds)-LNA:RNA compounds for all LNA-gapmers. It is that for all duplexes a similar overall conformation is observed thus indicating no major alteration in secondary structure. For ssLNA, all LNA-gapmers present bands as expected based on literature observations, [17,18] i.e. low positive bands around 270 nm and 220 nm and low negative bands around 240 nm and 210 nm. The dsRNA, defined as A-duplex, is characterized by a strong positive band at 270 nm coupled with a strong negative band at 210 nm [17,19,20], as it can be seen for dsLNA:RNA for all LNA-gapmers.

The *in vitro* cytotoxicity was assessed on 3T3 cells and using different concentrations of LNA-gapmer ASOs (10, 40 and 100 nM) (Figure II.3.2). These studies verify that all LNA-gapmers are non-cytotoxic in concentrations up to 40 nM, as the relative 3T3 cells viability was higher than 70 % under these conditions [21].
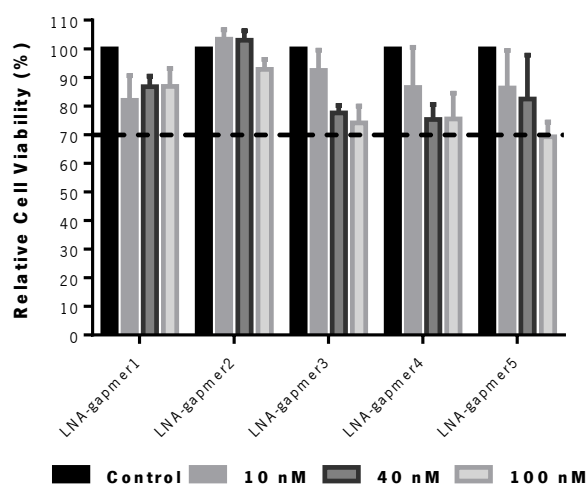
Figure II.3.2 Cytotoxicity of Anti-*EFG1* LNA-gapmer ASOs. Relative cell viability (%) determined by the absorbance (Abs (490 nm) cm^2) of formazan product obtained from 3T3 cells, treated with different concentrations of LNA-gapmers (10, 40, 100 nM). The control is compared to cells without ASO treatment.

b. Anti-*EFG1* LNA-gapmer ASOs *in vitro*

Based on the cytotoxicity results, an ASO concentration of 40 nM was selected for the *in vitro* experiments. The effect of all LNA-gapmer ASOs on *C. albicans* filamentation (Figure AIII.1 A) and on the

EFG1 gene expression (Figure AIII.1 B) was evaluated after 24 h of treatment. Figure II.3.3 A shows that all LNA-gapmers were able to control *C. albicans* filamentation with values of inhibition greater than 40 %. The LNA-gapmer1 was capable to reduce around 45 % of *C. albicans* filamentation, and a tendency of increment was observed when yeast's cells were treated with the other LNA-gapmers, however there were no statistically significant differences (P-value>0.05). The LNA-gapmer2 was able to reduce 50 % and the LNA-gapmer3, LNA-gapmer4 and LNA-gapmer5 reached 55 % of reduction (Figure II.3.3 A). The results revealed that the LNA-gapmers modified with PS-linkages and the palmitoyl-2'-amino-LNA display similar *in vitro* performance.
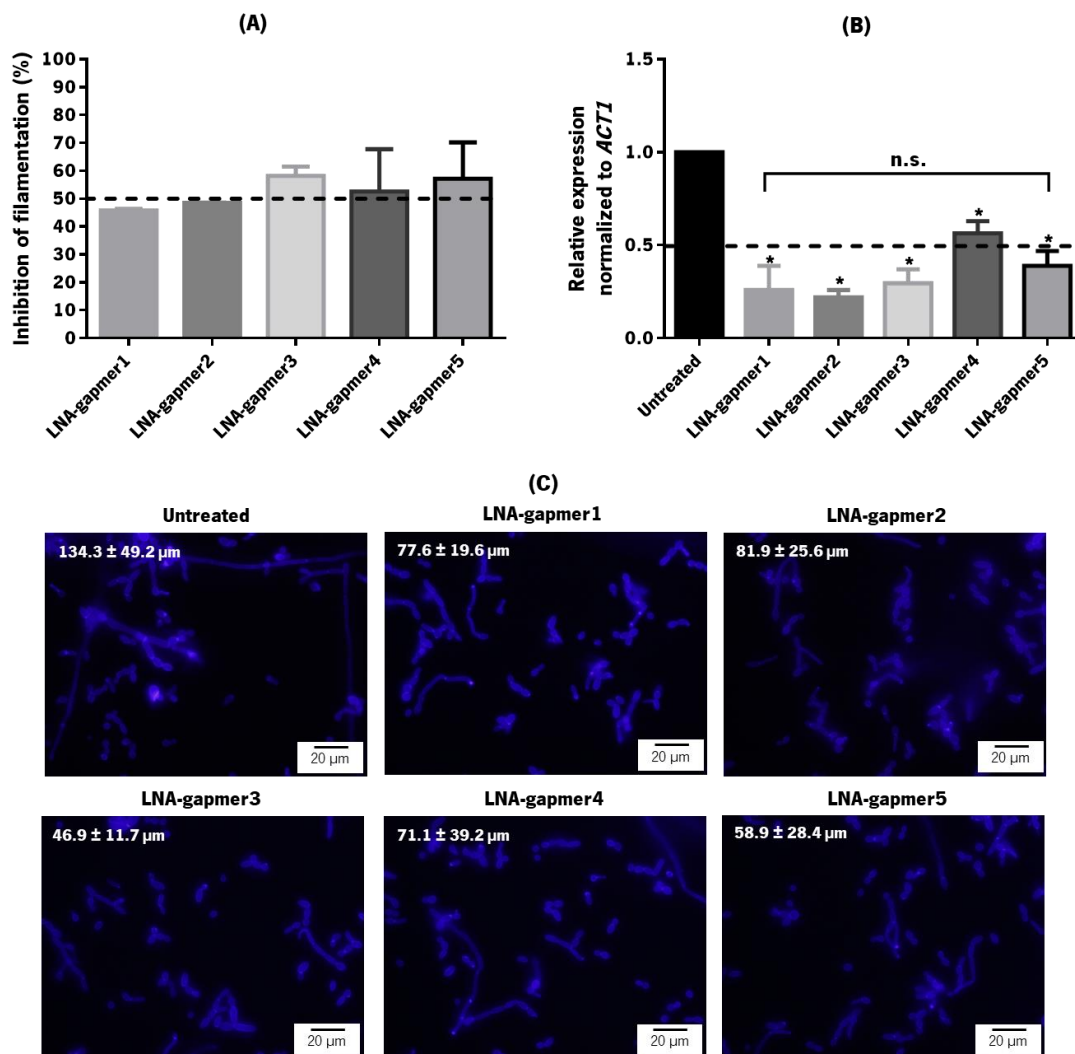
Figure II.3.3 Anti-*EFG1* LNA-gapmer ASOs *in vitro*. Effect of treatment of *Candida albicans* with LNA-gapmers (40 nM) during 24 h. **(A)** Filamentous inhibition (%). **(B)** Levels of *EFG1* gene expression evaluated by qRT-PCR. **(C)** Length of filaments determined by epifluorescence microscopy image analysis of yeast cells stained with calcofluor. Untreated represents an experiment prepared only with cells on RPMI (without ASOs). Error bars represent standard deviation. *****Significant differences between the untreated cells and the LNA-gapmers tested (P-value<0.05).

Figure II.3.3 B shows that all LNA-gapmers were able to reduce the levels of *EFG1* gene expression with values greater than 40 %. LNA-gapmer1 was able to reduce the levels of *EFG1* expression by approximately 74 %. The LNA-gapmer2 and LNA-gapmer3 had a similar performance to LNA-gapmer1, with reductions of approximately 78 % and 71 %, respectively. When using LNA-gapmer4 and LNA-gapmer5, the levels of gene inhibition were slightly reduced, reaching around 44 % and 61 %, respectively. It is important to note that the results were statistically significant when comparing the performance of all LNA-gapmers with the untreated cells (P-value<0.05), despite not presenting statistically significant differences among the LNA-gapmers (P-value>0.05).

Epifluorescence microscopy images (Figure II.3.3 C) confirmed decreases in the number of *C. albicans'* filaments which validate the ability of all LNA-gapmer ASOs to reduce the filament length. The highest impact was observed for LNA-gapmer3 and LNA-gapmer5 with reduction in filament lengths of 65 % and 56 %, respectively.

c.   Anti-*EFG1* LNA-gapmer ASOs *in vivo*

The effects of the anti-*EFG1* LNA-gapmer ASOs were in a next step evaluated using the *G. mellonella in vivo* model (Figure II.3.4) [22]. Notably, experiments showed the absence of *in vivo* toxicity for all the LNA-gapmers (40 nM) (Figure II.3.4 A). To evaluate the performance of the LNA-gapmers *in vivo*, *G. mellonella* larvae were injected with a lethal dose of *C. albicans* (7×10^7 cells mL^{-1}) together with 40 nM of each LNA-gapmer. As illustrated in Figure II.3.4 B, from the set of larvae injected with *C. albicans* cells (control) only 57 % at 24 h, 33 % at 48 h and 20 % at 72 h of larvae were alive. It is important to underline that the treatment with all LNA-gapmers increased the *G. mellonella* survival rate. The larvae injection with the LNA-gapmer1 and LNA-gapmer2, increased the survival, respectively, to 80 % and 67 % at 24 h, 53 % and 47 % at 48 h, with no effect observed at 72 h (with 20 % of survival in control and with both LNA-gapmers). The larvae which were injected with the LNA-gapmer3 and LNA-gapmer4 increased the survival rate to approximately 90 % and 83 % at 24h, 60 % at 48 h and 30 % and 33 % at 72 h, respectively. The most promising of all LNA-gapmers was the LNA-gapmer5, resulting in a survival rate of around 93 % at 24 h, 77 % at 48 h and 60 % at 72 h. In parallel, the fat body of larvae (Figure AIII.2) was recovered and processed for histological analysis (Figure II.3.4 C). As illustrated, yeast's cells are organized into clusters located around the organs or scattered around the adipose tissue. Sections of larvae infected only with *C. albicans* (control) showed intense *C. albicans* clusters composed mostly of filamentous forms, with a significant increase in the area of tissue engaged by hyphae from 24 h to 48 h

post infection. Larvae sections treated with LNA-gapmer4 and LNA-gapmer5 revealed a notable decrease in the number of *C. albicans* filamentous cells and consequently lead to a significant reduction in the area of fat body invaded by *G. mellonella*.
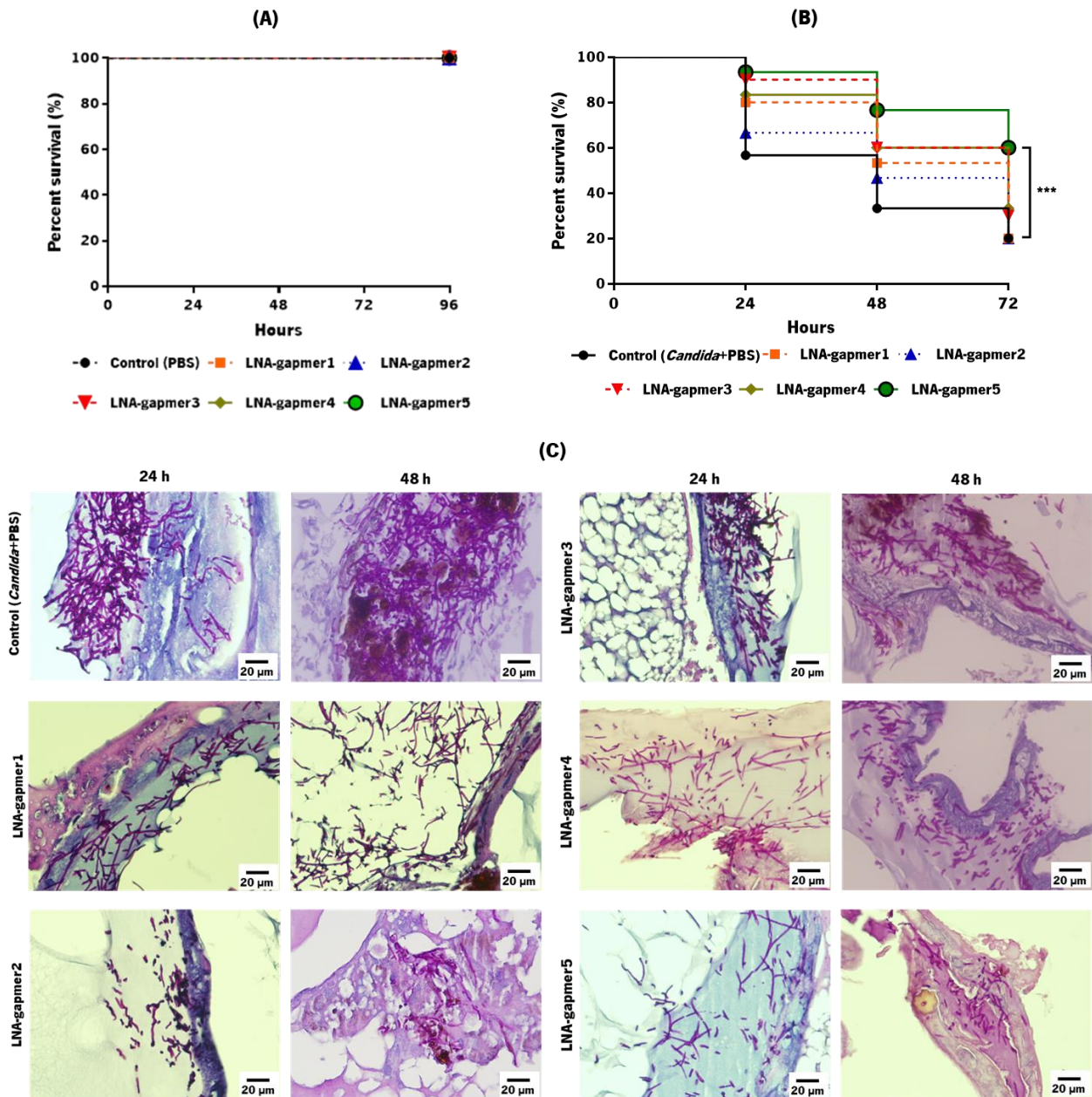
Figure II.3.4 Anti-*EFG1* LNA-gapmer ASOs *in vivo*. (A) Toxicity evaluation at 40 nM in the *Galleria mellonella* model evaluated (96 h post treatment); **(B)** Survival curves for *G. mellonella* larvae infected with *C. albicans* SC5314 (7×10^7 cells mL^{-1} injected per larva) and LNA-gapmers (40 nM) evaluated 72 h post treatment. Larvae were infected with a single dose of each LNA-gapmer at the same time of *C. albicans* cells. **(C)** Histological sections of the fat bodies of *G. mellonella* infected with *C. albicans* and treated with LNA-gapmers (40 nM) at 24 h and 48 h. The larvae sections were labelled with PAS coloration. The magnification was 400x. Results represent means of

three independent assays for 10 larvae per treatment. ******* Significant difference between the control (*Candida* + PBS) and the LNA-gapmer5 (P-value<0.001).

III.3.4 Discussion

In the last decade, the number of successful applications of ASOs for the treatment of human diseases [23–30] and to manage virus and bacterial infections [31–33] have increased. However, the ASO technology has been only poorly exploited to control *Candida* virulence determinants, and to date there are no reports of applications of LNA chemical modification to control *Candida* virulence determinants. Through this work, the efficacy of LNA-gapmer ASOs designed to hybridize specifically to an *EFG1* target, was compared in regard to the ability to control *EFG1* gene expression and to reduce the *in vitro* filamentation, in order to control *in vivo* *C. albicans* virulence. Therefore, it was designed and synthesized a set of five LNA-gapmers projected of different lengths and different chemical modifications, such as the PS-linkages or/and the palmitoyl-2'-amino-LNA chemical modifications.

Initially, all LNA-gapmers were characterized for hybridization ability, superficial charge, and secondary structure (Figure II.3.1). In many ways the LNA-gapmer ASOs behaved quite similarly. However, the inclusion of PS-linkages (LNA-gapmer3) lead to a decrease in duplex thermal denaturation temperature (T_m value) against RNA complement. As described in the literature [34,35], the PS modification and also the inclusion of palmitoyl-2'-amino-LNA (LNA-gapmer4 and LNA-gapmer5) reduced the thermal denaturation temperature of the corresponding duplexes when compared to the thermal denaturation temperatures of the duplexes involving the reference LNA-gapmer1. Of all LNA-gapmers characterized, LNA-gapmer5 displayed the lowest affinity and the highest superficial negative charge increase. The decrease in thermal denaturation temperature upon incorporation of the palmitoyl-2'-amino-LNA monomers corresponds with results reported earlier [8].

The *in vitro* and *in vivo* efficacy was evaluated for each LNA-gapmer at 40 nM since none of them showed *in vitro* (Figure II.3.2) or *in vivo* toxicity (Figure II.3.4 A) in concentrations up to 40 nM.

The *in vitro* results demonstrate the capacity of the LNA-gapmers to control *EFG1* gene expression by 40-60 % and the *C. albicans* filamentation around 50 % (Figure II.3.3). The addition of PS-linkages (LNA-gapmer3) was slightly favorable with respect to filamentation reduction but no additional effect on *EFG1* gene silencing. On the other hand, the inclusion of palmitoyl-2'-amino-LNA monomers, one in each of the two LNA wings (LNA-gapmer4 and LNA-gapmer5), did neither significantly enhance the filamentation control nor the gene silencing when compared to the performance of the other LNA-gapmers.

The *G. mellonella* caterpillar infection model was used to evaluate the effects of the LNA-gapmer ASOs on *C. albicans* virulence (Figure II.3.4). Interestingly, these *in vivo* experiments, contrary to the *in vitro* experiments, demonstrated pronounced differences between the individual LNA-gapmers. Thus, although the LNA-gapmer5 did not show the best performance *in vitro* (Figure II.3), this gapmer was the most efficient with respect to controlling *in vivo C. albicans'* virulence (Figure II.3.4 B and C). In fact, larvae treated with LNA-gapmer5 significantly increased *G. mellonella* survival from 20 % to 60 % (at 72 h of treatment). The histological images corroborated these findings with a notable reduction on the number of *C. albicans* filamentous cells and a consequent reduction in area of *G. mellonella* invasion (Figure II.3.4 C).

This work confirms the possibility to use LNA-modified ASOs to control virulence determinants of *C. albicans* and thus to control its pathogenicity. This work further revealed that LNA-type gapmer ASOs modifications with PS-linkages and palmitoyl-2'-amino-LNA monomers are favorable for *in vivo* performance and therefore constitute promising lead structures for development of drugs against *Candida* species.

References

1   Dias N and Stein C A (2002) Antisense oligonucleotides : basic concepts and mechanisms. *Mol Cancer Ther*. 1(5):347–55.

2   Chan J H P, Lim S and Wong W S F. (2006) Antisense Oligonucleotides: from design to therapeutic application. *Clin Exp Pharmacol Physiol*. 33:533–40.

3   Kurreck J. (2003) Antisense technologies: Improvement through novel chemical modifications. *Eur J Biochem*. 270(8):1628–44.

4   Khvorova A and Watts JK. (2017) The chemical evolution of oligonucleotide therapies of clinical utility. Nat Biotechnol. 35(3):238–48

5   Koshkin A A, Singh S K, Nielsen P, et al. (1998) LNA (Locked Nucleic Acids): Synthesis of the adenine, cytosine, guanine, 5-methylcytosine, thymine and uracil bicyclonucleoside monomers, oligomerisation, and unprecedented nucleic acid recognition. *Tetrahedron*. 54(14):3607–30.

6   Obika S, Nanbu D, Hari Y, et al. (1998) Stability and structural features of the duplexes containing nucleoside analogues with a fixed N-type conformation, 2'-O,4'-C-methyleneribonucleosides. *Tetrahedron Letters*. 39:5401-5404

7   Johannsen M W, Crispino L, Wamberg M C, et al. (2011) Amino acids attached to 2′-amino-LNA: Synthesis and excellent duplex stability. *Org Biomol Chem*. 9(1):243–52.

8   Ries A, Kumar R, Lou C, et al. (2016) Synthesis and biophysical investigations of oligonucleotides containing galactose-modified DNA, LNA, and 2′-Amino-LNA monomers. *J Org Chem*. 81(22):10845–56.

9   Fluiter K, Frieden M, Vreijling J, et al. (2005) On the *in vitro* and *in vivo* properties of four locked nucleic acid nucleotides incorporated into an anti-H-Ras antisense oligonucleotide. *ChemBioChem*. 6(6):1104–9.

10   DeVos S L and Miller T M. (2013) Antisense Oligonucleotides: Treating neurodegeneration at the level of RNA. *Neurotherapeutics*. 10:486–97.

11   Williams D W, Wilson M J, Lewis M A O, et al. (1995) Identification of *Candida* species by PCR and restriction fragment length polymorphism analysis of intergenic spacer regions of ribosomal DNA. *J Clin Microbiol*. 33(9):2476-9

12   Nailis H, Coenye T, Van Nieuwerburgh F, et al. (2006) Development and evaluation of different

normalization strategies for gene expression studies in *Candida albicans* biofilms by real-time PCR. *BMC Mol Biol.* 7:1–9.

13   Mil-Homens D, Bernardes N and Fialho A M. (2012) The antibacterial properties of docosahexaenoic omega-3 fatty acid against the cystic fibrosis multiresistant pathogen Burkholderia cenocepacia. FEMS Microbiol Lett. 328(1):61–9.

14   Mil-Homens D, Ferreira-Dias S and Fialho A M. (2016) Fish oils against *Burkholderia* and *Pseudomonas aeruginosa*: *In vitro* efficacy and their therapeutic and prophylactic effects on infected *Galleria mellonella* larvae. *J Appl Microbiol.* 120(6):1509–19.

15   Churukian C J and Schenk E A. (1977) Rapid Grocott's methenamine silver nitrate method for fungi and Pneumocystis carinii. *Am J Clin Pathol.* 68(3):427-8.

16   Perdoni F, Falleni M, Tosi D, et al. (2014) A histological procedure to study fungal infection in the wax moth *Galleria mellonella*. *Eur J Histochem.* 58(3):258–62.

17   Chauca-Diaz A M, Choi Y J and Resendiz M J E. (2015) Biophysical properties and thermal stability of oligonucleotides of RNA containing 7,8-dihydro-8-hydroxyadenosine. Biopolymers. 103(3):167–74.

18   Szabat M, Gudanis D, Kotkowiak W, et al. (2016) Thermodynamic features of structural motifs formed by β-L-RNA. PLoS One. 11(2):e0149478.

19   Tsai C S. (2007) Biomacromolecules structure: nucleic acids. Biomacromolecules : introduction to structure, function and informatics. First Edition, Canada, John Wiley & Sons, Inc, 55-93.

20   Choi Y J, Gibala K S, Ayele T, et al. (2017) Biophysical properties, thermal stability and functional impact of 8-oxo-7,8-dihydroguanine on oligonucleotides of RNA–a study of duplex, hairpins and the aptamer for preQ1 as models. *Nucleic Acids Res.* 45(4):2099–111.

21   International Organization for Standardization. ISO10993-5:2009. Biological evaluation of medical devices. Part 5: Tests for *in vitro* cytotoxicity. Third edition, 2009.

22   Junqueira J C. (2012) *Galleria mellonella* as a model host for human pathogens. *Virulence.* 3(6):474–6.

23   Jepsen J S, Sørensen M D and Wengel J. (2004) Locked nucleic acid: A potent nucleic acid analog in therapeutics and biotechnology. *Oligonucleotides.* 14, 130–46.

24   Frieden M and Orum H. (2008) Locked nucleic acid holds promise in the treatment of cancer. *Curr Pharm Des.* 14(11):1138–42.

25   Morinaga S, Nakamura Y, Atsumi Y, et al. (2016) Locked nucleic acid in situ hybridization analysis of microRNA-21 predicts clinical outcome in patients after resection for pancreatic cancer treated with adjuvant gemcitabine monotherapy. Anticancer Res. 36(3): 1083-1088.

26   Yamamichi N, Shimomura R, Inada K I, et al. (2009) Locked nucleic acid in situ hybridization analysis of miR-21 expression during colorectal cancer development. *Clin Cancer Res.* 15(12):4009–16.

27   Torres A, Kozak J, Korolczuk A, et al. (2016) Locked nucleic acid-inhibitor of miR-205 decreases endometrial cancer cells proliferation *in vitro* and *in vivo*. *Oncotarget.* 7(45):73651–63.

28   Ahmadi S, Sharifi M and Salehi R. (2016) Locked nucleic acid inhibits miR-92a-3p in human colorectal cancer, induces apoptosis and inhibits cell proliferation. *Cancer Gene Ther.* 23(7):199–205.

29   Nedaeinia R, Sharifi M, Avan A, et al. (2016) Locked nucleic acid anti-MIR-21 inhibits cell growth and invasive behaviors of a colorectal adenocarcinoma cell line: LNA-anti-MIR as a novel approach. *Cancer Gene Ther.* 23(8):246–53.

30   Ishige T, Itoga S and Matsushita K. (2018) Locked nucleic acid technology for highly sensitive detection of somatic mutations in cancer. *Advances in Clinical Chemistry.* 83:53–72.

31   Deng Y, Nong L, Huang W, et al. (2009) [Inhibition of hepatitis B virus (HBV) replication using antisense LNA targeting to both S and C genes in HBV]. *Zhonghua Gan Zang Bing Za Zhi.* 17:900–4.

32   Warren T K, Whitehouse C A, Wells J, et al. (2016) Delayed time-to-treatment of an antisense morpholino oligomer is effective against lethal Marburg virus infection in *Cynomolgus Macaques. PLoS Negl Trop Dis.* 10(2):1–18.

33   Sully E K and Geller B L. (2016) Antisense antimicrobial therapeutics. Curr Opin Microbiol. 3(33):47–55.

34   Crooke S T. (2004) Progress in antisense technology. Annu Ver Med. 55:61–95.

35   Lima J F, Cerqueira L, Figueiredo C, et al. (2018) Anti-miRNA oligonucleotides: A comprehensive guide for design. *RNA Biol.* 15(3):338-352

Chapter III

Creation of strategies for *C. albicans* antisense oligonucleotides cargo and delivery

Main goal

To create carrier's systems based on polymers and liposomes for the anti-*EFG1* 2'-*O*MethylRNA ASO cargo and delivery.

Chapter III.1

Polyamide microsized particulate polyplex carriers for 2'-*O*MethylRNA *EFG1* ASO

Main goal

To develop anionic and cationic polyplexes microparticles based on poly(γ-butyrolactam) (PA4) or poly(ε-caprolactam) (PA6) respectively, for anti-*EFG1* 2'-*O*MethylRNA ASO cargo and delivery.

Conclusions

This study showed that PA4 and PA6 polyplexes microparticles are feasible carriers for anti-*EFG1* 2'*O*Me ASO either using the entrapped and immobilized strategies, since the ASO released maintained its activity against *C. albicans* cells.

This chapter is based on the following article:

Araújo D, Braz J, Dencheva N, Carvalho I, Henriques M, Denchev Z, Malfois M, Silva S. Polyamide microsized particulate polyplex carriers for 2'-OMethylRNA *EFG1* antisense oligonucleotide. *ACS Applied Bio Materials*. doi.org/10.1021/acsabm.1c00334

III.1.1 Introduction

As described on Chapter I, delivery of ASOs to their site of action remains a challenge, and it appears that redesigning or finding new delivery vehicles is generally more problematic since there is no optimal delivery strategy [1]. As a result, development of such vehicles is necessary so as to ensure that ASOs are effectively protected from the environmental body conditions and to deliver them to their site of action. Polyplexes represent polymer materials and are mostly based on positively charged (cationic) polymers since the ASOs are negatively charged. The polymers can exhibit different polymeric architectures, such as linear, branched, hyperbranched, star-shaped, or dendritic structures [1–4]. Very recently, polyamide porous microparticles (MPs) were developed by activated anionic ring opening polymerization (AAROP) of lactams [5,6] and proven useful for protein recognition [7] or enzyme carriers [8]. To the best of the knowledge, so far, ASOs have not been introduced into porous microsized polyamide polyplexes. In this context, taking in account the promising results of the efficacy of anti-*EFG1* 2'-*O*MethylRNA ASO (Chapters II.1 and II.2), the main goal of this part of the work was to develop anionic and cationic polyplexes MPs based on poly(γ-butyrolactam) (PA4) or poly(ε-caprolactam) (PA6) respectively, for ASO's cargo and delivery.

III.1.2 Materials and Methods

a. Materials

The anti-*EFG1* 2'OMe ASO with the sequence 5' mG mG mC mA TACCGTTA mU mU mG mU 3' (m- 2'-*O*Me), was designed based on the second generation of nucleic acid mimics and synthesized according to the user's own specifications at EXIQON, as described in Chapter II.1. A stock of ASO at 4 μM was prepared in sterile ultrapure water and stored at -20 °C for later use.

The γ-*butyrolactam* (GBL) monomer used in the PA4-based polyplex preparation and all solvents in this work are of analytical grade supplied by Merck/Sigma Aldrich, Portugal. The ε-caprolactam, (ECL) (special grade for anionic polymerization) used in the PA6 polyplex preparation and the activator of AAROP (Brüggolen C20, containing 80 wt.% of aliphatic diisocyanate blocked in ε-caprolactam) are products of Brüggemann Chemical, Germany, which are used as received. The initiator of AAROP sodium dicaprolactamato-bis-(2-methoxyethoxo)-aluminate (dilactamate, DL) was a commercial product purchased from Katchem, Czech Republic, which is used as received.

b. Synthesis of PA4 and PA6 polyplex MPs

Two types of polyplex supports were prepared in this study wherein the ASO payload was either entrapped in the polyamide MPs during the AAROP or immobilized upon them by adsorption on prefabricated MPs. The AAROP of the respective lactams to PA4 and PA6 MPs was described in detail previously [6–8]. In a typical AAROP of GBL to PA4 MPs, 0.2 mol of the monomer was stirred for a period of 6 h with 1.5 mol. % of C20 and 3.0 mol % DL in an inert atmosphere at 40 °C, fixing the residual pressure to 50 mbar. The resulting solid reaction product was dispersed in acetone and filtered, followed by a two-fold wash with methanol. The fine white powder so produced was extracted with methanol in a Soxhlet for 4 h to get the neat PA4 MPs to produce the adsorption-immobilized ASO polyplex (PA4-Imm-ON). For the preparation of the polyplex with ASO entrapment (PA4-Ent-ON), the above AAROP was performed with 66 mmol GBL adding 4.0 µM (0.024 mg) of lyophilized ASO, using the same reaction conditions and concentrations of the activator/initiator complex as for the neat PA4 MPs.

In a typical AAROP of ECL to PA6 MPs, 50 mmol monomer dissolved in 90 mL of toluene/xylene mixture (1:1 by volume) were stirred for a period of 2 h with 1.5 mol. % of C20 and 3.0 mol % at 130 °C under reflux [5]. Then, the reaction mixture was vacuum-filtered, and the resulting fine white powder was washed and extracted with methanol, as in the case of PA4 MPs. Then the neat PA6 MPs were used to prepare the PA6-Imm-ON sample by physical adsorption of the ASO payload. For the preparation of the polyplex with ASO entrapment (PA6-Ent-ON), the above AAROP was performed with 50 mmol ECL adding 4.0 µM (0.024 mg) of lyophilized ASO at 90 °C using the same concentrations of the activator/initiator complex.

For the preparation of the PA6-Imm-ON and PA4-Imm-ON samples, 100 mg of each neat MP type was added to an Eppendorf tube containing 1 mL of a 4 µM aqueous solution of the ASO and incubated at 37 °C for 24 h using a laboratory orbital shaker. After centrifugation, the aqueous supernatant was decanted. The resulting PA6 or PA4 MPs with adsorption-immobilized ASO were washed with double distilled water and stored at 5 °C. Their immobilization efficiency was 100 % determined by the UV-vis absorbance at 260 nm before and after the immobilization (Figure AIV.1).

c. Structural and morphological characterization of the samples

Fourier-transform infra-red spectroscopy with attenuated total reflection (FTIR-ATR) was applied using a Perkin-Elmer Spectrum 100 apparatus with a horizontal ATR attachment with the ZnSe crystal. The spectra were acquired between 4000 and 600 cm^{-1} accumulating up to 16 spectra with a resolution of 2 cm^{-1}. The samples were studied in the form of fine powders.

The scanning electron microscopy (SEM) studies were performed on a NanoSEM-200 apparatus of FEI Nova (USA) using mixed secondary electron/black scattered electron in-lens detection. The pulverulent samples were observed after sputter-coating with the Au/Pd alloy in the 208 HR equipment of Cressington Scientific Instruments (UK) with high-resolution thickness control.

All the samples of this study were subjected to thermogravimetric analysis (TGA) in a Q500 gravimetric balance by TA Instruments, by heating the samples in the 40-600 °C range at a rate of 20 °C min^{-1} in a nitrogen atmosphere.

The differential scanning calorimetry was carried out in the 200 F3 equipment of Netzsch at a heating/cooling rate of 10 °C min^{-1} under nitrogen purge. The samples were heated to 290 °C, cooled down to 0 °C, and then heated back to 290 °C. The typical sample weights were in the 10-15 mg range.

Synchrotron wide- (WAXS) and small-angle X-ray scattering (SAXS) measurements were performed in the NCD-SWEET beamline of the ALBA Synchrotron facility in Barcelona, Spain.[9] Two-dimensional detectors were used, namely LH255-HS (Rayonix, USA) and Pilatus 1 M (Dectris, Switzerland) for registering the WAXS and SAXS patterns, respectively. The sample-to-detector distance was set to 131 mm for WAXS and 2690 mm for SAXS measurements, the λ of the incident beam being 0.1 nm and the beam size being 0.35 × 0.38 mm (h × v). The 2D data were reduced to 1D data using pyFAI software.[10] For processing of the WAXS and SAXS patterns the commercial packages Peakfit 4.12 by SeaSolve Software were implemented.

d. Polyplexes MPs cytotoxicity assays

The cytotoxicity side effects of the different polyplexes MPs were determined with MTS solution (CellTiter 96® Aqueous One Solution Cell Proliferation Assay, Promega) and 1 % of DMEM without phenol assays. For that, the 3T3 cell line (fibroblast cells, Embryonic tissues, Mouse from CCL3, American Type Culture Collection) was used and grown in DMEM (Biochrom, Germain) supplied with 10% FBS (Sigma Aldrich) and 1 % antibiotic- containing P/S (Biochrom, Germain). After cells detachment, 1 x 10^5 cells mL^{-1} of cells suspension was added to a 96-well plate, and cells grew until achieving 80 % of confluence. Different concentrations of neat polymers and polyplexes of PA4 and PA6 (1 and 5 mg mL^{-1}) were prepared in DMEM and 50 µL of each concentration was added each well. Negative control was prepared by adding 50 µL of DMSO to the cells and positive control by adding 50 µL of DMEM. The plates were incubated for 24 h at 37 °C and 5 % CO$_2$. The MTS procedure was carried out as described in the previous Chapter II.1.

e. Controlled release of anti-*EFG1* 2'OMe ASO from polyplexes MPs

The controlled release of anti-*EFG1* 2'OMe ASO from PA4 and PA6 polyplexes MPs was studied over 48 h. For that, approximately, 5-6 mg of each polyplex MP formulation [PA4 (PA4-Imm-ON and PA4-Ent-ON) and PA6 (PA6-Imm-ON and PA6-Ent-ON)] was added to 1 mL of phosphate-buffered saline (PBS; pH 7, 0.1 M) and incubated in 24-well plates at 37 °C and 120 rpm. At each specific time point (2, 4, 6, 8, 24, 26, 28, 30 and 48 h), an aliquot of 50 µL was recovered, and the polymer was obtained by centrifugation at 1000 g during 10 s. The related supernatants were collected, and the amount of ASO released from polyplexes MPs was determined by measuring the values of UV absorption at 260 nm (Figure AIV.2). The results are presented as the cumulative release of ASO quantity over time ($\mu M\ h^{-1}$). All experiments were performed in triplicate and in a minimum of three independent assays.

f. Microorganism and growth conditions

Candida used in this study was the reference strain *C. albicans* SC5314 belonging to *Candida* collection of the Biofilm group of the Centre of Biological Engineering and its identity was confirmed by PCR-based sequencing with specific primers (ITS1 and ITS4) [11].

The *Candida* cells were subcultured on Sabouraud dextrose agar (SDA; Merck, Germany) and incubated for 24 h at 37 °C. An inoculum was prepared in Sabouraud dextrose broth (SDB; Merck, Germany) and incubated overnight at 37 °C, 120 rpm. After incubation, the cell suspensions were centrifuged for 10 min at 3000 g at 4 °C and washed twice with PBS (pH 7, 0.1 M). Pellets were resuspended in 5 mL of Roswell Park Memorial Institute cell culture medium (RPMI, pH 7; Sigma, St Louis, USA), and the cellular density was adjusted for each experiment using a *Neubauer* chamber (Paul Marienfild, Lauda-Königshofen, Germany) to 1×10^6 cells mL^{-1}. All experiments were performed in triplicate and in a minimum of three independent assays.

g. Effect on *C. albicans* filamentation

The effect of anti-*EFG1* 2'OMe ASO released from PA4 and PA6 polyplexes MPs was evaluated in terms of its ability to reduce *C. albicans* filamentation. For that, on 24-well polystyrene microtiter plates (Orange Scientific, Braine-l'Alleud, Belgium), approximately 5-6 mg mL^{-1} of each MP with ASO was resuspended in RPMI together with a suspension of *C. albicans* SC5314 at 1×10^6 cells mL^{-1}. The suspensions were incubated at 37 °C at 120 rpm during 48 h. The positive control was prepared with 1 mL of *C. albicans* cells and the negative controls with each polyplex MPs without ASO together with *C. albicans* cells in RPMI. After 24 h and 48 h, the aliquots were recovered by centrifugation for 5 min at

6000 g and 4 °C, and in a total of 100 *C. albicans* cells, the number of cells as filaments was enumerated using a Neubauer chamber. The number of non-filamentous cells was normalized by the quantity of ASO released from each polyplex MPs at 24 h and 48 h. The results are presented as the number of non-filamentous cells per µM of ASO.

In parallel, epifluorescence microscopy images were obtained to confirm the levels of filamentation and to determine the filament length, as previously described in Chapter II.1.

h. Statistical analysis

Data are expressed as the mean ± standard deviation of a least three independent experiments. Results were compared using two-way ANOVA and Tukey's multiple comparisons tests using GraphPad Prism® (GraphPad Software, San Diego, CA, USA). All tests were performed with a confidence level of 95 %.

III.1.3 Results and Discussion

Generally, ASOs represent short chains of certain nucleic acids that can bind to the target RNA by means of standard Watson-Crick base pairing through hydrogen bonds [12]. This capacity for H-bond formation can be used to attach the ASO to a suitable polymeric carrier. The polyplex so-formed will be expected to display better *in vivo* stability to the bioactive entities in the body fluids, improving the cellular uptake and the protection against the serum nucleases and other enzymes [4,13,14]. The purpose of this work was to use as polymeric carriers, the microsized porous PA4 or PA6 MPs, for ASO cargo and future delivery. Two ways to obtain the respective polyplexes were studied: by physical adsorption of ASO upon prefabricated polyamide microcapsules or by their entrapment into polyamide MPs *in-situ* forming via AAROP. Thus, AAROP of GBL or ECL was performed without or with ASO inclusion in the reaction mixture, respectively. A simplified scheme of AAROP of ECL is presented in Figure AIV.3. It is expected that the presence of secondary amide groups in both PA4 and PA6 carriers would enable intensive H-bond formation with the nitrogen nucleobases in ASO leading to immobilization of the oligonucleotides in the polyamide particles. In the case of physical adsorption of ASO, one may expect only H-bond formation. In the case of *in-situ* entrapment during AAROP that occurs at 40 °C (PA4 carrier) or 90 °C (PA6 carrier), some chemical reactions between ASOs and the forming polyamide MP are theoretically possible. This is possible since in each step of polyamide chain growth or in the termination of AAROP, the necessary extraction of proton from primary or secondary amine or amide groups can involve some of the ASO

pyrimidine or purine bases causing incorporation of the oligonucleotide into the polyamide chain. Hence, this work will present a comparative discussion on the morphology, structure, and biological activity of polyplexes obtained by adsorption or entrapment on PA4 or PA6 MP carriers against *C. albicans* cells.

As seen from Table AIV.1, both types of empty MP carriers are negatively charged, the values varying between -23 (PA4 MP) and -12 eV (PA6 MP). At a pH slightly below the neutral and similar to the one at which the adsorption-immobilization process is carried out, the value of the negative charge will depend on the amount of terminal carboxyl groups in the PA6 or PA4 macromolecules, most probably being larger in the latter case. The second factor will be the protonation of the CONH group of the polyamide carrier that will depend on its crystalline structure. Having in mind that the ASO molecules are always negatively charged, it should be therefore concluded that the interaction between the ASO and the polyamide carrier in the adsorption immobilization is not based on electrostatic forces but on the formation of multiple hydrogen bonds that overcome the repulsion between the equally charged ASO and the polyamide carrier.

a. Characterization of PA4 and PA6 MPs and polyplexes on their basis
Microscopy studies

As explained in the experimental part, for the adsorption-immobilization approach the purified PA4 and PA6 MPs were incubated in aqueous solutions of ASO. Then, PA4-Imm-ON and PA6-Imm-ON were obtained after decanting the water and drying. PA4-Ent-ON and PA6-Ent-ON were synthesized by adding ASO molecules to the reaction mixture of AAROP of ECL or GBL, respectively. All polyplex samples represent are fine powders. Some of their properties are presented in Table III.1.1 in comparison to neat PA4 and PA6 MPs.

Table III.1.1 Designation and some characteristics of PA6 and PA4 MP and polyplexes

Sample	PA yield, %[a]	η, dL.g^{-1}	$d_{max,}$[b] μm	d_{max}/d_{min}[b]
PA4	50.4	0.926	5-10	1.1-1.3
PA4-Imm-ON	-	-	5-15	1.1-1.6
PA4-Ent-ON	46.6	0.833	10-25	1.1-1.6
PA6	52.0	0.983	20-30	1.2-1.4
PA6-Imm-ON	-	-	15-35	1.1-1.5
PA6-Ent-ON	39.8	0.902	20-60	1.1-1.5

(a)   relation to the lactam monomer;

(b)   Interval of values including >80 % of the particles number.

The intrinsic viscosity [η] of 0.983 dL g^1 of the neat PA6 (Table III.1.1, Annex IV) corresponds to circa (ca.) 27.500 g/mol. The same viscosity average molecular weight M_v is ascribed to the PA6-Imm-ON sample. For the PA4 and PA4-Imm-ON samples M_v cannot be calculated since the Mark-Houwink parameters K and α are unavailable. However, the [η] value of 0.926 dL g^1 for PA4 and PA4-Imm-ON reached in this study is similar to that of PA4 microspheres obtained by a different method involving AAROP of GBL [15]. The polymerization yields of the neat polyamides are 50-52 %, close to those found in previous studies. The AAROP during the entrapment of ASO in PA4 and PA6 occurred normally with similar yields of PA4-Ent-ON and PA6-Ent-ON. Judging from the lower [η] values of the entrapped samples, they are of lower molecular weights compared to the neat PA6 and PA4 MPs. The average maximum size of the particles d_{max} in all neat polyamides and polyplex samples based on optical microscopy with image-processing was found to be between 5 and 60 μm (Table III.1.1, Figure AIV.4). The d_{max} of neat PA4 MP is the smallest, ranging between 5 and 10 μm. Similar values of 5-15 μm are registered for the PA4-Imm-ON samples, while in the PA4-Ent-ON sample the upper limit of d_{max} grows above 25 μm. The neat PA6 produces MPs with d_{max} in the 20-30 μm range. The respective PA6-Imm-ON and PA6-Ent-ON polyplexes are characterized with very broad size distributions with upper limits in the latter case of 60 μm. As seen from Table III.1.1, the presence of ASO in both adsorption-immobilized or entrapped form leads to an increase of the roundness parameter d_{max}/d_{min} meaning less spherical MPs as compared to the neat PA4 and PA6 MPs. More details on the morphology of the empty supports and ASO-carrying particles can be obtained by SEM. Figure III.1.1 shows the micrographs of the neat PA6 (Figure III.1.1 A(a-c)) displaying spheroidal particles with sizes of the individual entity of 20-30 μm that can form also aggregates with average sizes close to 50 μm. At larger magnification, the PA6 particles display a highly porous, scaffold-like topology with average visible pore diameters larger than of 500 nm. The pore sizes do not seem to change significantly in the PA6-Ent-ON (Figure III.1.1 A(d-f)) and PA6-Imm-ON samples (Figure III.1.1 A(g-i)); however, both entrapment and adsorption of ASO results in more expressed agglomeration of MPs to aggregates with d_{max} of 60-100 μm, better expressed in the adsorption-immobilized polyplex.
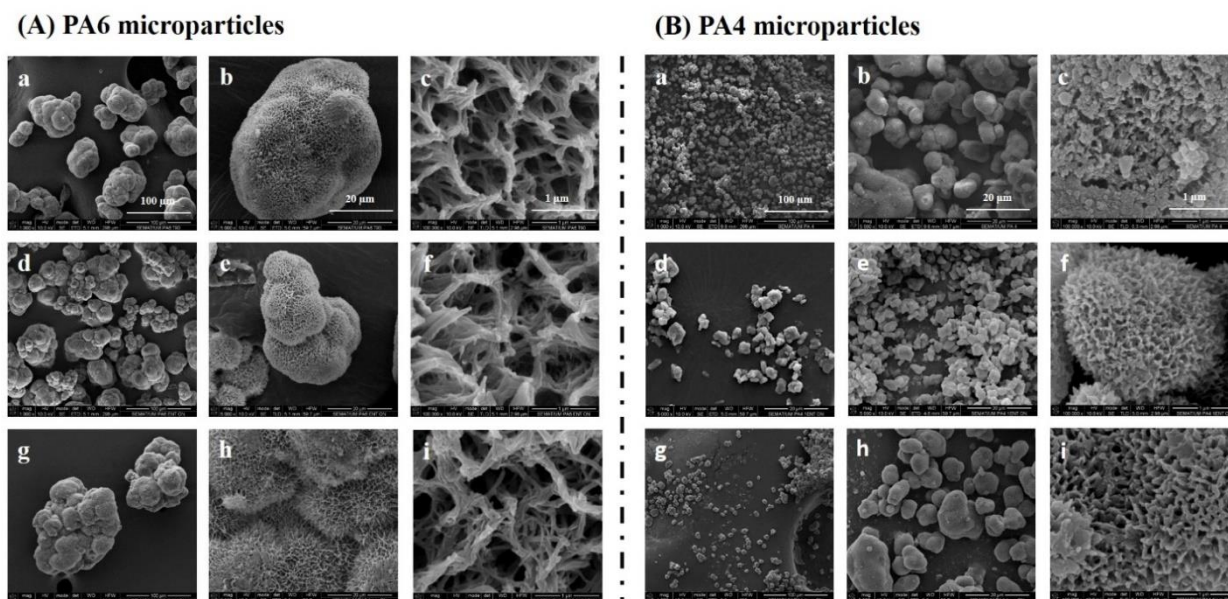
Figure III.1.1 Scanning electron microscopy of neat carriers and polyplex samples based on (A) PA6 microparticle and (B) PA4 microparticle: **(a-c)** neat microparticle; **(d-f)** Entrapped sample; **(g-i)** Immobilized sample. For sample designation see **Table III.1.1.**

As seen from Figure III.1.1 B, the average size of the ovoid PA4 neat MPs (Figure III.1.1 B(a-c)) is much smaller than in the PA6 neat carrier, being in the range of 6-10 μm, displaying pore sizes with visible diameters of 150-200 nm. In the ASO entrapped samples (Figure III.1.1 B(d-f)), the size of the PA4-Ent-ON sample is maintained around 10 μm; however, the shape of the particle's changes from ovoid to platelets with sharper edges, mostly due to different nucleation mechanisms during MPs crystallization. The shape and size of the PA4-Imm-ON sample (Figure III.1.1 B(g-i)) is remarkably similar to the neat PA4 used for its preparation, with analogous surface topography and average diameters of the pores on the surface ca. 200 nm. The variations in the shape, size, and surface topography of the PA6- and PA4-based samples can be explained with the different polymerization conditions of the polyamide carriers required by the different monomer activity and crystallization behavior during the polymerization.

FTIR Spectroscopy

An FT-IR spectral comparison between the PA6-based and PA4-based samples of this study is presented in Figure III.1.2a,b, respectively. In all samples, the bands at 3300 cm^{-1} were assigned to the valence stretching vibrations of hydrogen atoms in secondary NH groups of the polyamide carriers. Also,

the spectra show well-defined peaks for amide I at 1631.5 cm^{-1} and amide II at 1535.0 cm^{-1} with almost identical intensities. This is a clear indication for fixation of the trans-conformation of the NH-CO group, being typical for high molecular weight polyamides. This was important to confirm for the PA6-Ent-ON (Figure III.1.2a) and PA4-Ent-ON (Figure III.1.2b) samples.
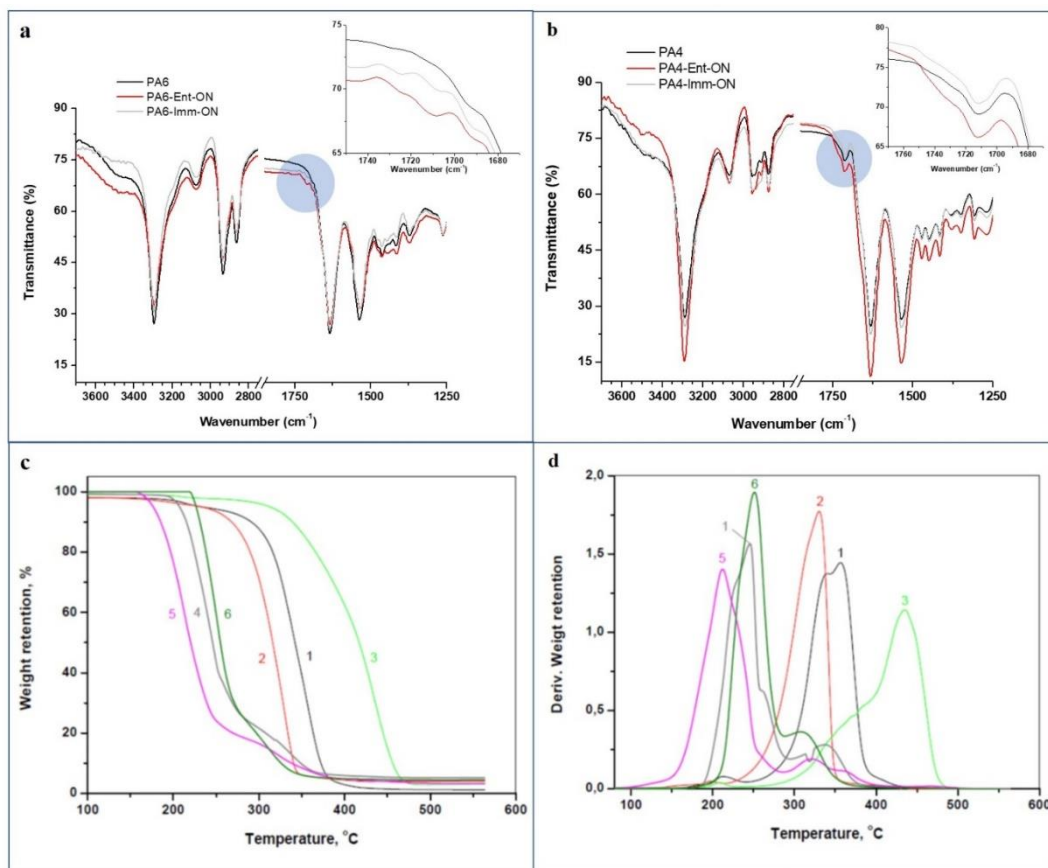
Figure III.1.2 Comparison of Fourier-transform infra-red spectroscopy with attenuated total reflection spectra of polyplexes based on (a) PA6 microparticle and **(b)** PA4 microparticle. The inset displays the area 1650-1800 cm^{-1} where the terminal carboxyl groups appear. **Thermogravimetric analysis traces of polyamide polyplexes (c)** integral curves; **(d)** first derivative curves: **(1)** PA6; **(2)** PA6-Ent-ON; **(3)** PA6-Imm-ON; **(4)** PA4; **(5)** PA4-Ent-ON; **(6)** PA4-Imm-ON.

All curves also display a weak peak at 1710-1712 cm^{-1} attributable to terminal carboxyl groups. In the neat PA6 sample (Figure III.1.2a, the inset), this peak appears as an unresolved shoulder of the amide I peak of PA6 belonging to the –COOH macromolecule terminus. In the macromolecule of the neat PA4, this COOH-related peak is even clearer (Figure III.1.2b, the inset). The immobilization of ASO by adsorption or entrapment in both carriers results in a series of additional small and unresolved peaks in this area. Theoretically, these peaks should result from the nucleobases of ASO and can be considered an indirect proof of the inclusion of the oligonucleotide in the polyplexes. However, FTIR cannot provide

more detailed quantitative or qualitative information about the entrapped or adsorbed ASO due to its low concentration.

Thermogravimetric analysis

Figure III.1.2 also displays the weight retention as a function of temperature in PA6- (curves 1-3) and PA4-based samples (curves 4-6) presented in the integral (Figure III.1.2c) or derivative form (Figure III.1.2 d).

Interestingly, the adsorption-immobilized PA6-Imm-ON and PA4-Imm-ON samples display better heat resistance than the respective neat MPs, expressed in higher temperature of initial degradation (T_d^{init}), the difference being ca. 80 °C for the PA6-based samples and ca. 15 °C for the PA4-based ones (Figure III.1.2c). On the contrary, the entrapment of ASO causes lower T_d^{init} values of the PA6-Ent-ON and PA4-Ent-ON samples with a difference of ca. −20 °C for both polyamides (Figure III.1.2c). Similar effects were observed in PA4 MPs carrying laccase [8] or protein [7] payloads introduced by adsorption immobilization or entrapment. Therefore, in the case of ASO adsorption, it seems that the ASO is deposited upon the MPs surface and during the TGA heating ramp, it manages to protect the COOH- end groups of the polyamide carriers from where the thermal degradation of polyamides normally starts [16]. In the case of ASO entrapment, it goes apparently to the nucleus of the MPs leaving their surface unprotected to thermal degradation. In this context, the changes in T_d^{init} of the entrapped and adsorption-immobilized samples can be considered another proof for the inclusion of ASO in the MPs.

Figure III.1.2d presents the derivative TGA curves, wherein the peak values represent the temperatures of maximal thermal degradation T_d^{max} and the number of peaks indicates the number of thermal degradation events. Hence, in neat PA6 (curve 1) there exist two degradation events with a T_d^{max} of 340 and 360 °C, and in neat PA4 (curve 4) at 225 and 240 °C. The entrapment of ASO also results in two degradation events: in PA4-Ent-ON, the better expressed one is at ca. 210 °C, with a small fraction of sample degrading most intensively at 320 °C. PA6-Ent-ON displays a degradation maximum at 330 °C. In summary, entrapment of ASO leads to faster degradation at lower temperatures than in the neat polyamide carriers. The adsorption of ASO maintains the primary T_d^{max} of PA4-Imm-ON in the range of 245-250 °C with a secondary event being fastest at 320 °C. The PA6-Imm-ON sample also displays dual degradation behavior with the primary degradation occurring in a broad range centered at 350 °C and a second intensive degradation at ca. 440 °C. In summary, the TGA data suggest that in comparison to the neat PA4 and PA6 supports, the entrapped samples possess lower thermal stability and the adsorption-immobilized ones – higher thermal stability. This is due to different mechanisms of thermal

degradation caused by the ASO component. As mentioned before, in the adsorption-immobilized samples, it is on the particles surface making them less thermoconductive and therefore more resistant to pyrolysis.

Synchrotron WAXS

The FTIR and TGA experiments, as well as the microscopy studies provided evidence about the presence of ASO in the polyplexes studied, being physically adsorbed onto, or entrapped into the polyamide MPs. The postulated intense H-bond formation between ASO molecules and the polyamide supports may theoretically alter the crystalline structure of the polymeric support that can be probed by X-ray scattering techniques. In an attempt to evaluate these factors in empty polyamide supports and in the respective ASO-adsorbed or entrapped polyplexes, synchrotron WAXS and SAXS were employed.

Figure III.1.3 shows a comparison between the linear WAXS patterns of PA6-based polyplexes (Figure III.1.3a) and PA4-based ones (Figure III.1.3b). All WAXS patterns display two strong reflections at q values of 14.5 and 17.0 nm^{-1} that should be ascribed to the monoclinic unit cell of α-PA4 and α-PA6. The visual inspection of the WAXS patterns of the PA6-Ent-ON and PA4-Ent-ON samples (curves 1 and 3 in Figure III.1.3a, b) suggests that the entrapment of ASO does not seem to significantly change the polyamide crystalline structure, maintaining the angular position and the intensities of the two α-polymorph reflections. Figure III.1.3a, b also displays the pattern of the PA6-Imm-ON and PA4-Imm-ON samples. Therefore, the two WAXS reflections for the α-PA6 and α-PA4 apparently maintain their form and position; however, there appears a hump in the background at high q values related to a new diffuse reflection centered at high q values.

Figure III.1.3 Linear synchrotron wide-angle X-ray scattering patterns of: **(a)** PA6-based polyplexes; **(b)** PA4-based polyplexes. **(1)** neat polyamide carriers; **(2)** PA-Imm-ON samples; **(3)** PA-Ent-ON samples.

Further information about the crystalline structure of the samples can be extracted after processing the WAXS patterns shown in Figure III.1.4 by peak fitting. This procedure and the subsequent quantification of the degree of WAXS crystallinity X_c^{WAXS} and the polymorphism in the polyamide supports is made according to earlier publications resolving the crystalline parameters of PA4 [6] and PA6 [17]. All structural information from the fitted WAXS patterns is presented in Figure III.1.4 A. All data treatments in Figure III.1.4 A show that excellent fits with regression coefficients $R^2 \geq 0.999$ were only possible if along with the two peaks of the α-polyamide crystalline form and the two amorphous halos AH_1 and AH_2, two more crystalline peaks are considered that should be assigned to an additional monoclinic phase. In the case of PA6, this polymorph is designated as γ-phase[17] or as β-phase in PA4 [18,19].

(A)

Sample	a, %	β or g, %	X_c^{WAXS} %	a/b(g)	q_{max}, nm^{-1}
PA4	28.6	28.1	56.7	1.02	-
PA4-Ent-ON	24.0	25.6	49.6	0.94	-
PA4-Imm-ON	16.8	20.6	37.4	0.82	19.5
PA6	22.3	19.8	42.1	1.13	-
PA6-Ent-ON	21.1	19.3	40.4	1.09	-
PA6-Imm-ON	17.5	13.8	31.3	1.27	19.9

Note: Data obtained after deconvolution of the linear WAXS profiles as indicated in Figure III.1.3. q_{max} is the angular position of the AH3 diffuse peak in Fig III.1.4c and III.1.4f; X_c^{WAXS} = WAXS crystallinity index. For more information, see the text.

(B)

Figure III.1.4 (A) Synchrotron wide-angle X-ray scattering analysis of neat MP and polyplexes. **(B)** Deconvolution of polyamide-based polyplexes: **(a)** PA4; **(b)** PA4-Ent-ON; **(c)** PA4-Imm-ON and PA6-based polyplexes: **(d)** PA6; **(e)** PA6-Ent-ON; **(f)** PA6-Imm-ON.

In accordance with previous synchrotron WAXS studies [6,8], the appearance of a new diffuse halo in the PA4-Imm-ON and PA6-Imm-ON means that in the adsorption-immobilized polyplexes there exist possibilities for lateral interaction between oligonucleotides through H-bond formation between N-bases. Moreover, these bases seem to also form H-bonds with the polyamide amide groups in the amorphous phase of the carrier leading to its much denser packing. Hence, as seen from Figure III.1.4 A, the new amorphous peak in the adsorption-immobilized samples (Figure III.1.4 B(c, f) designated as AH3 is centered at $q_{max} \approx 20$ nm^{-1}. Meanwhile, the main amorphous peak of the same PA-Imm-ON samples, as well as those of the neat PA4 (Figure III.1.4 B(a)) and PA6 (Figure III.1.4 B(d)) are in the q-range of 15.5-16.0 nm^{-1}, meaning less dense packing in the amorphous phase of the polyamide carriers in the absence of ASO.

In the ASO-entrapped samples (Figure III.1.3(a,b), curve 2) an additional diffuse peak AH3 does not appear. This observation leads to two conclusions for the PA6-Ent-ON and PA4-Ent-ON samples: (i) the ASO in them that is arrested in the polyamide particles during AAROP cannot form a separate amorphous reflection, and (ii) the entrapped ASO does not upset the crystallization of both polyamide polymorphs. It can be therefore hypothesized that in the PA-Ent-ON series the ASO molecules are distributed within the amorphous phase of the semicrystalline polyamide support quite homogeneously with no significant interaction between one another.

Synchrotron SAXS

The use of synchrotron SAXS allows further clarification of the structure of the PA6- and PA4-based polyplexes. This method probes density periodicities with dimensions in the 20-250 angstroms range, which includes the sizes of the crystalline lamellae typically found in semi-crystalline polymers.

The background-subtracted and Lorentz-corrected SAXS linear profiles of the three PA4 samples (Figure III.1.5 a) can be compared to those of PA6-based samples (Figure III.1.5 b). It can be seen that the PA4 support and the PA4-Imm-ON sample (Figure III.1.5 a, curves 1 and 2) show relatively well resolved Bragg peaks indicating the lamellar stack morphology with a long spacing value $L_B = 61$ Å, i.e., that is close to the 63-66 Å established previously in PA4 bulk samples [19]. Apparently, the adsorption of ASO upon the PA4 MPs does not change the lamellar crystal structure of the support. However, the entrapment of the oligonucleotide (Figure III.1.5 a, curve 3) deteriorates the lamellar periodicity (i.e., the SAXS peak becomes less resolved), increasing the L_B to 70 Å. These effects can be explained with a decrease of the density gradient between the crystalline and amorphous phase in the lamellar stacks of the PA4 support due to the incorporation in it of the ASO molecules.

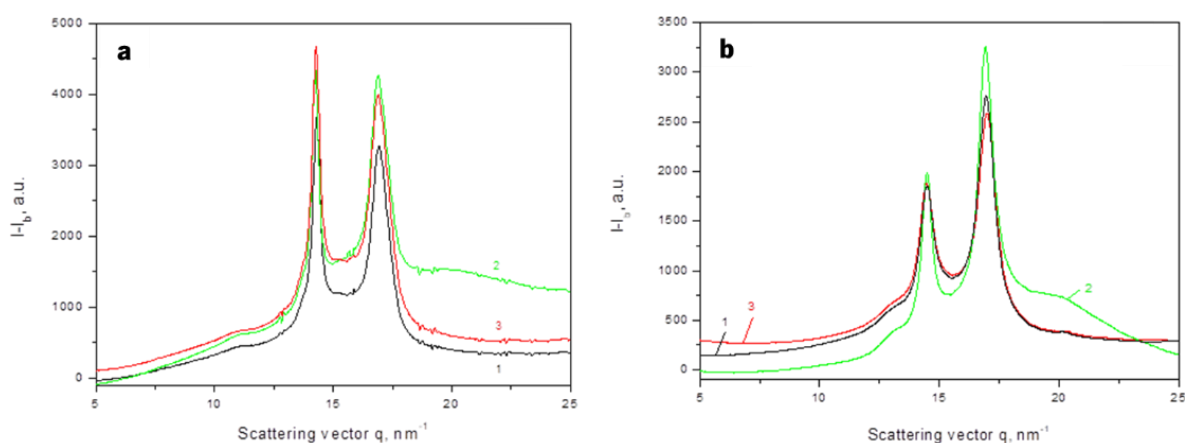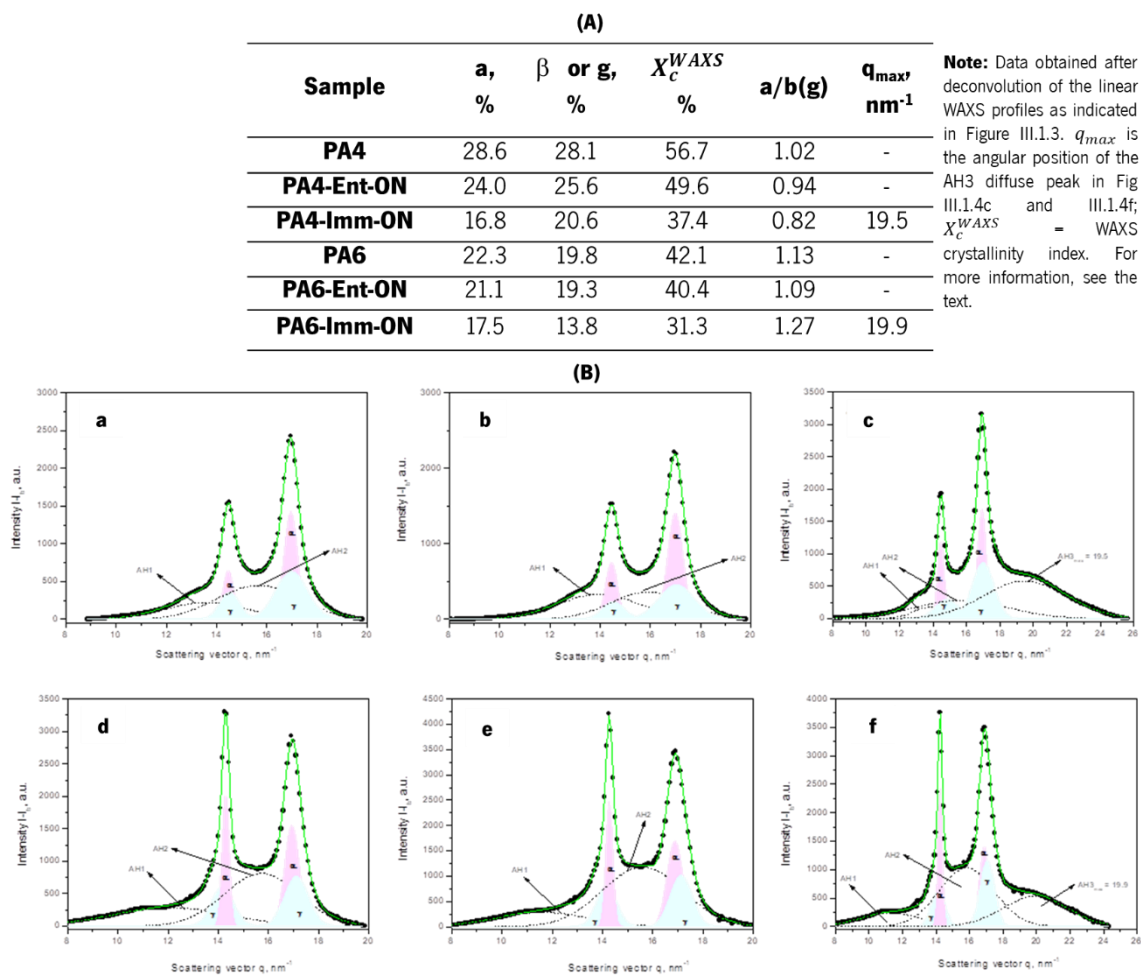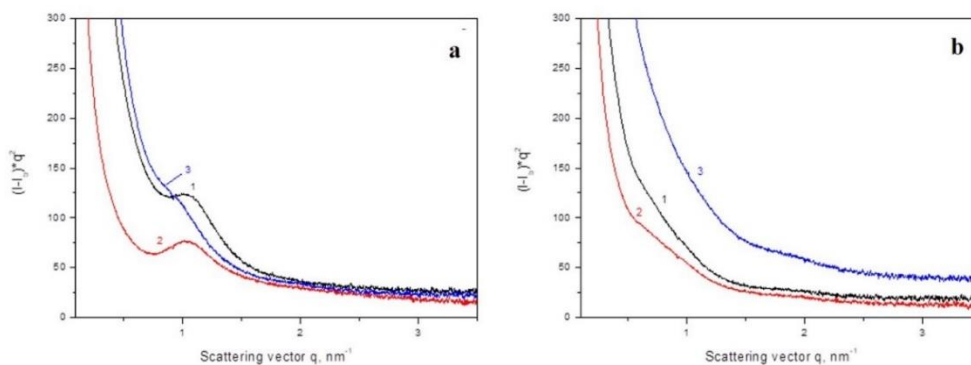**Figure III.1.5 Linear small-angle X-ray scattering patterns of (a)** PA4-based polyplexes; and **(b)** PA6-based polyplexes. **(1)** neat polyamide carriers; **(2)** PA-Imm-ON samples; and **(3)** PA-Ent-ON samples.

Figure III.1.5b makes clear that all PA6-based samples display very poorly resolved Bragg peaks whose maxima cannot be established from the linear SAXS profiles. This can be explained with the extremely high porosity of the PA6 carrier (See Figure III.1.1 A(c,f,i), which strongly deteriorates the phase contrast between the crystalline and amorphous PA6 resulting in the absence of the SAXS peak in Figure III.1.3a.

The SAXS data in Figure III.1.5 confirm the hypothesis that in PA4-Ent-ON and PA6-Ent-ON samples the ASO component is arrested within the amorphous phase of the polyamide support. In the ASO adsorbed samples (PA6-Imm-ON and PA4-Imm-ON), the ASO phase seems to be located within the pores of the polyamide MPs.

b. Cytotoxicity tests of polyplexes MPs

In the previous Chapter II.1, it was demonstrated the absence of anti-*EFG1* 2'OMe ASO molecule cytotoxicity. Figure III.1.6 presents the results of the polymers and polyplexes of PA4 and PA6 cytotoxicity on the 3T3 cell line through the MTS assay. Hereby, it was demonstrated that both polymers (PA4 and PA6) as well as the MPs of PA4 and PA6 Imm-ON and Ent-ON at the concentrations tested, are no cytotoxic in accordance with the International Standard (2009), ISO10993-5 (P-value>0.05) [20]. To note, the relative cell viability of 3T3 cells is higher than 70 % of the control (absence of polyplexes MPs).
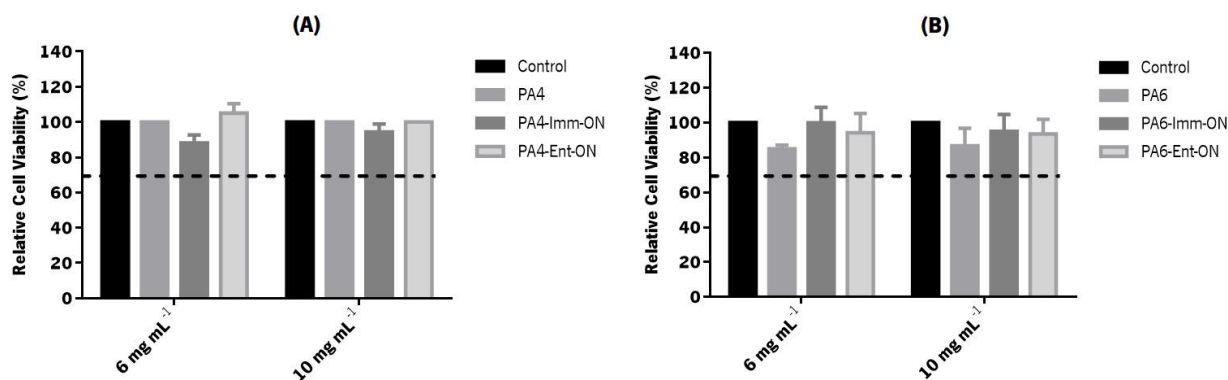
Figure III.1.6 Relative cell viability of **(A)** PA4-based polyplexes and **(B)** PA6-based polyplexes microparticles determined by the absorbance values (Abs (490 nm) cm^{-2})) of the formazan product obtained from 3T3 cells in contact with 6 and 10 mg mL^{-1} microparticles. The control refers to cells without any treatment. Error bars represent standard deviation.

c. Controlled release of anti-*EFG1* 2'OMe ASO from polyplexes MPs

Figure III.1.7 presents the cumulative release concentration of anti-*EFG1* 2'OMe ASO from PA4 and PA6 MPs over 48 h. For all polyplexes MPs, the release of anti-*EFG1* 2'OMe ASO increases over the time; however, the release rate was polyplex type dependent.
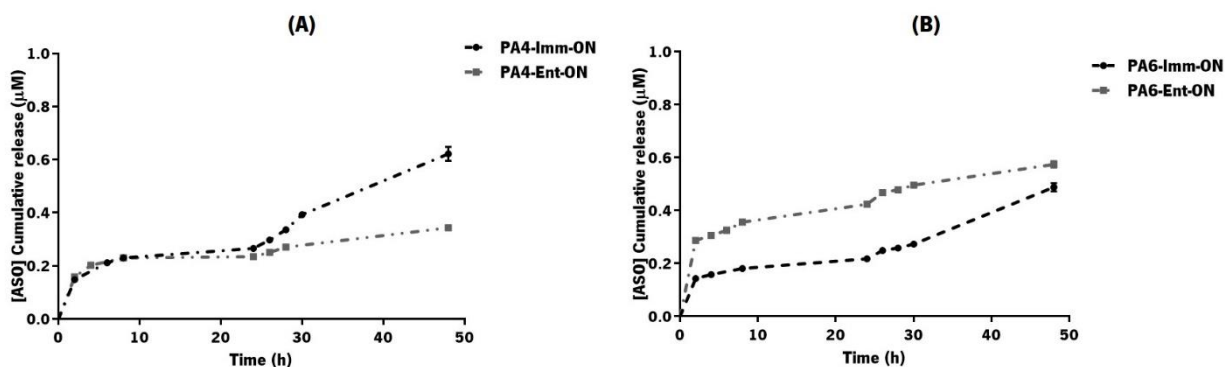
Figure III.1.7 Cumulative controlled release profiles of anti-*EFG1* 2'OMe ASO immobilized (Imm) and entrapped (Ent) into **(A)** PA4-based polyplexes and **(B)** PA6-based polyplexes over time.

In the case of PA4-Imm-ON, the release rate was similar to PA4-Ent-ON until the first 24 h (Figure III.1.7 A). However, after 24 h, it was observed a significant increase on anti-*EFG1* 2'OMe release from PA4-Imm-ON. These results seem to be consistent with the ASO molecule localization on the surface of MP after the immobilization process, suggesting that they can be more easily freed. The profile of anti-*EFG1* 2'OMe ASO released from PA6 MPs was significantly different from that observed from PA4 MPs.

It was observed that anti-*EFG1* 2'OMe ASO is more easily released from PA6-Ent-ON than from PA6-Imm-ON over the time, despite reaching similar values after 48 h of incubation (Figure III.1.7 B).

In other instance, the release rate of PA6-Ent-ON (Figure III.1.7 B) was higher than that observed in the case of PA4-Ent-ON (Figure III.1.7 A). This is an expectable result, once as SEM images revealed that the size pore of PA6 is higher than that observed on PA4 (Figure III.1.1). The release curves of PA4-Imm-ON (Figure III.1.7 A) and PA6-Imm-ON (Figure III.1.7 B) were remarkably similar.

d. Effect of anti-*EFG1* 2'OMe ASO released from polyplexes MPs on *C. albicans*

The anti-*EFG1* 2'OMe ASO was designed to bind to the *EFG1* mRNA in order to degrade it, blocking its translation into proteins and, consequently, reducing the transition of *C. albicans* from yeast to filamentous forms. As previously shown, the anti-*EFG1* 2'OMe ASO significantly reduced *EFG1* gene expression and Efg1p translation and consequently reduced *C. albicans* cell filamentation. In the present work, was evaluated the possibility to use PA4 and PA6 carriers for anti-*EFG1* 2'OMe ASO cargo and delivery. For that, the efficacy of anti-*EFG1* 2'OMe released from polyplexes MPs (PA4-Imm-ON, PA4-Ent-ON, PA6-Imm-ON, PA6-Ent-ON) on *C. albicans* cells filamentation was determined, as well as their effect on *C. albicans* filament length (Figure III.1.8). Figure III.1.8 A presents the results as the number of non-filamentous cells per µM of ASO released. Importantly, it was observed an effect on *C. albicans* cells filamentation for all polyplexes MPs, however dependent on the polyplex type and time. In accordance with Figure III.1.7, all polyplexes MPs presenting different release rates and consequently ASOs molecules could not be immediately available to interact with *C. albicans* cells. To note that at 24 h, the highest performance was observed in the case of PA6-Imm-ON and the lower in the case of PA6-Ent-ON (P-value<0.05). The lower performance of PA6-Ent-ON in terms of *C. albicans* filamentation reduction could be related with the temperature (80-85 °C) used to polymerize the polymer. Concerning, the number of non-filamentous cells counting after incubation with PA4-Imm-ON and PA4-Ent-ON, it was observed a similar pattern (P-value>0.05) (Figure III.1.8A). After 48 h of incubation, it was observed in general a decrease on the effect of the ASO release from all polyplexes MPs, with exception of PA4-Ent-ON and PA6-Ent-ON, which maintains its low performance (P-value>0.05). The loss of effect observed over the time may reflect excess ASOs molecules free that are competed to cross the *C. albicans* cells wall. The highest effect at 48 h was observed in the case PA4-Ent-ON (Figure III.1.8 A) which is the polyplex MPs with lower values of ASO released (Figure III.1.7 A).

In Figure III.1.8 B, is presented the epifluorescence images for all MPs after 24 h and 48 h. The examination of epifluorescence microscopy images confirms the results of reduction on filamentation obtained and it is also possible to observe a consistent relevant decrease in terms of the filaments' lengths. As can be seen, after 24 h, PA6-Ent-ON presented the major reduction of the filament length of around 60 % (135 to 57 µm) and subsequently the highest release rate of ASO (Figure III.1.7 B). In contrast, the more pronounced reduction of hyphae length after 48 h was in PA4-Imm-ON, with around 74 % (270 to 69 µm), presenting the highest release rate of ASO (Figure III.1.7 A).
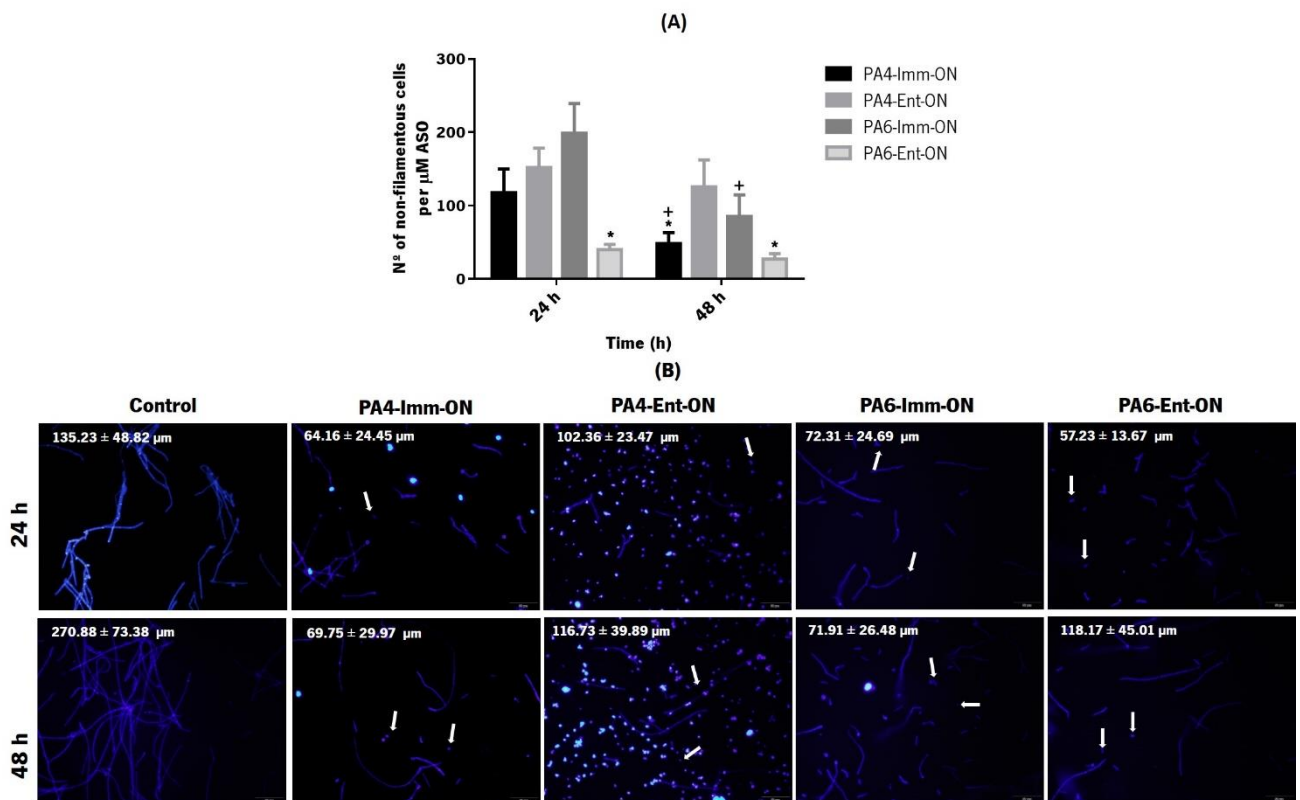
Figure III.1.8 Effect of anti-*EFG1* 2'OMe ASO released from immobilized (Imm) and entrapped (Ent) polyplexes microparticles on *C. albicans* cells filamentation. (A) Number of non-filamentous *C. albicans* cells normalized by the quantity of ASO released at each time; **(B)** Epifluorescence microscopy images of *C. albicans* stained with Calcofluor after 24 h and 48 h in contact with the polyplex microparticles and the average of the hyphae size for each condition. The assays were performed for *C. albicans* SC5314. Error bars represent standard deviation. ***Significant differences between samples of the same polymer at each time (P-value<0.05). +Significant differences between both times analysed for the samples of the same polyplex microparticle (P-value<0.05). Arrows highlight yeast cells.

Anti-*EFG1* 2'OMe is an ASO able to recognize and block the *EFG1* gene and to control *C. albicans* filamentation. The delivery of these molecules remains a challenge and there is no optimal delivery strategy. This data confirms that PA4 and PA6 polyplexes MPs are feasible carriers for anti-*EFG1* 2'OMe ASO molecules either using the entrapped and immobilized strategies, once all the ASO released maintains its activity against *C. albicans* cells.

References

1   Juliano R L. (2016) The delivery of therapeutic oligonucleotides. *Nucleic Acids Res.* 44, 6518–6548.

2   Yin H, Kanasty R L, Eltoukhy A A et al. (2014) Non-viral vectors for gene-based therapy. *Nat Rev Genet.* 15(8), 541–555.

3   Crespo-Barreda A, Encabo-Berzosa M M and González-Pastor R. (2016) Chapter 11 - Viral and nonviral vectors for *in vivo* and *ex vivo* gene therapies. In *Translating Regenerative Medicine to the Clinic*; Laurence, J., Ed.; Academic Press: Boston, MA, USA, pp. 155–177

4   Hattori Y. (2017) Progress in the development of lipoplex and polyplex modified with anionic polymer for efficient gene delivery. *J. Genet. Med. Gene Ther.* 1, 003–018.

5   Dencheva N, Denchev Z, Lanceros-Méndez S and Sanz T E. (2015) One-Step in situ synthesis of polyamide microcapsules with inorganic payload and their transformation into responsive thermoplastic composite materials. *Macromol. Mater. Eng.* 301, 119–124

6   Dencheva N, Braz J, Nunes T G, et al. (2018) One-pot low temperature synthesis and characterization of hybrid poly(2-pyrrolidone) microparticles suitable for protein immobilization. *Polymer* 145, 402–415

7   Dencheva N, Oliveira F D, Braz J F and Denchev Z Z. (2020) Bovine serum albumin-imprinted magnetic poly(2-pyrrolidone) microparticles for protein recognition. *Eur. Polym. J.* 122, 109375

8   Dencheva N, Braz J and Scheibel D. (2020) Polymer-assisted biocatalysis: polyamide 4 microparticles as promising carriers of enzymatic function. *Catalysts* 10, 767

9   González J B, González N, Colldelram C, et al. (2015) NCD-SWEET beamline upgrade. In: Proc. 10th Mech. Eng. Des. Synchrotron Radiat. Equip. Instrum. pp. 374–376.

10   Ashiotis G, Deschildre A, Nawaz Z et al. (2015) The fast azimuthal integration Python library: pyFAI. *J. Appl. Crystallogr.*, 48: 510–519.

11   Williams D W, Wilson M J, Lewis M A and Potts A J. (1995) Identification of *Candida* species by PCR and restriction fragment length polymorphism analysis of intergenic spacer regions of ribosomal DNA. *J. Chin. Microbiol.* 33, 2476-2479.

12   DeVos S L and Miller T M. (2013) Antisense oligonucleotides: treating neurodegeneration at the level of RNA. *Neurotherapeutics* 10(3), 486-97.

13   Wang H, Jiang Y, Peng H et al. (2015) Recent progress in microRNA delivery for cancer therapy by non-viral synthetic vectors. *Advanced Drug Delivery Reviews* 81, 142–160.

14   Roberts T C, Ezzat K, Andaloussi S E, Weinberg M S. (2016) Synthetic SiRNA delivery: Progress and prospects. *Methods in Molecular Biology* 1364, 291–310

15   Kim N, Kim J H, Nam S W, et al. (2015) Preparation of nylon 4 microspheres via heterogeneous polymerization of 2-pyrrolidone in a paraffin oil continuous phase. *J. Ind. Eng. Chem.* 28: 236-240.

16   Tachibana K, Hashimoto K, Tansho N and Okawa H. (2011) Chemical modification of chain end in nylon 4 and improvement of its thermal stability. *J. Polym. Sci. Part A: Polym. Chem.* 49, 2495-2503.

17   Dencheva N, Nunes T, Oliveira M J and Denchev Z. (2005) Microfibrillar composites based on polyamide/polyethylene blends. 1. Structure investigations in oriented and isotropic PA6. *Polymer* 46, 887-901.

18   Fredericks J, Doyne T H and Spague R S. (1966) Crystallographic studies of nylon 4. II. On the β and δ polymorphs of Nylon 4. *J. Polym. Sci. Polym. Phys.* 4, 913-922.

19   Bellinger M A, Waddon A J, Atkins E D T and MacKnight W J. (1994) Structure and morphology of nylon 4

chain-folded lamellar crystals. *Macromolecules* 27(8), 2130-2135.

20   International   Organization   for   Standardization   ISO   10993-5:2009.   (2009)   Biological evaluation   of   medical   devices.   Part   5:   tests   for   in   vitro   cytotoxicity,   third   edition, (2009-06-01).

Chapter III.2

Cationic lipid-based formulations for

encapsulation and delivery of anti-*EFG1*

2'-*O*MethylRNA antisense oligonucleotide

Main goal

To develop lipid-based formulations for anti-*EFG1* 2'-*O*MethylRNA antisense oligonucleotide cargo and delivery, prepared with cationic and neutral lipids, and to evaluate its efficacy to control *Candida albicans* filamentation *in vitro* and *in vivo*.

Conclusions

The results obtained showed that all lipid-based formulations are feasible nanocarriers for anti-*EFG1* 2'OMe ASO cargo, specially the DOTAP/DOPC 80/20 ρ=3 formulation that considerable contributed to the increase of the *G. mellonella* survival infected with *C. albicans*.

III.2.1 Introduction

As mentioned in Chapter III.1, the cargo and delivery of ASOs to its site of action remains a key challenge. For the last years, various non-viral vectors have been engineered for improved gene and drug delivery strategies [1–3]. Some of the most promising strategies for delivery of nucleic acids encompass complexation of nucleic acids, which are anionic, with liposomes of fixed or ionizable cationic charge [4–8]. Due to the attractive interactions between cationic liposomes and nucleic acids, new nanostructured complexes tend to be formed, and are referred to as lipoplexes [9–12]. Besides facilitating the formation of nanostructured particles with high encapsulation efficiency, the cationic charge of liposomes also favour attractive interactions with cell and endosomal membranes, improving cellular uptake and endosomal release [13–15]. Typically, cationic liposomes used in nucleic acid delivery are composed by at least two lipid components: a cationic lipid (e.g. 1,2-dioleoyl-3-trimethylammoniumpropane - DOTAP) and a neutral or zwitterionic lipid (e.g. dioleoylphosphocholine - DOPC). The role of the neutral lipid is to help in the adjustment of the amount of positive charge per liposome area (i.e. membrane charge density - σ_M), and can also have fusogenic properties that help the lipid-nucleic acid complex to fuse with endosomal membranes, as in the case of dioleoylphosphatidylethanolamine (DOPE) and monoolein (MONO) [2,16,17]. Both the ability to modulate membrane charge density (σ_M) and fusogenicity properties are known to influence the transfection efficiency [13,14].

So, the main purpose of this section of the work was to develop lipid-based formulations for anti-*EFG1* 2'-*O*Methyl ASO cargo and delivery, using the DOTAP as cationic lipid and the DOPC, DOPE or MONO as neutral lipids. The anti-*EFG1* 2'OMe ASO lipid-based formulations efficacy was evaluate in terms of its capability for controlling *C. albicans* filamentation *in vitro* and *in vivo* (using the *Galleria mellonella* model).

III.2.2 Materials and Methods

a. Materials

The anti-*EFG1* 2'OMe ASO with the sequence 5'-mG mG mC mA TACCGTTA mU mU mG mU-3' (m- 2'OMe), was designed and synthesized as described in the previous Chapter II.1. For that, a stock of ASO at 4 µM was prepared in sterile ultrapure water and stored at -20 °C for later use.

The lipids 1,2-dioleoyl-3-trimethylammoniumpropane (DOTAP), dioleoylphosphocholine (DOPC), and dioleoylphosphatidylethanolamine, (DOPE), in chloroform, were purchased from the Avanti Polar

Lipids (USA). Monoolein (MONO) was purchased from Nu-Chek Prep (Elysian, MN, USA). All lipids were used as received.

b. Liposomes and lipoplexes preparation

Liposomes were prepared according to the thin film hydration method followed by sonication. For this end, DOTAP (cationic lipid) and the helper lipids DOPC, DOPE and MONO were mixed in chloroform to the different molar ratios as described in Table III.2.1. The resulting mixture was dried using a constant nitrogen gas stream, and then placed in vacuum overnight. The lipid film was resuspended in ultrapure nuclease free Milli-Q water to a total lipid concentration of 2 mM. The suspensions were vortexed and sonicated using a tip sonicator for 1 min, with 10 % amplitude and 50 % duty cycle using a Branson Digital Sonifier 250 Model.

Table III.2.1 Different liposomes prepared and its molar ratios, cationic-to-anionic charge ratio (ρ_{chg}) and type of lipoplexes structure

Cationic Lipid	Helper Lipid	Cationic/helper lipid molar %	Typical lipoplex structure
DOTAP	DOPC	80/20	Lamellar [18]
		30/70	Lamellar [18]
	DOPE	80/20	Lamellar [19]
		30/70	Inverted hexagonal phase [19]
	MONO	80/20	Lamellar [20]
		30/70	Inverted hexagonal phase [20]

For lipoplex formation, equal volumes of liposomes and ASO solutions previously diluted to the right concentrations were mixed for a final anti-*EFG1* 2'OMe ASO concentration of 40 nM. The resulting mixture was promptly vortexed for 30 sec and left at least 30 min under stirring conditions. The formed complexes were stored at 4 °C. Lipoplexes were prepared with a cationic-to-anionic charge ratio (ρ_{chg}) of 3 and 10. The ρ_{chg} is calculated as the total number of positive charges (from the number of DOTAP molecules) divided by the total number of negative charges (from the number and valence of ASO molecules).

c. *In vitro* effect of the lipoplexes against *C. albicans* cells

Microorganisms and growth conditions

The *Candida* strain used in this study was *C. albicans* SC5314, which is a reference strain from *Candida* collection of the Biofilm group of the Centre of Biological Engineering. The identification of all strains was confirmed using a chromogenic medium, specifically CHROMagar™ *Candida*, through the distinction of colonies' colours and by PCR-based sequencing with specific primers (ITS1 and ITS4) [21].

For all experiments, the yeast strain was subcultured on sabouraud dextrose agar (SDA; Merck, Germany) and incubated for 24 h at 37 °C. Cells were then inoculated in sabouraud dextrose broth (SDB; Merck, Germany) and incubated overnight at 37 °C and 120 rpm. After incubation, cells' suspensions were centrifuged for 10 min at 3000 g and 4 °C, and washed twice with phosphate-buffered saline (PBS; pH 7, 0.1 M). Pellets were suspended in 5 mL of Roswell Park Memorial Institute (RPMI; Sigma, St Louis, USA), and the cellular density was adjusted for each experiment using a *Neubauer* chamber (Paul Marienfild, Lauda-Königshofen, Germany) to 1×10^6 cells mL^{-1}.

Effect on *C. albicans* filamentation

The lipoplexes performance was evaluated in terms of the ability of the anti-*EFG1* 2'OMe ASO released from each formulation to control *C. albicans* filamentation. For that, on 24-well polystyrene microtiter plates (Orange Scientific, Braine- l'Alleud, Belgium) 500 µL of each lipoplex was added to 500 µL of a suspension of *C. albicans* at 1×10^6 cells mL^{-1}. The solutions were incubated at 37 °C and 120 rpm during 72 h. A control was prepared with *C. albicans* cells treated with 40 nM of ASO-free. Moreover, the positive control was prepared only with *C. albicans* cells and the negative controls with the empty lipoplexes together with *C. albicans* cells in RPMI. The results were presented as percentage (%) of filamentation reduction, as previously described in Chapter II.1. In addition to the filamentation inhibition studies, the length of the filaments was quantified through fluorescence microscopy analysis as previously described in Chapter II.1.

d. *In vivo* effect of the lipoplexes using the *G. mellonella* model

Galleria mellonella larvae

Galleria mellonella larvae were reared on a pollen grain and bee wax diet at 25 °C in the darkness and used in a final stage with a weight of approximately 250 mg. The larvae were injected into hemolymph via the hindmost left proleg, previously sanitized with 70 %(v/v) ethanol, using a micro syringe adapted in a micrometer to control the volume of injection [22,23].

Toxicity evaluation

The lipoplexes for *in vivo* assays were selected based on the *in vitro* results. Namely, the DOTAP/DOPC 80/20 ρ=10; DOTAP/DOPE 80/20 ρ=10; DOTAP/MONO 80/20 ρ=10 for presenting a better performance and the DOTAP/DOPC 80/20 ρ=3 for presenting the worst performance *in vitro*.

To test *in vivo* the lipoplexes toxicity, 10 *G. mellonella* larvae were injected with 5 μL of each formulation. As control a set of larvae were injected with the same volume of free-ASO and only with PBS. Larvae were placed in petri dishes and stored in the dark at 37 °C. Larvae survival was recorded over 72 h and survival curves were constructed.

Galleria mellonella survival

To study the *in vivo* effect of lipoplexes, *G. mellonella* larvae were previously infected with a lethal dose of *C. albicans* cells ($7x10^7$ cells mL^{-1} in PBS) and randomly allocated to different experimental groups (a set of 10 larvae). A set of larvae was treated with a single-dose of lipoplex (0 h post infection) and another with a double dose of each lipoplex (0 h and 12 h post infections). As control larvae were treated with free ASO or only with PBS. Larvae were placed in petri dishes and stored in the dark at 37 °C over 3 days, and consequently, the survival curves were constructed. Caterpillars were considered dead when they displayed no movement in response to touch [23].

e. Statistical analysis

Data are expressed as the mean ± standard deviation of at least three independent experiments. Results were compared using two-way ANOVA and Tukey's multiple comparisons tests. Kaplan-Meier survival curves were plotted and differences in survival were calculated by using log-rank Mantel-Cox statistical test. All performed with GraphPad Prism 6® (GraphPad Software, San Diego, CA, USA).

III.2.3 Results and Discussion

The use of ASOs for the treatment of important genetic diseases have emerged as a promising approach [24–28] and more recently for *C. albicans* infections [29]. However, the ASOs' penetration into *Candida* cells can be limited by the cell wall envelope, which is composed of several layers that surround the cytosol. So, delivery strategies are needed to ensure that ASOs cross *Candida*'s cell wall and also that their protection against the degradation by serum proteases and nucleases be guaranteed [30]. At the present time, major somatic ASOs transfer approaches employ either viral or non-viral vectors [1]. Viral vectors show high gene transfer efficiency, however they present risks, including the induction of a host inflammatory and immune response [1,31]. Some of these problems can be circumvented by employing non-viral vectors, such as cationic lipoplexes [2,32–34], which are assemblies that result from the electrostatic complexation between cationic liposomes and negative charged ASOs [16], forming well-ordered hexagonal or multilamellar structures with the ASOs sandwiched between the bilayers [2]. Thus, the main goal of this part of the work was to develop lipid-based formulations to anti-*EFG1* 2'OMe ASO cargo and delivery.

a. *In vitro* effect of the lipoplexes on *C. albicans* filamentation

During this study, the use of liposomes composed by the DOTAP as cationic lipid and DOPC, DOPE and MONO as neutral lipids to develop anti-*EFG1* 2'OMe ASO lipid-based formulations was investigated. To note that cationic and neutral lipids are usually used to form liposomes for gene delivery due to their favourable interactions with the negatively charged RNA or DNA and with cell membranes [16]. Moreover, the neutral lipids are usually included as 'helper' lipids to enhance the transfection activity and nanoparticle stability [1,2,34]. From a lamellar to a hexagonal, liposomes can adopt different structures depending on the number of cationic and neutral charges in its composition (Table III.2.1). A liposome with a higher number of DOPE molecules comparing to the DOTAP lipids, have a tendency to adopt an hexagonal phase [17], as is the case of the DOTAP/DOPE 30/70 [19] and the DOTAP/MONO 30/70 [20]. Lipoplexes with a cationic/helper lipid molar ratio of 80/20 have a high cationic content and a higher number of positive charges per liposome area, compared to the 30/70 lipoplexes. In other words, they have a higher cationic membrane σ_M. The lipoplexes with ρ_{chg}=10 have a higher excess of DOTAP liposomes than the lipoplexes with ρ_{chg}=3.

The anti-*EFG1* 2'OMe ASO lipid-based formulations efficacy was evaluate in terms of its ability for controlling *C. albicans* filamentation *in vitro* and *in vivo* (using the *G. mellonella* model). Figure III.2.1 presents the *in vitro* effect of lipoplexes on *C. albicans* filamentation over 72 h of treatment. To note, all

106

formulations were able to control *C. albicans* filamentation, although at different levels. It is important to address that in general the reduction on *C. albicans* filamentation increase over the time for all lipoplexes, as well as, for ASO-free.

Figure III.2.1 *In vitro* **effect of anti-*EFG1* 2'OMe ASO lipid-based formulations on *C. albicans* filamentation.** Levels of *C. albicans* filamentation reduction (%) of **(A)** DOTAP/DOPC; **(B)** DOTAP/DOPE and **(C)** DOTAP/MONO after 24, 48 and 72 h of treatment with each lipoplex. As positive control, *C. albicans* cells were incubated in same conditions with the anti-*EFG1* 2'OMe ASO-free. Error bars represent standard deviation. *Significant differences between anti-*EFG1* 2'OMe ASO lipid-based formulations and ASO-free at each time of incubation (P-value<0.05). +Significant differences between DOTAP/DOPE 80/20 ρ=10 and DOTAP/DOPE 30/70 ρ=10 at 24 h of incubation (P-value<0.05).

It should be noted that the encapsulation of anti-*EFG1* 2'OMe ASO on DOTAP/DOPC liposomes (Figure III.2.1 A) slight improve the effect of treatment of *C. albicans* cells after 48 h and 72 h comparing to ASO-free performance (P-value>0.05). Figure III.2.1 B presents the treatment of *C. albicans* cells with the DOTAP/DOPE lipoplexes. All the DOTAP/DOPE formulations feature a similar or superior performance than the ASO-free. The highest performance was observed in the case of the DOTAP/DOPE 30/70 ρ=10, with statistically differences at 48 h (P-value<0.05) and the lower performance was observed in the case of DOTAP/DOPE 30/70 ρ=3 (P-value>0.05). All the DOTAP/MONO lipoplexes presented a better performance comparatively to ASO-free, specially at 48 h (P-value<0.05). Within those lipoplexes, the DOTAP/MONO 80/20 ρ=10 which assumes a lamellar structure and that is constitute by an excess of positive charges demonstrated to be the formulation with the highest ability to control *C. albicans* filamentation. So, it is believe that, the best performance *in vitro* of DOTAP/MONO 80/20 compared to the remaining formulations may be related with the superior number of charges of DOTAP, combined with the fusogenicity of MONO, which may facilitate the fusion of the lipoplex membranes with endosomal membranes and consequently facilitate endosomal release [35,36]. The DOTAP/MONO 30/70 formulation has a slightly lower ability to inhibit *C. albicans* filamentation. From the lipoplexes with this composition is expected to result on an inverted hexagonal structure. Overall, these results are in agreement with the findings for an analogous system composed by DOTAP/MONO but encapsulating siRNA [37]. The lamellar phase containing MONO was found to have a higher gene silencing efficiency than the inverted hexagonal phase, but it was also found that the lamellar had a higher non-specific gene knockdown [37].

There are not significant differences between the formulations constituted by 80/20 or by 30/70 of lipoplexes, and even between the both ρ_{chg} tested (ρ=3 and ρ=10) (P-value>0.05), with an exception between DOTAP/DOPE 80/20 and 30/70 ρ=10 at 24 h (Figure III.2.1 B) (P-value<0.05). Consistently, the ratio between positive and neutral lipids do not have a huge influence in the anti-*EFG1* 2'OMe ASO lipid-based formulations efficacy.

Figure III.2.2 shows that all lipoplexes tested were also able to reduce the filament's length of *C. albicans* on into approximately 40 to 70 % when compared to ASO-free performance (P-value>0.05), with exception of the DOTAP/DOPC 30/70 ρ=3 and the DOTAP/MONO 30/70 ρ=3 formulations, for which the levels of reduction were significantly lower comparatively to ASO-free performance (P-value<0.05).
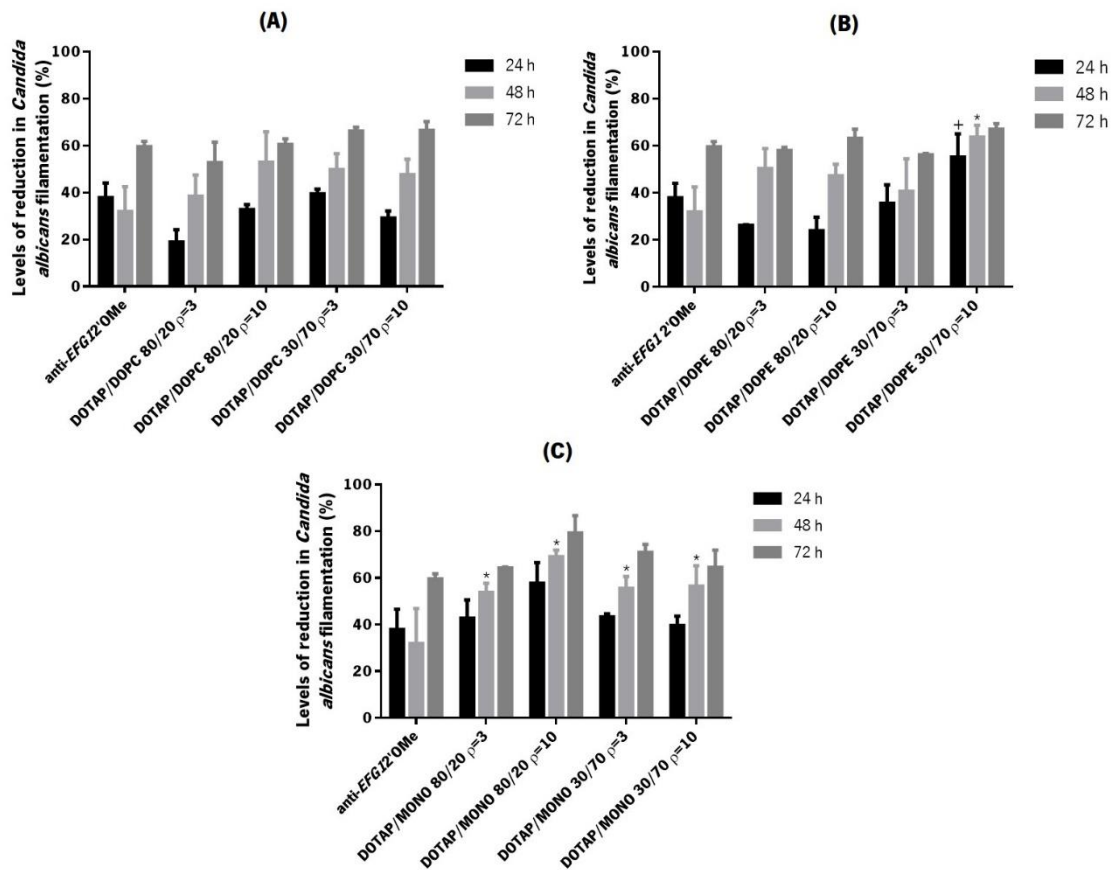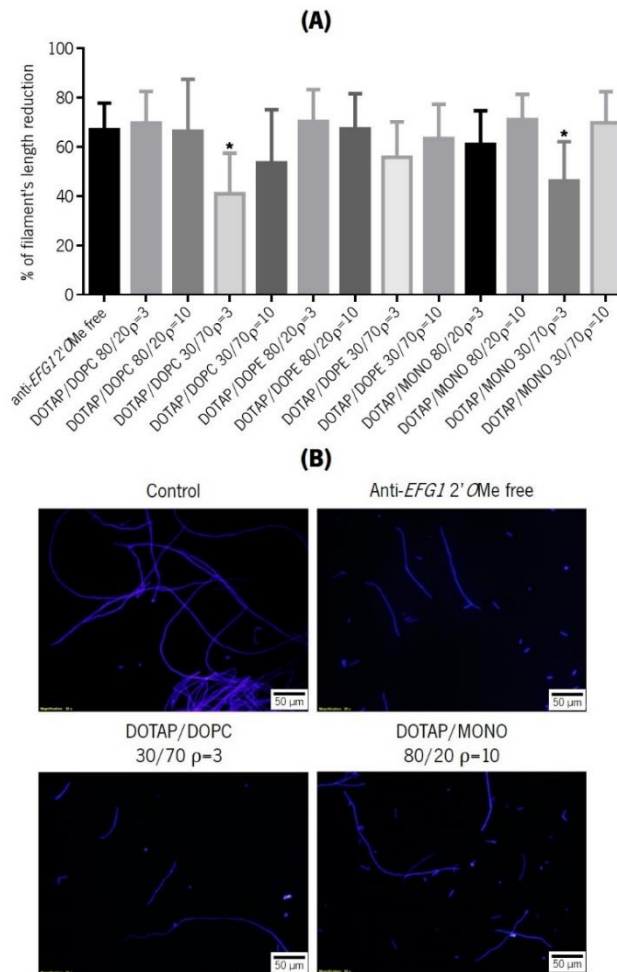
Figure III.2.2 *In vitro* **effect of anti-*EFG1* 2'OMe ASO lipid-based formulations on *C. albicans* filament's length. (A)** Filament's length inhibition (%) determined by using ImageJ software and **(B)** epifluorescence microscopy images of *C. albicans* cells stained with calcofluor after 72 h of incubation with lipoplexes. Control represents an experiment prepared only with cells on RPMI. Anti-*EFG1* 2'OMe free represents the cells treated with free ASO. *****Significant differences between anti-*EFG1* 2'OMe ASO lipid-based formulations and ASO-free (P-value<0.05).

b. *In vivo* effect of the lipoplexes on *G. mellonella* survival

The invertebrate model of *G. mellonella* was used to test *in vivo* the efficacy of anti-*EFG1* 2'OMe ASO lipid-based formulations. The lipoplexes tested were: DOTAP/DOPC 80/20 ρ=3, DOTAP/DOPC 80/20 ρ=10, DOTAP/DOPE 80/20 ρ=10 and DOTAP/MONO 80/20 ρ=10. Two of that lipoplexes were selected based on its *in vitro* performance: the DOTAP/MONO 80/20 ρ=10 with the best and the DOTAP/DOPC 80/20 ρ=3 with the worst performance. The other two lamellar lipoplexes (DOTAP/DOPC 80/20 ρ=10 and DOTAP/DOPE 80/20 ρ=10), were also tested.

Indeed, the toxicity of the anti-*EFG1* 2'OMe ASO lipid-based formulations was evaluate and notably, the results in Figure III.2.3 A showed the absence of toxicity for all lipoplexes tested. Moreover, it was observed no effect with lipid-based formulations empty of ASO in the *G. mellonella* survival (Figure III.2.3 B).
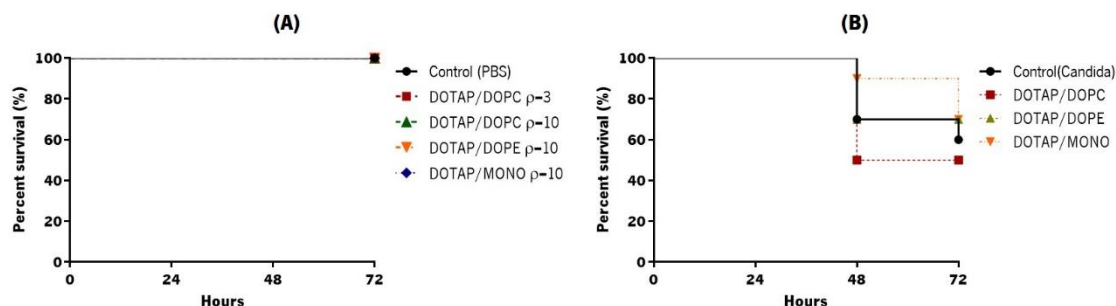

Figure III.2.3 (A) Anti-*EFG1* 2'OMe ASO lipid-based formulations toxicity evaluation on *Galleria mellonella* model. For each condition, 10 larvae were injected with each lipoplex and their survival was monitored over 72 h. As control larvae were injected only with PBS. **(B)** Effect of Lipid-based formulations empty of ASO on the *Galleria mellonella* survival infected with *Candida albicans.*

To study the effect of anti-*EFG1* 2'OMe ASO lipid-based formulations *in vivo*, *G. mellonella* larvae infected with a lethal dose of *C. albicans* were treated with a single-dose (0 h post infection) (Figure III.2.4) and with a double-dose (0 h and 12 h post infection) of the DOTAP/DOPC 80/20 ρ=3 (Figure III.2.5). In general, the treatment of the infected *G. mellonella* with a single-dose of each lipoplex enhanced the survival of larvae over 72 h (Figure III.2.4 A, B and C). To note, that the DOTAP/DOPC 80/20 ρ=3 presented the best performance, enhancing the *G. mellonella* survival by 19 % at 24 h and 48 h and 14 % at 72 h (P-value<0.05). The results also revealed that the ρ_{chg} (ρ=3 and ρ=10) influences the *in vivo* DOTAP/DOPC 80/20 lipoplexes performance (Figure III.2.4 A), once the ρ=3 formulation presented a better performance than ρ=10 (an increase on *G. mellonella* survival below 10 %). In contrast, DOTAP/DOPC 80/20 ρ=10 revealed to be a worst performance after 72 h of treatment. It was also observed that DOTAP/DOPE 80/20 ρ=10 (Figure III.2.4 B) increased the *G. mellonella* survival over 72 h (P-value<0.05), however in a slight extension comparing to the performance of DOTAP/DOPC 80/20 ρ=3. Although the *G. mellonella* survival increased after 24 h and 48 h of treatment with the DOTAP/MONO 80/20 ρ=10 lipoplex in comparison to the untreated larvae, no statistic differences were observed after 72 h (Figure III.2.4 C) (P-value>0.05).
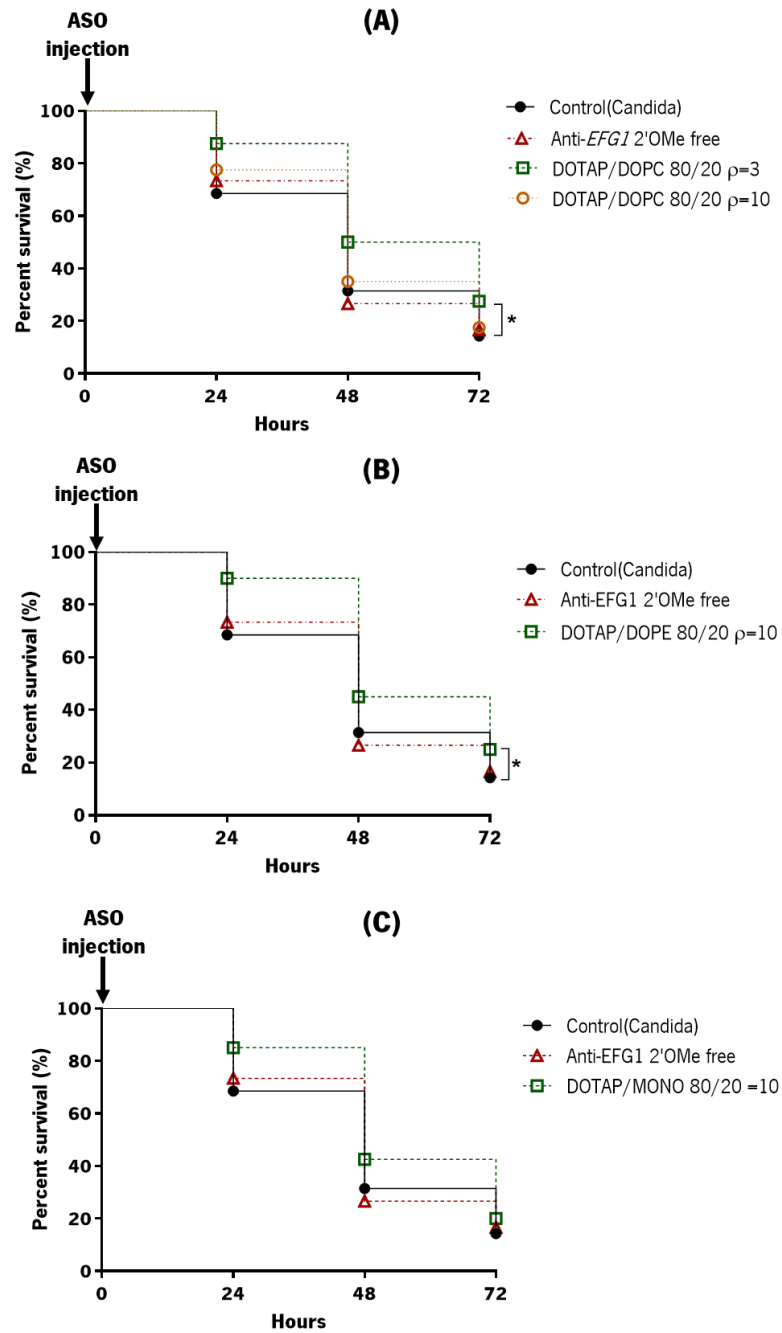
Figure III.2.4 Single dose anti-*EFG1* 2'OMe ASO lipid-based formulations effect on the survival of *Galleria mellonella* survival infected with *Candida albicans.* Survival curves of infected larvae treated with a single-dose (0 h post infection) of **(A)** DOTAP/DOPC lipoplexes; **(B)** DOTAP/DOPE lipoplexes and **(C)** DOTAP/MONO lipoplexes. As control larvae infected were injected with anti-*EFG1* 2'OMe ASO-free and only with PBS.

In a clinical context, normally the treatments are not carried out by a single antimicrobial administration [38,39]. Thus, to mimic that, it was analysed the performance of a double-dose administration of the DOTAP/DOPC 80/20 ρ=3 formulation (the lipoplex with the best performance in

the single-dose studies). To note, the double-dose administration of DOTAP/DOPC 80/20 ρ=3 enhances the *G. mellonella* survival on around 1.5 times more comparing to the single-dose administration, increasing the larvae survival into 40 % after 48 h and into 25 % after 72 h of treatment (P-value<0.005) (Figure III.2.5). It is important to point out that the double-dose administration also potentiates the effect of ASO-free on around 1 time more (18 % after 24 h and 13 % after 72 h of infection (P-value<0.05)).
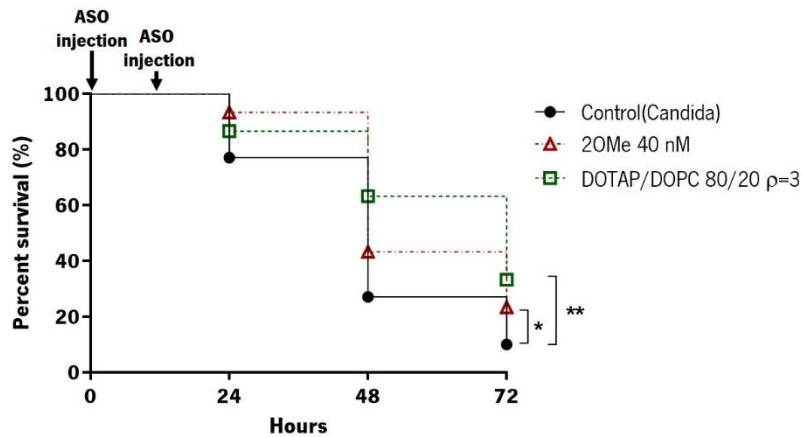

Figure III.2.5 Double-dose anti-*EFG1* 2'OMe ASO lipid-based formulations effect on *Galleria mellonella* survival infected with *Candida albicans*. Survival curves of infected larvae treated with a double-dose (0 h and 12 h post infection) of DOTAP/DOPC 80/20 ρ=3 lipoplex. As control larvae infected were injected only with anti-*EFG1* 2'OMe ASO-free and only with PBS.

Effectively, the survival rate of *G. mellonella* when treated with the anti-*EFG1* 2'OMe ASO lipid-based formulations was significantly higher than when treated with ASO-free. This evidence confirms the importance of the encapsulation process for protecting ASOs against the degradation by serum proteases and nucleases.

Among non-viral vectors, cationic liposomes have been more commonly used [1,2] and this data confirms also its viability to anti-*EFG1* 2'OMe ASO cargo and delivery into *C. albicans* cells. In accordance with the *in vitro* results, seems to be irrelevant the proportions between cationic and neutral lipids, and between cationic charges of the liposomes and ASOs negative charges on the performance of anti-*EFG1* 2'OMe ASO lipid-based formulations. However, by considering the *in vivo* results, the excess of cationic charges as is the case of DOTAP/DOPC 80/20 ρ=10 seems to have a negative impact with a lower rate of larvae survival.

This study demonstrated the successful delivery of anti-*EFG1* 2'OMe ASO encapsulated in lipid-based formulations, providing valuable information for further assays. The DOTAP/DOPC 80/20 ρ=3 formulation has the potential to improve nanodrug administration for *C. albicans* species.

112

References

1   Hattori Y. (2017) Progress in the development of lipoplex and polyplex modified with anionic polymer for efficient gene delivery. *J. Genet. Med. Gene Ther.* 1, 003–018.

2   Barba A A, Bochicchio S, Dalmoro A, et al (2019) Lipid delivery systems for nucleic-acid-based-drugs: From production to clinical applications. *Pharmaceutics* 11, 5–7

3   Wang Y, Miao L, Satterlee A and Huang L. (2015) Delivery of oligonucleotides with lipid nanoparticles. *Adv Drug Delive Rev.* 87, 68–80

4   Ewert K K, Ahmad A, Evans H M and Safynia C R. (2005) Cationic lipid-DNA complexes for non-viral gene therapy: Relating supramolecular structures to cellular pathways. *Expert Opinion on Biological Therapy*, 5(1), 33–53

5   Semple S C, Akinc A, Chen J, et al. (2010) Rational design of cationic lipids for siRNA delivery. *Nat. Biotechnol.* 28, 172–176

6   Kranz L M, Diken M, Haas H, et al. (2016) Systemic RNA delivery to dendritic cells exploits antiviral defence for cancer immunotherapy. *Nature* 534, 396–401

7   Akinc A, Maier M, Manoharan M, et al. (2019) The Onpattro story and the clinical translation of nanomedicines containing nucleic acid-based drugs. *Nature Nanotechnology*, 14, 1084–1087

8   Gaspar R, Coelho F and Silva B F B. (2020) Lipid-Nucleic Acid Complexes: Physicochemical Aspects and Prospects for Cancer Treatment. *molecules* 25(21), 5006

9   Weisman S, Hirsch-Lerner D, Barenholz Y and Talmon Y. (2004) Nanostructure of cationic lipid-oligonucleotide complexes. *Biophys. J.* 87(1), 609–614

10   Tros de Ilarduya C, Sun Y and Düzgüneş N. (2010) Gene delivery by lipoplexes and polyplexes. *European Journal of Pharmaceutical Sciences*, 40, 159–170

11   Safinya C R, Ewert K K, Majzoub R N and Leal C. (2014) Cationic liposome-nucleic acid complexes for gene delivery and gene silencing. *New Journal of Chemistry*, 38 (11), 5164–5172

12   Silva B F B, Majzoub R N, Chan C L, et al. (2014) PEGylated cationic liposome-DNA complexation in brine is pathway-dependent. *Biochim. Biophys. Acta - Biomembr.* 1838, 398–412

13   Lin A J, Slack N L, Ahmad A, et al. (2003) Three-dimensional imaging of lipid gene-carriers: Membrane charge density controls universal transfection behavior in lamellar cationic liposome-DNA complexes. *Biophys. J.* 84, 3307–3316

14   Ahmad A, Evans H M, Ewert K, et al. (2005) New multivalent cationic lipids reveal bell curve for transfection efficiency versus membrane charge density: Lipid - DNA complexes for gene delivery. *J. Gene Med.* 7, 739–748

15   Majzoub R N, Ewert K K and Safinya C R. (2016) Cationic liposome-nucleic acid nanoparticle assemblies with applications in gene delivery and gene silencing. *Philos. Trans. A* 374, 20150129

16   Bochicchio S, Dalmoro A, Barba A A, et al. (2014) Liposomes as siRNA Delivery Vectors. *Curr. Drug Metab.* 15, 882–892

17   Lin Q, Chen J, Zhang Z and Zheng G. (2014) Lipid-based nanoparticles in the systemic delivery of siRNA. , *Nanomedicine*, 9, 105–120

18   Rädler J O, Koltover I, Salditt T and Safinya C R. (1997) Structure of DNA-cationic liposome complexes: DNA intercalation in multilamellar membranes in distinct interhelical packing regimes. *Science.* 275, 810–814

19   Koltover I, Salditt T, Rädler J O and Safinya C R. (1998) An inverted hexagonal phase of cationic liposome-DNA complexes related to DNA release and delivery. *Science.* 281, 78–81

20   Ewert K K, Zidovska A, Ahmad A, et al. (2010) Cationic lipid-nucleic acid complexes for gene delivery and silencing: pathways and mechanisms for plasmid DNA and siRNA. *Top Curr Chem.* 296, 191–226

21   Williams D W, Wilson M J, Lewis M A and Potts A J. (1995) Identification of *Candida* species by PCR and restriction fragment length polymorphism analysis of intergenic spacer regions of ribosomal DNA. *J Clin Microbiol.* 33(9), 2476-2479

22   Mil-Homens D, Bernardes N and Fialho A M. (2012) The antibacterial properties of docosahexaenoic omega-3 fatty acid against the cystic fibrosis multiresistant pathogen *Burkholderia cenocepacia*. FEMS Microbiol Lett. 328(1):61–9.

23   Mil-Homens D, Ferreira-Dias S and Fialho A M. (2016) Fish oils against Burkholderia and *Pseudomonas*

aeruginosa: In vitro efficacy and their therapeutic and prophylactic effects on infected *Galleria mellonella* larvae. *J Appl Microbiol* 120:1509–19.

24   Wesolowski D, Alonso D and Altman S. (2013) Combined effect of a peptide-morpholino oligonucleotide conjugate and a cell-penetrating peptide as an antibiotic. *Pnas* 110, 8686–8689

25   Van Hauwermeiren F, Vandenbroucke R E, Gine L, et al. (2014) Antisense oligonucleotides against TNFR1 prevent toxicity of TNF/IFNγ treatment in mouse tumor models. *Int. J. Cancer* 135, 742–750

26   Kenney S P and Meng X J. (2015) Therapeutic targets for the treatment of hepatitis E virus infection. *Expert Opin. Ther. Targets* 19, 1245–60

27   Liang S, He Y, Xia Y et al. (2015) Inhibiting the growth of methicillin-resistant *Staphylococcus aureus* in vitro with antisense peptide nucleic acid conjugates targeting the ftsZ gene. *Int. J. Infect. Dis.* 30, e1–e6

28   Sully E K and Geller B L. (2016) Antisense antimicrobial therapeutics. *Curr Opin Microbiol* 3, 47–55

29   Silva S, Araújo D, Azevedo N M et al. (2020) Antisense oligomers for controlling *Candida albicans* infections. P.N.: 115349.

30   Juliano R L and Carver K. (2015) Cellular uptake and intracellular trafficking of oligonucleotides. *Adv. Drug Deliv. Rev.* 87, 35–45

31   Young L S, Searle P F, Onion D and Mautner V. (2006) Viral gene therapy strategies: from basic science to clinical application. *J. Pathol. J Pathol* 208, 299–318

32   Yin H, Kanasty R L, Eltoukhy A A, et al. (2014) Non-viral vectors for gene-based therapy. *Nature Reviews Genetics*, 15, 541–555

33   Juliano R L. (2016) The delivery of therapeutic oligonucleotides. *Nucleic Acids Res.* 44, 6518–6548

34   Crespo-Barreda A, Encabo-Berzosa M M and González-Pastor R. (2016) Chapter 11 - Viral and nonviral vectors for *in vivo* and *ex vivo* gene therapies. In *Translating Regenerative Medicine to the Clinic*; Laurence, J., Ed.; Academic Press: Boston, MA, USA, pp. 155–177

35   Leal C, Ewert K K, Shirazi R S, et al. (2011) Nanogyroids incorporating multivalent lipids: Enhanced membrane charge density and pore forming ability for gene silencing. *Langmuir* 27, 7691–7697

36   Oliveira A C N, Martens T F, Raemdonck K, et al. (2014) Dioctadecyldimethylammonium: monoolein nanocarriers for efficient *in vitro* gene silencing. *ACS Appl. Mater. Interfaces* 6, 6977–6989

37   Leal C, Bouxsein N F, Ewert K K and Safinya C R. (2010) Highly efficient gene silencing activity of siRNA embedded in a nanostructured gyroid cubic lipid matrix. *J. Am. Chem. Soc* 132, 16841–16847

38   Torres A, Kozak J, Korolczuk A, et al. (2016) Locked nucleic acid-inhibitor of miR-205 decreases endometrial cancer cells proliferation *in vitro* and *in vivo*. *Oncotarget* 7, 73651–73663

39   Kloezen W, Parel F, Brüggemann R, et al. (2018) Amphotericin B and terbinafine but not the azoles prolong survival in *Galleria mellonella* larvae infected with Madurella mycetomatis. *Med. Mycol.* 56, 469–478

Chapter IV

General conclusions and work perspectives

IV.1 General conclusions

The incidence of *Candida* infections has increased remarkably in the last years, being attributed to the rise of the elderly population, to the number of immunocompromised patients, and to the widespread use of indwelling medical devices. *Candida albicans* remains as the most prevalent of all *Candida* species and its pathogenicity is promoted by several virulence factors, being the ability to switch from yeast to filamentous forms one of the most alarming. This phenomenon is regulated by a complex regulatory network of genes and *EFG1* is one of the most important virulence determinants. It is well known that the high levels of morbidity and mortality related to *C. albicans* is mainly due to the rise in antifungal resistance and the limited number of efficient antifungal drugs. In this sense, it is urgent to develop new strategies to prevent and control *C. albicans* infections. The key hypothesis that supports this research is: "If a particular gene, as is the case of *EFG1* gene, is known as a determinant of *C. albicans* filamentation, it could be the target by antisense oligonucleotides, which will bind to the respective mRNA causing its inactivation and translation into protein and thus it will be possible to control *C. albicans* virulence".

Antisense therapy (AST) is being applied in a large number of human genetic diseases, however poorly explored in case of microbial infections, particularly candidiasis. Therefore, the main goal of this research was to promote the development of novel therapeutic approach based on AST to track *C. albicans* filamentation employing the established and the emerging generations of ASOs. To reach on such aim, two complementary objectives were addressed: I) Exploitation and application of ASOs to control the *EFG1* gene and consequently *C. albicans* filamentation; II) Creation of strategies for *C. albicans* ASOs cargo and delivery.

The unmodified ASOs have a limited clinical use since they are rapidly degraded by intracellular endonucleases and exonucleases, being destroyed before binding their respective target. To overcome these issues, ASOs have been chemically modified and up to now there are three different generations of chemical modifications. The first aim of this researcher was achieved through the development of ASOs based on the second and the third generation of ASOs targeting the *EFG1* gene (Chapter II). Regarding the second generation of ASOs, it was projected the anti-*EFG1* 2'-*O*MethylRNA ASO (Chapter II.1), applying the 2'-*O*Methyl chemical modification. This modification is a sugar modification that is described as improving the nuclease resistance and increasing the hybridization affinity for target mRNA. The results revealed that the anti-*EFG1* 2'OMe ASO is able to significantly reduce the levels of *EFG1* gene expression and of Efg1p protein translation (both approximately 60 %), and effectively prevent filamentation of *C.*

albicans cells (by 80%). Moreover, it was also verified that anti-*EFG1* 2'OMe ASO keeps the efficacy in different simulated human body fluids. To test whether anti-*EFG1* 2'OMe ASO could have a therapeutic potential *in vivo*, its efficacy was assessed using a *G. mellonella* caterpillar model of infection (Chapter II.2). It was clear that treatment with a single-dose (0 h post infection) of anti-*EFG1* 2'OMe is able to enhance the larvae survival over 24 h (by 20-30 %). It was also evident, that a double-dose (0 h and 12 h post infection) of the anti-*EFG1* 2'OMe ASO is needed to prolong its effectiveness until 72 h of infection (by 30 %).

The third generation of ASOs was developed to further enhance biostability and pharmacokinetics of the molecules in addition to enhance nuclease resistance and the target affinity. In this sense, a set of LNA-ASO were projected (Chapter II.3), in the so-called gapmer constitution, to control also the *EFG1* gene expression and to reduce *in vitro C. albicans* filamentation. It is important to address that *in vitro* all LNA-ASOs projected were able to reduce *C. albicans* filamentation (by 50 %) and the levels of *EFG1* gene expression (by 40 – 80 %) as in the case of anti-*EFG1* 2'OMe. Although, the *in vivo* studies using the *G. mellonella* model revealed important differences among the LNA-ASOs performances. The inclusion of PS-linkage and palmitoyl-2'-amino-LNA chemical modification into the same gapmer demonstrated to be the most promising combination. In fact, an increasing on *G. mellonella* survival of around 40 % (at 72 h) was observed with a single-dose administration in comparison to the treatment with the anti-*EFG1* 2'OMe (no effect was observed at 72 h with a single-dose administration). Given these findings, with this first part of the research, it is possible to conclude that the second and third generation of ASOs are viable approaches to target specific genes and control *C. albicans* virulence.

The second goal of this research was to create strategies for *C. albicans* ASOs cargo and delivery (Chapter III). It is known that the delivery of ASOs to its site of action remains a key challenge. The development of non-viral vectors has been widely studied to ensure that these molecules become effectively protected from the environmental body conditions and to deliver them to their site of action. Polymers and liposomes become the most non-viral vectors researched in this sense, and specifically, the cationic polymers and liposomes due to their favourable interactions with the negatively charged RNA or DNA and cell membranes. Aiming for the future to coat medical devices with the anti-*EFG1* 2'OMe ASO, novel anionic and cationic polyplexes microparticles based on poly(γ-butyrolactam) (PA4) or poly(ε-caprolactam) (PA6) respectively, were developed using the entrapped and immobilized approaches (Chapter III.1). To note, that PA4 and PA6 polyplexes microparticles proved to be feasible carriers for anti-*EFG1* 2'OMe ASO either using the entrapped and immobilized strategies, once all the ASO released maintains its activity against *C. albicans* cells. In another instance, aiming hereafter to develop a liposomal

nanocarrier to oral or cutaneous administration, lipid-based formulations to anti-*EFG1* 2'OMe ASO cargo and delivery, prepared with DOTAP (cationic lipid) and DOPC, DOPE or MONO (neutral lipids) were developed (Chapter III.2). Importantly, all the lipid-based formulations revealed to be also feasible nanocarriers for anti-*EFG1* 2'OMe ASO cargo, specially the DOTAP/DOPC 80/20 ρ=3 formulation that considerably contributed to increase *G. mellonella* survival when infected with *C. albicans* (in to 40 % after 48 h and 25 % after 72 h with a double-dose administration). The real importance of the development of nanocarriers for *C. albicans* ASOs cargo and the lipoplexes and polyplexes feasibility become clear with this part of the work.

In summary, the research developed under this work provides potentially valuable information for future research into the management of *Candida* infections, regarding the development of a credible and alternative method to control *C. albicans* infections, based on AST methodology. Undoubtedly, this work validates the *in vitro* and *in vivo* therapeutic potential of ASO for controlling *C. albicans* infections.

IV.2 Work perspectives

The work described in this thesis provided a useful approach to control *Candida* infections. However only a part of the work was performed, and some important facts have been left behind, leading to interesting new questions for further research. Some of these suggestions should be considered for further investigations:

a) To extend the studies performed with PA4 and PA6 microparticles to their application on medical surfaces (e.g. latex, silicone, acrylic) to control *C. albicans* proliferation.

b) To further investigate other strategies to improve the lipoplexes formulations. For example, the incorporation of PEGylated lipids into the lipoplexes studied to overcome specific cellular barriers and immune defense mechanisms innate. In addition to the ratios between the cationic and neutral lipids, it is intended to vary the degree of PEG coverage to optimize ASOs stability and efficiency, and to evaluate its impact on *C. albicans* filamentation *in vitro* and *in vivo*.

c) To extend the *in vivo* studies performed on the *G. mellonella* larvae to other *in vivo* models (e.g. mouse-models). The mouse-model will enable a realistic approach of the ASOs effect, and it will be interesting to evaluate the pharmacokinetics, pharmacodynamics and toxicology events behind molecules administration.

d) As in the case of anti-*EFG1* 2'OMe, further studies to improve the stability with the anti-*EFG1* LNA-gapmer5 should be performed. It would be interesting to study the encapsulation

of anti-*EFG1* LNA-gapmer5 on polyplexes and lipoplexes formulations as a strategy to improve its delivery and its effect on *C. albicans* filamentation. Moreover, to further investigate if the administration of a double-dose of this LNA-gapmer will enhance the control of *C. albicans* filamentation on *G. mellonella* larvae and to extend these studies to other *in vivo* models.
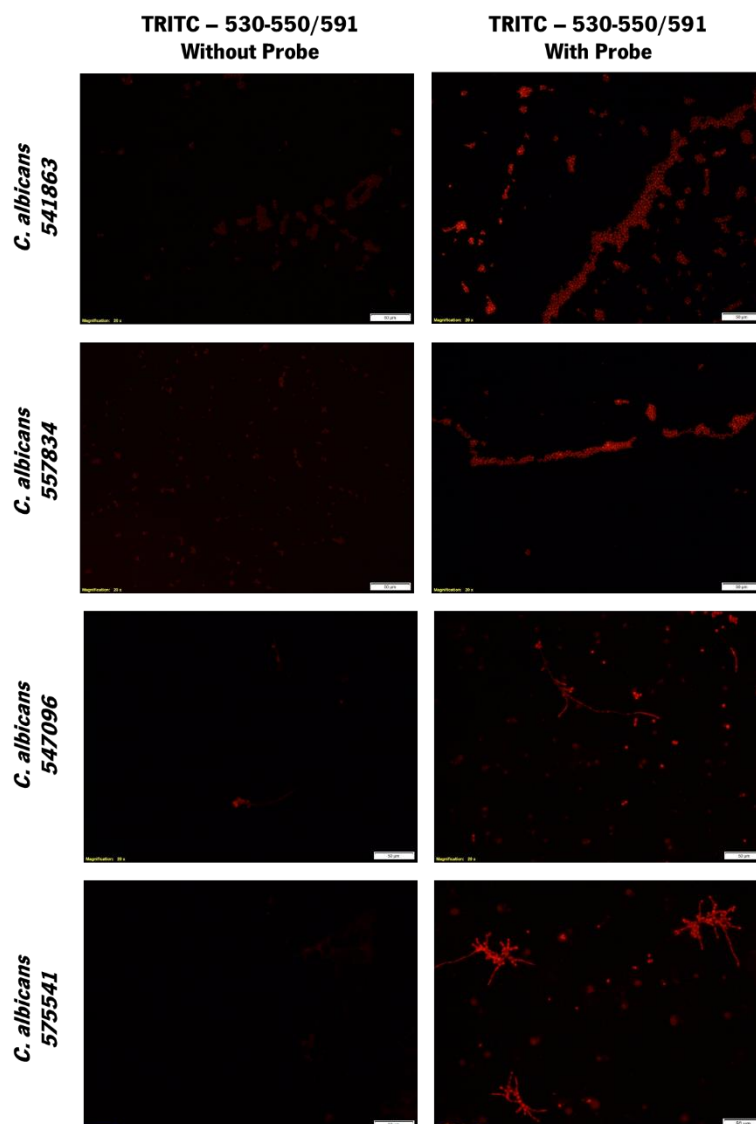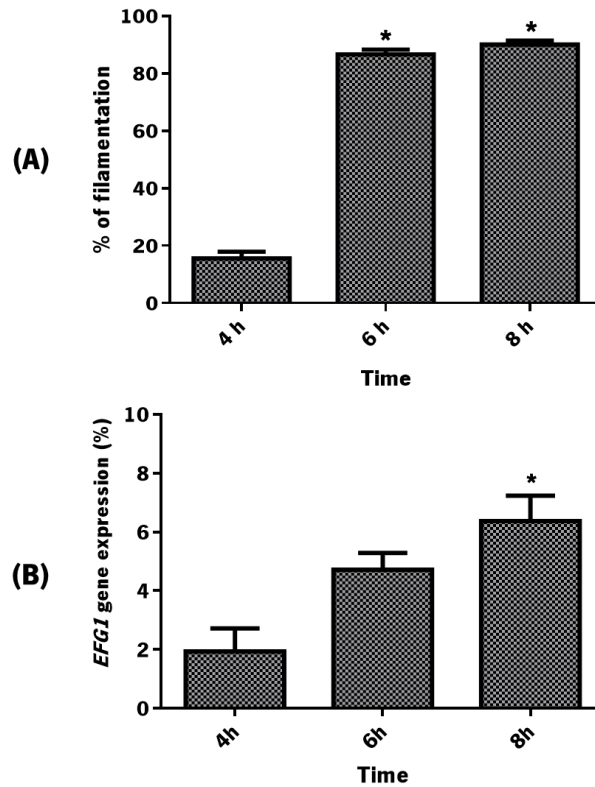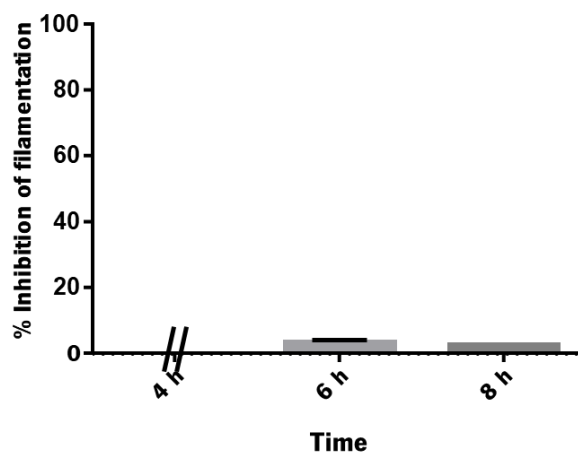
Annex I

Figure AI.1 Anti-*EFG1* 2'OMe *Candida albicans* strains sensitivity determined by fluorescence *in situ* hybridization (FISH). The images were obtained by epifluorescence microscopy with the same exposure time for cells incubated in absence and presence of ASO. The values of exposure time used varied between 32.05 ms and 340.7 ms. Negative controls were prepared only with 20 µL of hybridization solution without probe.

Annex AI.2 Evaluation of *C. albicans* filamentation and *EFG1* gene expression in the untreated cells. (A) Percentage of filamentous forms (%) of *Candida albicans* SC5314 at different time points (4, 6 and 8 h) in RPMI (Without ASO); **(B)** Percentage of *EFG1* gene expression obtained from *Candida albicans* SC5314 at different time points (4, 6 and 8 h). Error bars represent standard deviation. *Significantly differences between 4 h and the other times tested (P-value<0.05).

Annex AI.3 Scrambled ASO effect on *Candida albicans* filamentation. Percentage of inhibition of filamentous forms (%) at different time points (4, 6 and 8 h) with 40 nM of scrambled ASO in RPMI.
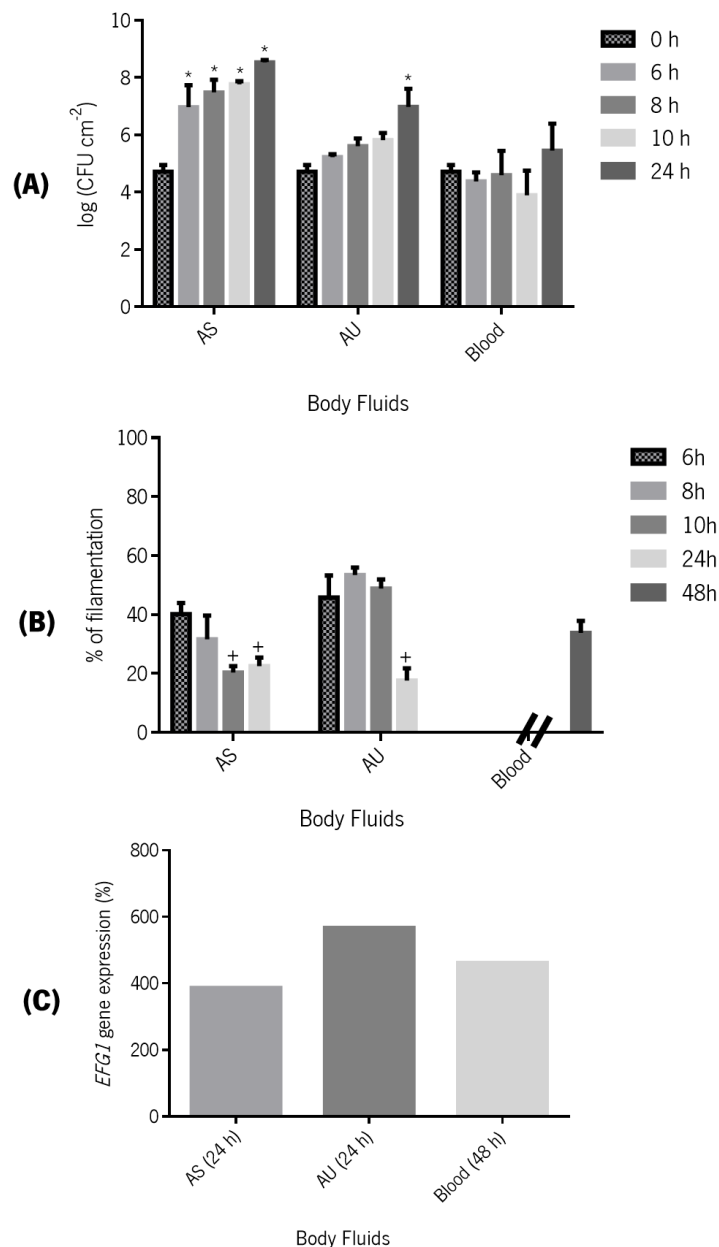
Annex AI.4 *Candida albicans* **behaviour on different simulated human body fluids. (A)** Number of cultivable cells (log CFUs cm^{-2}) at different time points (0, 6, 8, 10 and 24 h); **(B)** Percentage of filamentous forms (%) at different time points (6, 8, 10, 24 and 48 h) and **(C)** Percentage of *EFG1* gene expression in different simulated human body fluids (AS, AU at 24 h and horse blood at 48 h); without ASO obtained from *Candida albicans* SC5314. Error bars represent standard deviation. *Significantly differences between 0 h and the other times tested (P-value<0.05). ⁺Significantly differences between 6 h and the other times tested (P-value<0.05).
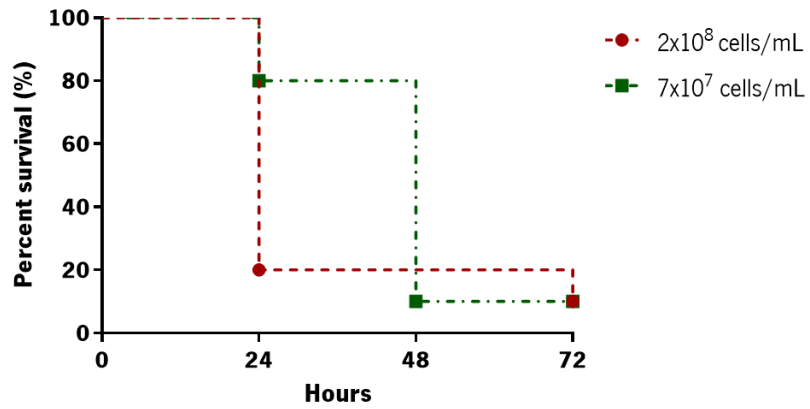
Annex II

Figure AII.1 Study of *Galleria mellonella* lethality. For each control, 10 larvae were injected with two different concentrations of *Candida albicans* cells (2 x 10⁸ and 7 x 10⁷ cells mL⁻¹ cells mL⁻¹)..
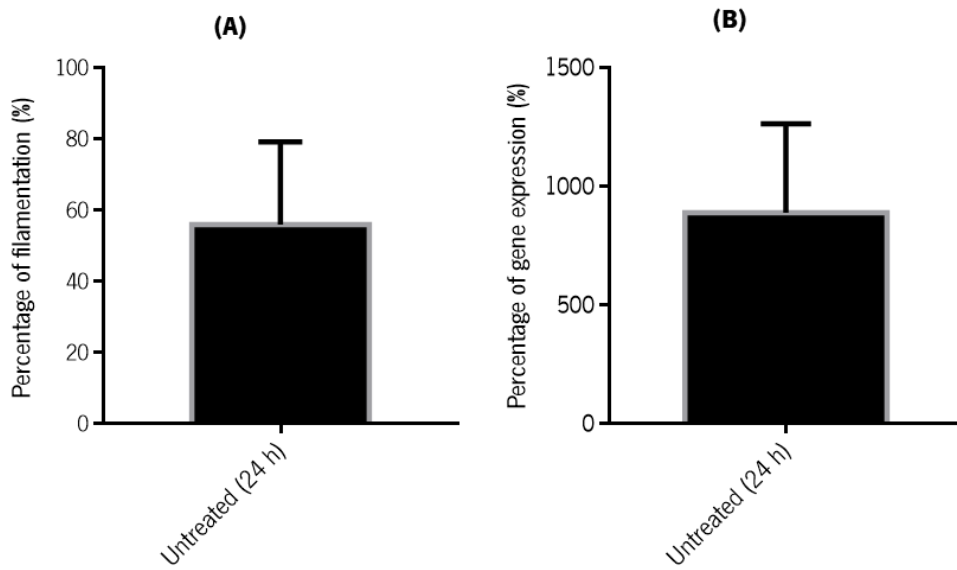
Annex III

(A)

(B)

Figure AIII.1 Evaluation of *C. albicans* filamentation and *EFG1* gene expression in the untreated cells. Percentage of **(A)** *Candida albicans* filamentation and **(B)** *EFG1* gene expression after 24 h of incubation on RPMI (without ASO).
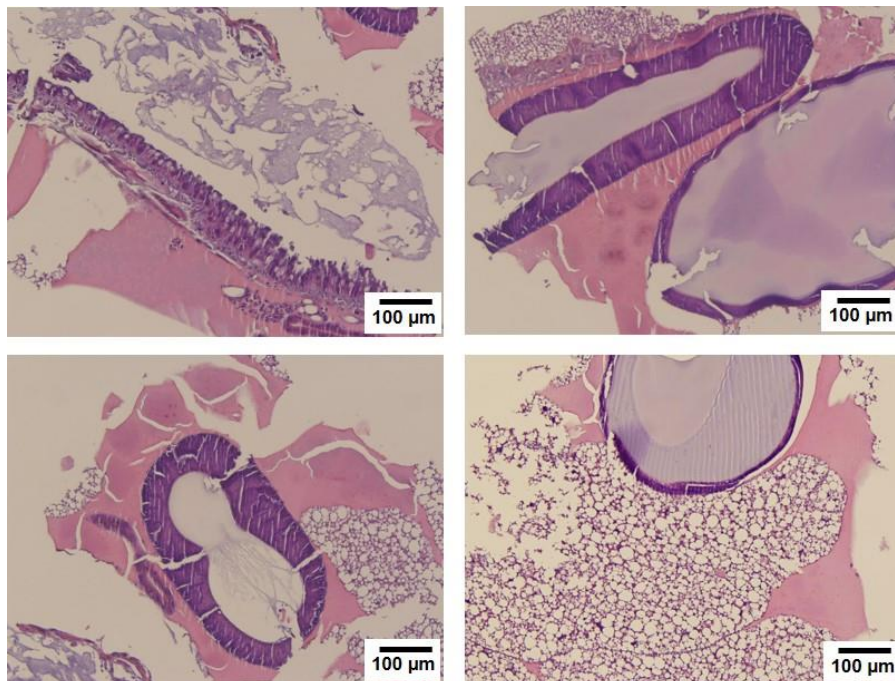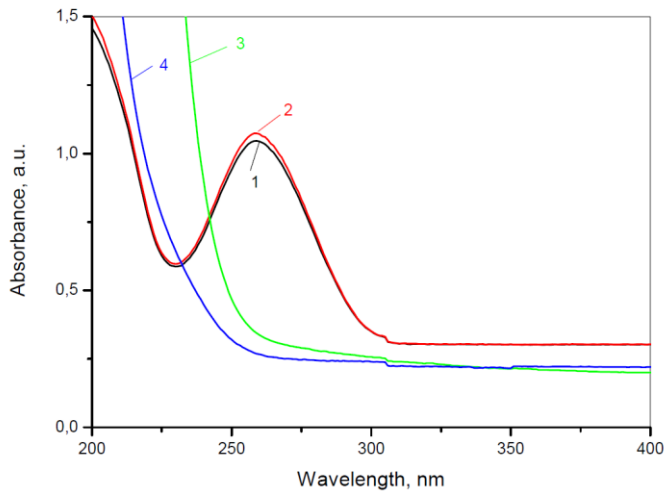

Figure AIII.2 Histological sections of the fat body of *Galleria mellonella* (control, without *Candida albicans* cells). The larvae sections were labelled with haematoxylin-eosin (HE) coloration. The magnification images were at 100x.

Annex IV

UV-VIS spectra of 4 µM ASO (DDW) before (1,2) and after (3,4) adsorption immobilization on polyamide supports. 1 and 3 – PA4 supports; 2 and 4 – PA6 supports.

Figure AIV.1 UV-VIS analysis for ASO before and after adsorption immobilization on PA4 and PA6 carriers.
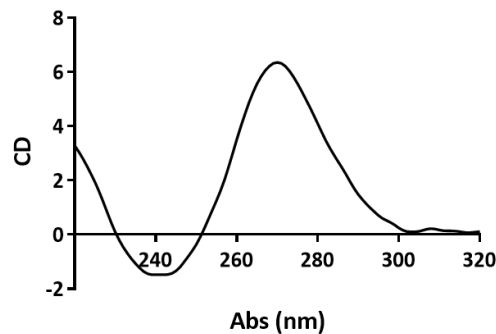

Figure AIV.2 Circular dichroism of anti-*EFG1* 2'-*O*MethylRNA. The spectra were recovered on a JASCO DC 1500 spectrophotometer using cuvettes with a 0.1 cm path length. Spectra were averaged over three scans (320-200 nm, 50nm/min intervals, 1 nm bandwidth, and 1 s response time) and background corrected with the solvent (5 mM $MgCl_2$, 10 mM NaCl and 1 mM sodium phosphate).
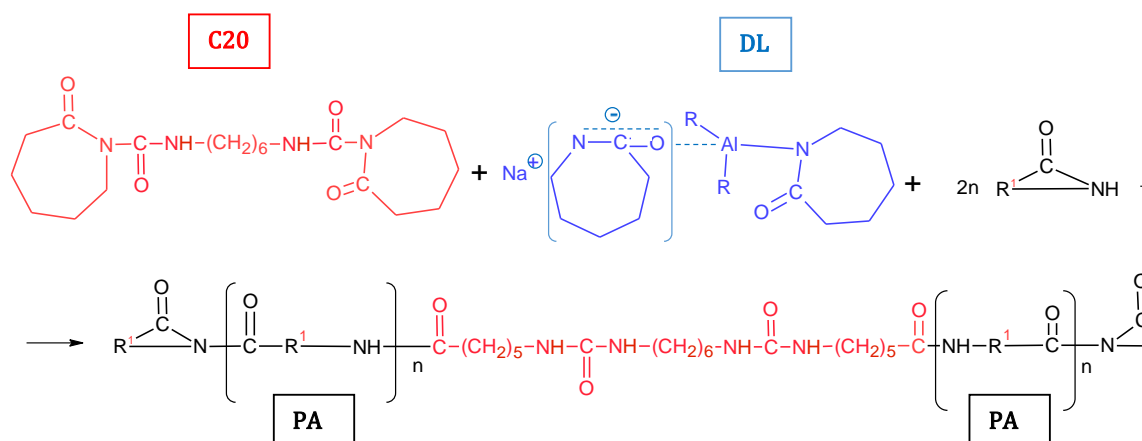
Figure AIV.3 Chemical reactions occurring during AAROP of GBL ($R^1 = (CH_2)_3$) or ECL ($R^1 = (CH_2)_5$) to PA4 or PA6 MPs. The active substance of the AAROP activator is designated as C20; The chemical structure of the AAROP initiator dicaprolactamato-bis-(2-methoxyethoxo)-aluminate wherein $R = OCH_2CH_2OCH_3$ is designated by DL.

Viscosity measurements

The intrinsic viscosity measurements were performed with PA4 and PA6 MP samples in 97% sulfuric acid at a concentration of 0.2 g/dL with a suspended level Ubbelohde viscometer thermostatted at 23°C. Flow times are recorded as an average of at least 10 runs.
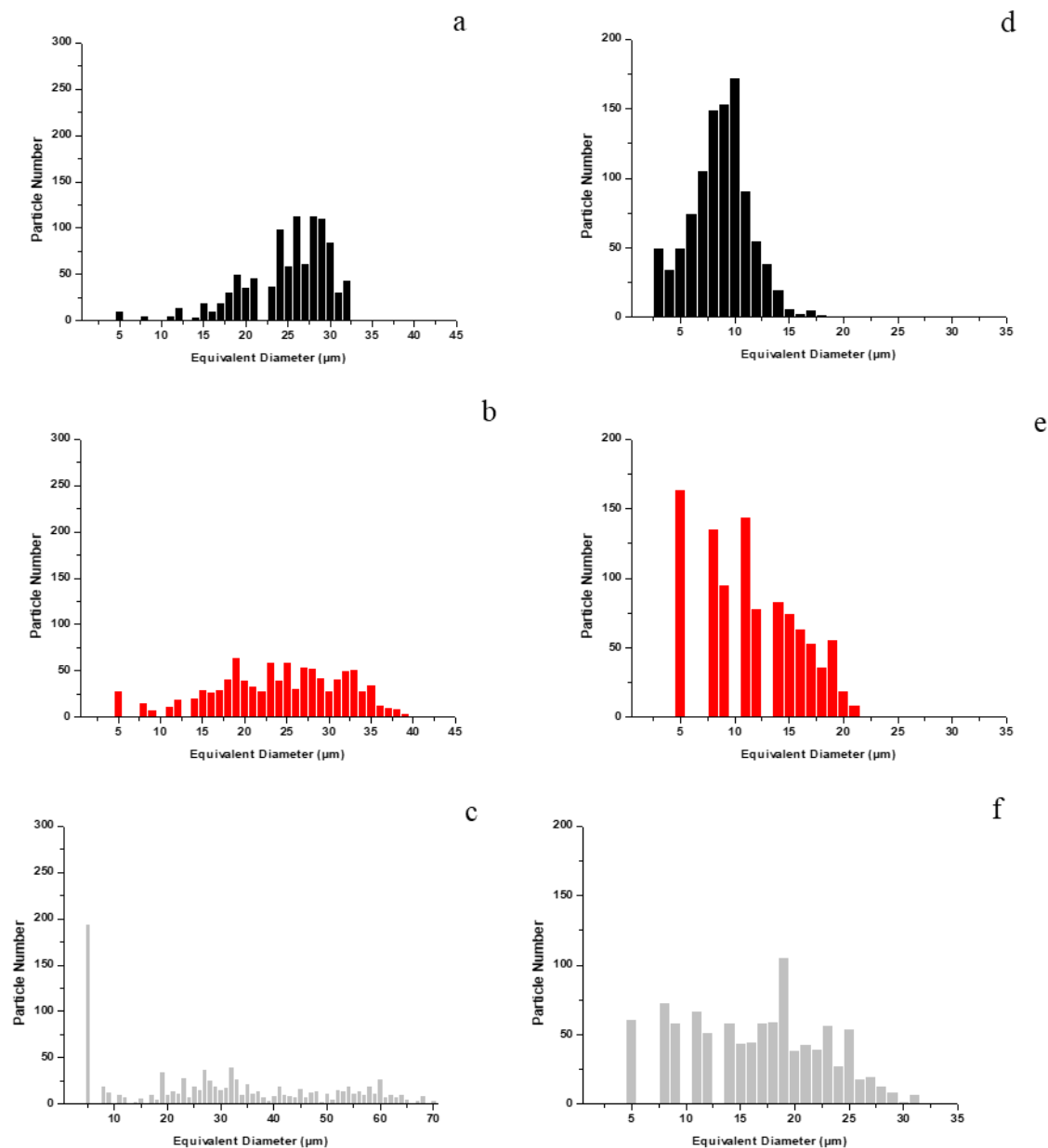
Figure AIV.4 Size distribution curves in neat PA6 and PA4 MP supports and in the respective polyplexes: a – PA6; b – PA6-Ent-ON; c – PA6-Imm-ON; d – PA4; e – PA4-Ent-ON; f – PA4-Imm-ON. Bright field optical microscopy of all samples was performed evaluating the particles' sizes, roundness, and their distributions were performed in an Olympus BH-2 microscope (Japan) equipped with the Leica Application Suite 4.4 software for image processing.

Z-potential measurements

The electric charge of the PA6 and PA4 empty carriers, as well as that of the respective polyplexes was evaluated by zeta potential determined at pH = 6.34 in deionized water at 25.0 ± 0.1 °C. Measurements

were performed with a microelectrophoresis cell (DLS Nanosizer, Malvern) in a Zetasizer Nano ZS apparatus of Malvern Instruments. The applied voltage was 200 V and each mean value consisted of 100 recordings.

Table AIV.1 Z-potential of neat polyamide MPs and their polyplexes. Amount of particles: 0.5 mg/mL

Sample designation	Z potential mV
PA4	-23.3 ± 0.9
PA4-Imm-ON	-4.4 ± 3.9
PA4-Ent-ON	-30.0 ± 2.0
PA6	-12.4 ± 4.1
PA6-Imm-ON	-13.6 ± 1.8
PA6-Ent-ON	-4.6 ± 1.4